UNIVERSITY OF CALIFORNIA, SAN DIEGO

Black Carbon Transport and Deposition to the California Mountain Snow Pack

A dissertation submitted in partial satisfaction of the requirements for the degree

Doctor of Philosophy

in

Earth Sciences

by

Odelle L. Hadley

Committee in charge:

V. Ramanathan, Chair
Steven Buckley
Daniel Cayan
Joel Norris
Lynn Russell

2008

The dissertation of Odelle L. Hadley is approved, and it is acceptable in quality and form for publication on microfilm:

Chair

University of California, San Diego

2008

For Grandma and Grandpa

TABLE OF CONTENTS

LIST OF SYMBOLS

α	absorption
a	fraction of attenuation from black carbon
A	area of the sample spot on a filter
ATN	attenuation
BC	mass of black carbon
c	coefficient of attenuation
c_1	coefficient of attenuation for BC
c_2	coefficient of attenuation for char
EC	mass of elemental graphitic carbon
I	radiant intensity
k	absorption angstrom exponent (AAE)
LAC	mass of light absorbing carbon (black carbon and char)
MAE	mass attenuation efficiency
T	temperature
TC	mass of carbon
TOA	thermal-optical analysis
OC	mass of organic carbon
σ	uncertainty
λ	wavelength of light

LIST OF FIGURES

LIST OF TABLES

ACKNOWLEDGEMENTS

First and foremost I would like to thank Professor Ramanathan for his careful guidance of my research over the years, as well as for providing me with many opportunities to participate in and travel to conferences and workshops, both nationally and abroad. I am grateful to the scientists and students in Professor Ramanathan's group for their wonderful support and advice over the years: Craig Corrigan, Greg Roberts, M. Ramana, Deohy Kim, Yan Feng, Katrin Lehman, and my office partner and fellow student, Aihua Zhu.

I wish to thank the members of my PhD committee for their thoughtful advice and comments regarding the progression of my research: Lynn Russell, Dan Cayan, Joel Norris and Steven Buckley.

With support from NSF NSF (ATM0201946), and NOAA (NA17RJ1231-VR03) I was able to participate in the Cloud Indirect Forcing Experiment (CIFEX), which provided much of the data and instigated the first portion of my research. I also thank the U. of Wyoming, King Air crew, (without whom much of the CIFEX data could not have been collected) and all the site operators for the IMPROVE monitoring network and the analysis team at the Desert Research Institute for providing long term measurements of aerosols at the IMPROVE aerosol observatories. Data from the IMPROVE network proved integral to a large portion of the research presented within these pages. I would like to express my gratitude to Guido Franco and the California Energy Commission for their continuing support of and belief in the research conducted for this dissertation.

I would like to acknowledge my collaborators outside of SIO, Tom Kirchstetter at Lawrence Berkeley National Lab and Steven Cliff at the University of California Davis. Without either of these two people, neither the laboratory nor the field phase of this work would have been accomplished so successfully.

I am grateful to my family for all their support, especially my father-in-law Patrick Hadley, who provided a lovely home and haven during my time at SIO, and my mom for her advice, support, understanding, and her editing and comments on various papers and chapters of this thesis over the years. Lastly, and most importantly, I thank with all my heart my husband, Mason Hadley, for his patience, support, encouragement, love, and the occasional awesome graphic. I could have done none of this without him.

The text of Chapter 2, in full, is a reprint of a published paper, Hadley OL, Ramanathan V, Carmichael GR, , "Trans-Pacific Transport of black carbon and fine aerosols into North America" *Journal of Geophysical Research-Atm* 112 (D5): Art. No. D05309 MAR 14 2007. I was the primary researcher and author. A large segment of the text of Chapter 3 was submitted to Environmental Science and Technology in February 2008. In addition to myself, the primary author, co-authors on this paper are Dr. Craig E. Corrigan and Dr. Thomas W. Kirchstetter.

VITA

June 1995	B.A. Liberal Arts, The Evergreen State College, Olympia, WA
Summer 1999	NASA Space Grant, O.U.R. Earth Summer Research Internship, University of Washington, Seattle
September 2000	B.S. Physical Chemistry, The Evergreen State College, Olympia, WA
2000-2002	Air Quality Specialist and Monitoring Technician, Olympic Region Clean Air Agency, Olympia, WA
2002-2008	Graduate Student Researcher, Center for Atmospheric Sciences, Scripps Institution of Oceanography, University of California, San Diego
Summer 2006	Senior Learning Skills Counselor - Jacobs School of Engineering, COSMOS (California State Summer School for Mathematics and Science)
June 2008	Ph.D. Earth Sciences, Scripps Institution of Oceanography, University of California, San Diego

PUBLICATIONS

Hadley OL, Corrigan CE, Kirchstetter TW, et al, "Modified Thermal-Optical Analysis using Spectral Absorption Selectivity to Distinguish Black Carbon from Pyrolized Organic Carbon" (submitted to *Environmental Science and Technology, February 2008*)

Hadley OL, Ramanathan V, Carmichael GR, et al, "Trans-Pacific Transport of black carbon and fine aerosols into North America" *Journal of Geophysical Research-Atm* 112 (D5): Art. No. D05309 MAR 14 2007

Roberts G, Mauger G, Hadley O, et al., "North American and Asian aerosols over the eastern Pacific Ocean and their role in regulating cloud condensation nuclei" *Journal of Geophysical Research-Atm* 111 (D13): Art. No. D13205 JUL 12 2006

ABSTRACT OF THE DISSERTATION

Black Carbon Transport and Deposition to the California Mountain Snow Pack

By

Odelle Lariviere Hadley

Doctor of Philosophy in Earth Sciences

University of California, San Diego, 2008

Professor V. Ramanathan, Chair

Black carbon (BC), a main component of combustion-generated soot, is a strong absorber of sunlight and contributor to climate change. This dissertation is divided into three separate sections. Part one presents estimates of long range transport of black carbon (BC) and aerosol fine mass across the Pacific Ocean into North America during April 2004. The BC and aerosol transport estimates were based on simulations by the CFORS (Chemical weather FORecast System) model. Model validation was accomplished using aircraft data and surface measurements of fine mass and BC at 30 IMPROVE (Interagency Monitoring of Protected Visual Environments) ground observatories located in the Western United States. The transported BC mass at 130°W in the spring of 2004 amounted to approximately 77% of the total BC emitted in North America during the same period.

The second section highlights a new analysis method for measuring BC particles in snow and rain water. This includes a description of the development of a laboratory standard of known amounts of BC in water, evaluation of sample filtration efficiency, and modifications to the thermal-optical analysis method (TOA), developed specifically for this research in order to make accurate measurements of BC in snow and rain water. Changes in the wavelength dependence of absorption during TOA are used to separate BC from charring organics, yielding a more accurate measurement of BC mass on the filter.

The final section of this dissertation presents the first measurements BC deposition in rain and snow in California, as well as a general estimate of contribution from Asian BC. The average BC concentration in coastal rain was 5 ng/g, and slightly higher in the mountain snow, at 6 ng/g and 7 ng/g. The data revealed that snow was able to efficiently remove almost all of the atmospheric BC to the snowpack. Measurements of aerosol elemental composition, combined with meteorological data and calculated air mass back trajectories, indicated that transported Asian aerosols contribute as much as 40% to the observed BC in California's mountains and therefore in the snow pack as well.

Chapter 1

Introduction

1.0 Black Carbon Aerosols and their Impact on Climate

Analysis of atmospheric aerosol pollution, which affect Earth's radiative balance and the hydrologic cycle, has long been recognized as integral to achieving a better understanding of anthropogenic influence on global and regional climate change [*Penner, et al.*, 2001]. Aerosols and their associated feedbacks introduce some of the largest uncertainties facing climate forecasters today [*Ramaswamy, et al.*, 2001]. The first order effect that atmospheric aerosols have on global climate is that they enhance the planetary albedo by scattering incoming solar radiation back to space. This diminishes the amount of energy absorbed at the surface of the Earth and causes a small cooling. More importantly, less energy reaching the surface means that evaporation from the oceans is reduced, effectively slowing down the hydrologic cycle [*Ramanathan and Carmichael*, 2008]. Secondary climate effects of aerosols include: increasing cloud albedo by increasing the number of cloud droplets [*Twomey*, 1977], reducing droplet size and therefore suppressing precipitation [*Rosenfeld*, 2000], and extending cloud lifetimes [*Quaas, et al.*, 2004]. Of all the aerosol types present in our atmosphere, the unique optical properties of BC (black carbon) or soot represent one of the largest sources of uncertainty in quantifying the net effect of aerosols on climate change [*Jacobson*, 2001; *Penner, et al.*, 2003; *Ramaswamy, et al.*, 2001].

BC plays an important role in total aerosol radiative effects. Instead of merely scattering solar radiation, BC aerosols absorb solar radiation and exert a positive forcing on the climate system [*Jacobson*, 2001; *Ramanathan and Carmichael*, 2008; *Ramanathan, et al.*, 2007]. This forcing causes a redistribution of energy within the atmosphere, increases vertical stability and possibly leads to decreased convection and precipitation [*Chung and Zhang*, 2004; *Menon, et al.*, 2002]. Furthermore, freshly emitted BC tends to be hydrophobic and therefore thought to have a longer atmospheric lifetime compared to other particles, which may be removed more efficiently by precipitation and cloud processing [*Lim, et al.*, 2003]. BC atmospheric residence time largely depends on how quickly the BC particles are processed by atmospheric oxidants [*Johnson, et al.*, 2005; *Park, et al.*, 2005]. These "processed" BC particles develop a hydrophilic coating, which allows them to act as CCN (cloud condensation nuclei) [*Chughtai, et al.*, 1996; *Zuberi, et al.*, 2005] and subsequently be removed via wet deposition. Entrainment of BC into clouds may also shorten the cloud lifetime through enhanced absorption of radiation and resultant in-cloud heating and evaporation [*Ackerman, et al.*, 2000; *Chylek, et al.*, 1999; *Conant, et al.*, 2002; *Jiang, et al.*, 2006; *Nenes, et al.*, 2002]. Reducing cloud lifetime decreases the cooling effect of the cloud and acts as a positive forcing on the radiation budget. Lastly, BC deposited onto snow and ice decreases the surface albedo and leads to faster melting of glaciers, polar ice, and mountain snow packs [*Chylek, et al.*, 1983; *Clarke and Noone*, 1985; *Conway, et al.*, 1996; *Flanner, et al.*, 2007; *Hansen and Nazarenko*, 2004; *Jacobson*, 2004; *Painter, et al.*, 2007; *Warren and Wiscombe*, 1980], all of

which have serious implications for the global energy balance, sea level rise, polar and high elevation ecology, and fresh water resources for many population centers world wide.

1.1 What is BC? Chemical Properties

Although BC is widely recognized as an important variable in aerosol and climate science, the definition of BC is subject to interpretation and use of this term has been criticized as being ill-defined. Other labels that have been used in place of BC include: soot, elemental carbon (EC), light absorbing carbon (LAC), and graphitic carbon (GC) [*Bond and Bergstrom*, 2006]. The term "black carbon" originates from measurement methods that rely on its light absorption properties. Black carbon aerosol efficiently absorbs light at all wavelengths, making it appear visibly black when viewed with the naked eye. A variation of the Beer-Lambert law is used to convert BC absorption to BC mass (Chapter 3); however this calculation depends on knowing the BC mass absorption efficiency, which numerous field and laboratory studies have found to vary by over a factor of seven depending on the mixing state, size, and morphology of the BC aerosol. Optical measurements of BC correlate very highly with AMS (aerosol mass spectrometer) and thermally evolved carbon analysis [*Kirchstetter and Novakov*, 2007], which measure EC rather than BC, thus the two variables are nearly interchangeable. Simultaneous EC and BC measurements have provided the range of values used for BC mass absorption efficiency. Since BC aerosol may contain a fraction of light absorbing organic carbon (OC), which tend to

have stronger absorption wavelength dependence than typically used for BC, the term light absorbing carbon or LAC has recently been introduced [*Bond and Bergstrom*, 2006].

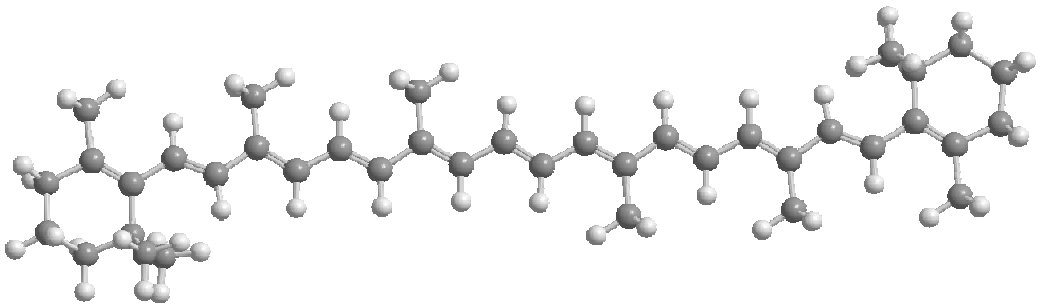

Figure 1.1 Conjugated bonds, like those in this beta-carotene molecule form delocalized pi bonds that reduce the energy needed for electron orbital transitions and allow electro-magnetic radiation (light) to be absorbed at lower energies.

The high absorption efficiency of BC is due to the bond type and morphology of the carbon-carbon bonds in a BC molecule. BC consists of long chains, rings, and partial rings of carbon atoms held together by alternating single and double carbon bonds, as seen in the beta-carotene molecule (Figure 1.1). This pattern of alternating single double bonds is called conjugated carbon bonding. The degree of conjugation is based on the number of alternating single-double bonds in the molecule. Conjugated carbon bonding results in the formation of delocalized pi-bonds that lower the energy gap required for electron orbital transition [*Solomons and Fryhle*, 2000]. Smaller molecules containing conjugated double bonds absorb light at very specific wavelengths, for example beta-carotene (Figure 1.1) which has 11 conjugated double bonds absorbs light at $\lambda = 497$ nm, and has a red-orange color [*Solomons and Fryhle*, 2000]. Molecules with a smaller number of conjugated bonds require more energy for

an electron orbital transition and therefore absorb higher energy light. Black carbon molecules contain hundreds to thousands of conjugated bonds in random formation, which allows the efficient absorption of all wavelengths of light [*Bond and Bergstrom*, 2006]. The most commonly used spectral dependence of BC on absorption follows the form $\alpha = \lambda^{-k}$ [*Bergstrom, et al.*, 2007; *Hansen*, 2003; *Kirchstetter, et al.*, 2004; *Weingartner, et al.*, 2003], where α is absorption and k is the absorption angstrom exponent (AAE). When BC is mixed with organic molecules containing fewer conjugated bonds, the AAE increases and may be as high as 2 or 3, but an AAE of 1 is most commonly assumed for BC that is close to pure EC [*Bergstrom, et al.*, 2007; *Kirchstetter, et al.*, 2004]. Since many organic molecules, such as polyaromatic hydrocarbons (PAH), contain conjugated carbon bonds, the line separating BC, EC, and OC is often indistinct. As most of the measurements of BC made during this research were optically based, this dissertation uses the term BC throughout to describe carbonaceous aerosol that efficiently absorbs light at all wavelengths and has an atmospheric mass absorption efficiency greater than 7 m^2/g.

1.3 Where does BC come from? Sources

Black carbon aerosols are generated during combustion of fossil fuels and biomass. In urban environments combustion of gasoline and diesel in motor vehicles contribute the majority of the BC aerosol, while in rural regions the most significant contributor is land clearing burns and residential heating. Although most of the global BC emissions are over land, ships and aircraft contribute a significant amount to the

atmospheric burden of BC over oceans [*Ramanathan and Carmichael*, 2008]. Global emissions of BC are currently estimated at approximately 8000 Gg per year [*Bond, et al.*, 2004]. Globally, Asia is the largest emitter of BC from contained combustion (mostly fossil fuel) at around 2000 Gg. Africa contributes the most BC from open burning at about 1500 Gg [*Bond, et al.*, 2004].

1.4 Where does BC go? Long Range transport and deposition to high elevation sites in Western North America

The research presented in this dissertation focuses on what happens to BC aerosols after they are emitted to the atmosphere. The two regions of interest are: East Asia, currently the largest emitter of BC, and the Western United States, downwind of the Asian continental outflow. Chapter 2 presents an evaluation of BC transport from East Asia to North America in the spring of 2004. Spring is the peak season for trans-Pacific transport of dust and pollutants, including BC [*Bey, et al.*, 2001; *Liu, et al.*, 2003; *Park, et al.*, 2005]. The bulk of the transport occurs between 2 and 6 km [*de Gouw, et al.*, 2004]. Asian aerosols reaching North America at these altitudes do not significantly contribute to pollution observed at low elevations (<1000 amsl) [*Goldstein, et al.*, 2004], but may have considerable impact at higher elevations in coastal mountain ranges, specifically the Cascades and the Sierra Nevadas [*Jaffe, et al.*, 2005; *VanCuren*, 2003; *VanCuren and Cahill*, 2002]. The timing of this transport and its observed contribution to total aerosol concentration in the coastal mountains has the potential to impact mountain snow pack albedo and melt rate.

The elemental composition and mass distribution of ambient aerosols and ambient BC mass concentration were measured at multiple locations in Northern CA. Coastal rain water and mountain snow samples were collected as the drops/crystals fell, and were analyzed for BC concentration, as well as 26 additional elements. Chapter 3 describes the analysis methods used to measure BC in precipitation samples. Chapters 4 and 5 present the data from the field study and provide the analysis and discussion as to the source type and regional origins of the BC and other aerosol observed in the mountains. Chapter 4 also includes a short discussion as to the potential impacts that the observed BC may have on snow albedo and subsequent melt rates in the spring.

References

Ackerman, A. S., O. B. Toon, D. E. Stevens, A. J. Heymsfield, V. Ramanathan, and E. J. Welton (2000), Reduction of tropical cloudiness by soot, *Science*, *288*, 1042-1047.

Bergstrom, R. W., P. Pilewskie, P. B. Russell, J. Redemann, T. C. Bond, P. K. Quinn, and B. Sierau (2007), Spectral Absorption Properties of Atmospheric Aerosols, *Atmos Chem Phys*, *Discuss., 7*, 10669-10686.

Bey, I., D. J. Jacob, J. A. Logan, and R. M. Yantosca (2001), Asian chemical outflow to the Pacific in spring: Origins, pathways, and budgets, *J Geophys Res-Atmos*, *106*, 23097-23113.

Bond, T. C., and R. W. Bergstrom (2006), Light absorption by carbonaceous particles: An investigative review, *Aerosol Sci Tech*, *40*, 27-67.

Bond, T. C., D. G. Streets, K. F. Yarber, S. M. Nelson, J. H. Woo, and Z. Klimont (2004), A technology-based global inventory of black and organic carbon emissions from combustion, *J Geophys Res-Atmos*, *109*, doi:10.1029/2003JD003697.

Chughtai, A. R., M. E. Brooks, and D. M. Smith (1996), Hydration of black carbon, *J Geophys Res-Atmos*, *101*, 19505-19514.

Chung, C. E., and G. J. Zhang (2004), Impact of absorbing aerosol on precipitation: Dynamic aspects in association with convective available potential energy and convective parameterization closure and dependence on aerosol heating profile, *J Geophys Res*, *109*, D22103.

Chylek, P., L. Kou, B. Johnson, F. Boudala, and G. Lesins (1999), Black carbon concentrations in precipitation and near surface air in and near Halifax, Nova Scotia, *Atmos Environ*, *33*, 2269-2277.

Chylek, P., V. Ramaswamy, and V. Srivastava (1983), Albedo of Soot-Contaminated Snow, *J Geophys Res-Oc Atm*, *88*, 837-843.

Clarke, A. D., and K. J. Noone (1985), Soot in the Arctic Snowpack - a Cause for Perturbations in Radiative-Transfer, *Atmos Environ*, *19*, 2045-2053.

Conant, W. C., A. Nenes, and J. H. Seinfeld (2002), Black carbon radiative heating effects on cloud microphysics and implications for the aerosol indirect effect - 1. Extended Kohler theory, *J Geophys Res-Atmos*, *107*, doi:10.1029/2002JD002094.

Conway, H., A. Gades, and C. F. Raymond (1996), Albedo of dirty snow during conditions of melt, *Water Resour Res*, *32*, 1713-1718.

de Gouw, J. A., et al. (2004), Chemical composition of air masses transported from Asia to the U. S. West Coast during ITCT 2K2: Fossil fuel combustion versus biomass-burning signatures, *J Geophys Res*, *109*, D23S20, doi:10.1029/2003JD004202.

Flanner, M. G., C. S. Zender, J. T. Randerson, and P. J. Rasch (2007), Present-day climate forcing and response from black carbon in snow, *J Geophys Res-Atmos*, *112*, -.

Goldstein, A. H., et al. (2004), Impact of Asian emissions on observations at Trinidad Head, California, during ITCT 2K2, *J Geophys Res*, *109*, D23S17, doi:10.1029/2003JD004406.

Hansen, A. D. A. (2003), *The Aethalometer*, Magee Scientific Company, Berkely CA.

Hansen, J., and L. Nazarenko (2004), Soot climate forcing via snow and ice albedos, *P Natl Acad Sci USA*, *101*, 423-428.

Jacobson, M. Z. (2001), Strong radiative heating due to the mixing state of black carbon in atmospheric aerosols, *Nature*, *409*, 695-697.

Jacobson, M. Z. (2004), Climate response of fossil fuel and biofuel soot, accounting for soot's feedback to snow and sea ice albedo and emissivity, *J Geophys Res-Atmos*, *109*, D21201, doi:21210.21029/22004JD004945.

Jaffe, D., S. Tamura, and J. Harris (2005), Seasonal cycle and composition of background fine particles along the west coast of the US, *Atmos Environ*, *39*, 297-306.

Jiang, H. L., H. W. Xue, A. Teller, G. Feingold, and Z. Levin (2006), Aerosol effects on the lifetime of shallow cumulus, *Geophys Res Lett*, *33*, L14806.

Johnson, K. S., B. Zuberi, L. T. Molina, M. J. Molina, M. J. Iedema, J. P. Cowin, D. J. Gaspar, C. Wang, and A. Laskin (2005), Processing of soot in an urban environment: case study from the Mexico City Metropolitan Area, *Atmos Chem Phys*, *5*, 3033-3043.

Kirchstetter, T. W., and T. Novakov (2007), Controlled generation of black carbon particles from a diffusion flame and applications in evaluating black carbon measurement methods, *Atmos Environ*, *41*, 1874-1888.

Kirchstetter, T. W., T. Novakov, and P. V. Hobbs (2004), Evidence that the spectral dependence of light absorption by aerosols is affected by organic carbon, *J Geophys Res-Atmos*, *109*, D21208, doi:21210.21029/22004JD004999.

Lim, H. J., B. J. Turpin, L. M. Russell, and T. S. Bates (2003), Organic and elemental carbon measurements during ACE-Asia suggest a longer atmospheric lifetime for elemental carbon, *Environ Sci Technol*, *37*, 3055-3061.

Liu, H. Y., D. J. Jacob, I. Bey, R. M. Yantosca, B. N. Duncan, and G. W. Sachse (2003), Transport pathways for Asian pollution outflow over the Pacific: Interannual and seasonal variations, *J Geophys Res-Atmos*, *108*, (D20), 8786, doi:8710.1029/2002JD003102.

Menon, S., J. Hansen, L. Nazarenko, and Y. F. Luo (2002), Climate effects of black carbon aerosols in China and India, *Science*, *297*, 2250-2253.

Nenes, A., W. C. Conant, and J. H. Seinfeld (2002), Black carbon radiative heating effects on cloud microphysics and implications for the aerosol indirect effect - 2. Cloud microphysics, *J Geophys Res-Atmos*, *107*, 4605, doi:4610.1029/2002JD002101.

Painter, T. H., A. P. Barrett, C. C. Landry, J. C. Neff, M. Cassidy, C. R. Lawrence, K. E. McBride, and G. L. Farmer (2007), Impact of disturbed desert soils on duration of mountain snow cover, *Geophys Res Lett*, *34*, L12502, doi:12510.11029/12007GL030284.

Park, R. J., et al. (2005), Export efficiency of black carbon aerosol in continental outflow: Global implications, *J Geophys Res-Atmos*, *110*, D11205, doi:11210.11029/12004JD005432.

Penner, J. E., et al. (2001), Aerosols, their Direct and Indirect Effects, in *Climate Change 2001: The Scientific Basis. Contribution of Working Group I to*

the Third Assessment Report of the Intergovernmental Panel on Climate Change, edited by J. T. Houghton, et al., pp. 289 - 348, Cambridge University Press, Cambridge, United Kingdom and New York, NY, USA.

Penner, J. E., S. Y. Zhang, and C. C. Chuang (2003), Soot and smoke aerosol may not warm climate, *J Geophys Res-Atmos*, *108*, 4657, doi:4610.1029/2003JD003409.

Quaas, J., O. Boucher, J. L. Dufresne, and H. Le Trent (2004), Impacts of greenhouse gases and aerosol direct and indirect effects on clouds and radiation in atmospheric GCM simulations of the 1930-1989 period, *Clim Dynam*, *23*, 779-789.

Ramanathan, V., and G. Carmichael (2008), Global and regional climate changes due to black carbon, *Nature Geoscience*, *156*, 221-227.

Ramanathan, V., M. V. Ramana, G. Roberts, D. Kim, C. Corrigan, C. Chung, and D. Winker (2007), Warming trends in Asia amplified by brown cloud solar absorption, *Nature*, *448*, 575-U575.

Ramaswamy, V., O. Boucher, J. Haigh, D. Hauglustaine, J. Haywood, G. Myhre, T. Nakajima, G. Y. Shi, and S. Solomon (2001), Radiative Forcing of Climate Change, in *Climate Change 2001: The Scientific Basis. Contribution of Working Group I to the Third Assessment Report of the Intergovernmental Panel on Climate Change*, edited by J. T. Houghton, et al., pp. 351 - 416, Cambridge University Press, Cambridge, United Kingdom and New York, NY, USA.

Rosenfeld, D. (2000), Suppression of rain and snow by urban and industrial air pollution, *Science*, *287*, 1793-1796.

Solomons, T. W. G., and C. B. Fryhle (2000), *Organic Chemistry*, 7th edition ed., 1258 pp., John Wiley & Sons, New York, New York.

Twomey, S. (1977), Influence of Pollution on Shortwave Albedo of Clouds, *Journal of the Atmospheric Sciences*, *34*, 1149-1152.

VanCuren, R. A. (2003), Asian aerosols in North America: Extracting the chemical composition and mass concentration of the Asian continental aerosol plume from long-term aerosol records in the western United States, *J Geophys Res-Atmos*, *108*, -.

VanCuren, R. A., and T. A. Cahill (2002), Asian aerosols in North America: Frequency and concentration of fine dust, *J Geophys Res-Atmos*, *107(D24)*, 4804, doi:4810.1029/2002JD002204.

Warren, S. G., and W. J. Wiscombe (1980), A Model for the Spectral Albedo of Snow.2. Snow Containing Atmospheric Aerosols, *J Atmos Sci*, *37*, 2734-2745.

Weingartner, E., H. Saathoff, M. Schnaiter, N. Streit, B. Bitnar, and U. Baltensperger (2003), Absorption of light by soot particles: determination of the absorption coefficient by means of aethalometers, *J Aerosol Sci*, *34*, 1445-1463.

Zuberi, B., K. S. Johnson, G. K. Aleks, L. T. Molina, and A. Laskin (2005), Hydrophilic properties of aged soot, *Geophys Res Lett*, *32*, L01807, doi:01810.01029/02004GL021496.

Chapter 2

Trans-Pacific Transport of Black Carbon and Fine Aerosols (D<2.5 μm) into North America

2.1 Introduction

Growing interest in trans-Pacific transport of pollutants has motivated a number of field experiments as well as the development of chemical transport models. Employing both field data and models, several studies have characterized trans-Pacific transport of carbon monoxide and ozone[*Bertschi and Jaffe,* 2005; *Goldstein, et al.*, 2004; *Liang, et al.*, 2004; *Yienger, et al.*, 2000], as well as various other pollutants [*Jacob, et al.*, 2003; *Parrish, et al.*, 2004]. Observational and modeling analyses have identified episodic and significant enhancement from Asian dust and pollution emissions at a multitude of surface sites in the western United States [*Heald, et al.*, 2006; *Jaffe, et al.*, 2005; *VanCuren and Cahill*, 2002].This study assesses transport of BC (black carbon), as well as fine aerosol mass, into North America during April 2004.

Past research has shown that continental outflow of Asian pollution [*Bey, et al.*, 2001] , including BC [*Park, et al.*, 2005], is largest during March, April and May. This is due to the high frequency of vernal cold fronts moving across the Northwest Pacific, which rapidly lift the prefrontal aerosols and other pollutants to altitudes where they are captured by high winds and carried long distances [*Jacob, et al.*, 2003; *Liu, et al.*, 2003; *Stohl*, 2001]. Spring also marks the end of the dry season in Asia and therefore increased desert dust emission. Although spring meteorology enhances

Asian aerosol transport, long and short term surface aerosol analysis during the ITCT 2K2 (Intercontinental Transport and Chemical Transformation 2002) field study provide evidence that Asian pollution impacts the Northeast Pacific Ocean and the west coast of North America year round and that background levels of tropospheric aerosol at altitudes greater than 1 km over the Western United States are largely of Asian origin [*VanCuren, et al.*, 2005].

Table 2.1 Wyoming King Air instrument payload during CIFEX, April 2004 [adapted from [*Roberts, et al.*, 2006]

Instrument	**Measurement**	**Sample rate (sec)**
Condensation Particle Counter (CPC 3760; TSI)	concentration (N_{CN}; D_p > 10nm)	1
Scanning Mobility Particle Sizer (SMPS; TSI)	size distribution (n(D_p); 10 < D_p < 400 nm)	50
Passive Cavity Aerosol Spectrometer Probe (PCASP-100X; PMS)	size distribution (n(D_p); 0.2 < D_p < 3 μm)	1
Integrating nephelometer (Radiance Research)	hemispherical scattering (σ_b; λ = 530 nm)	1
Forward Scattering Spectrometer Probe (FSSP-100; PMS/DMT)	size distribution (n_D (D_p); 1 < D_p < 45 μm)	1

The CIFEX[1] campaign took place during April 2004 off the coast of Northern California. Aerosol and cloud data were collected on board the King Air, a twin turbo-prop aircraft operated by the University of Wyoming, which flew 24 missions [*Roberts, et al.*, 2006] from April 1 - 24 in the region bound by 37ºN to 43ºN and 124ºW to 127.5ºW (Figure 2.1, right panel). The King Air is equipped with multiple aerosol instruments for tropospheric measurements (Table 2.1, *adapted from* [*Roberts, et al.*, 2006]). This was ideal for CIFEX, which focused on the measurement of aerosol and cloud properties to assess the impact of long-range transport on aerosol-

[1] http://borneo.ucsd.edu/cifex/

cloud interactions. The experiment operated from the Eureka/Arcata airport in Northern California (near the Trinidad Head site operated by the NOAA Climate Monitoring and Diagnostics Laboratory; CMDL), where we intercepted plumes of pollution and dust transported from the Asian continent across the Pacific Ocean. A wide variety of aerosols observed included those of long-range transport from Asia, clean marine boundary layer, and North American emissions. These aerosols, classified by their size distribution and history, were found in stratified layers between 500 to 7500 meters above sea level and thicknesses from 100 to 3000 meters [*Roberts, et al.*, 2006].

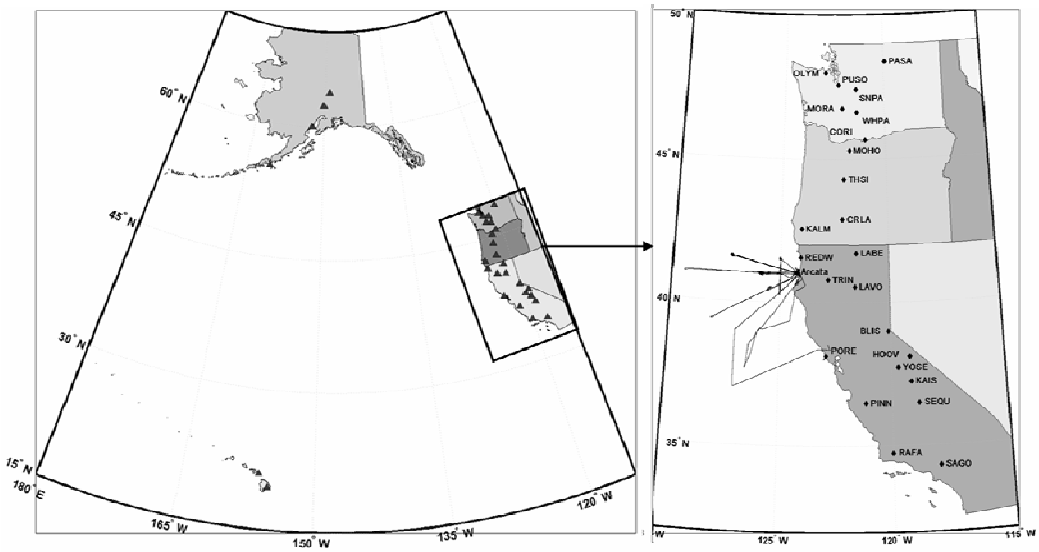

Figure 2.1. IMPROVE site locations and the WY King Air flight tracks

In addition to the airborne measurements, we employed measurements of EC (elemental carbon), OC (organic carbon), sulfate, and fine dust (<2.5 microns) from various IMPROVE (Interagency Monitoring of Protected Visual Environments) sites in Alaska, Hawaii, Oregon, Washington, and California (Figure 2.1). The IMPROVE

sites sampled varied fractions of Asian air mass ranging from less than 10% for low elevation sites to an excess of 40% for the higher elevation sites (Table 2.2).

Table 2.2. IMPROVE sites: location and percentage of air mass trajectories originating from Asia

Site	Latitude	Longitude	Elevation (meters)	% Asian traj
BLIS CA	39	-120.1	2130.7	55
CORI WA	45.7	-121	178.5	5
CRLA OR	42.9	-122.1	1996	40
DENA AK	63.7	-149	658.2	0
HALE HW	20.8	-156.3	1153	25
HAVO HW	19.4	-155.3	1258.5	25
HOOV CA	38.1	-119.2	2560.7	45
KAIS CA	37.2	-119.2	2597.5	55
KALM OR	42.6	-124.1	80	15
LABE CA	41.7	-121.5	1459.5	30
LAVO CA	40.5	-121.6	1732.7	40
MOHO OR	45.3	-121.8	1531	20
MORA WA	46.8	-122.1	439	10
OLYM WA	48	-123	599.7	20
PASA WA	48.4	-119.9	1627.3	25
PINN CA	36.5	-121.2	302	5
PORE CA	38.1	-122.9	97	15
PUSO WA	47.6	-122.3	97.7	0
RAFA CA	34.7	-120	956.5	10
REDW CA	41.6	-124.1	243.7	20
SAGO CA	34.3	-118	1791	35
SEQU CA	36.5	-118.8	519.3	0
SIME AK	55.3	-160.5	57	10
SNPA WA	47.4	-121.4	1049	30
THSI OR	44.3	-122	885	15
TRCR AK	62.3	-150.3	155	0
TRIN CA	40.8	-122.8	1014	35
TUXE AK	60	-152.7	15	0
WHPA WA	46.6	-121.4	1827.3	45
YOSE CA	37.7	-119.7	1603	45

2.2 CFORS (Chemical weather FORecast System) model

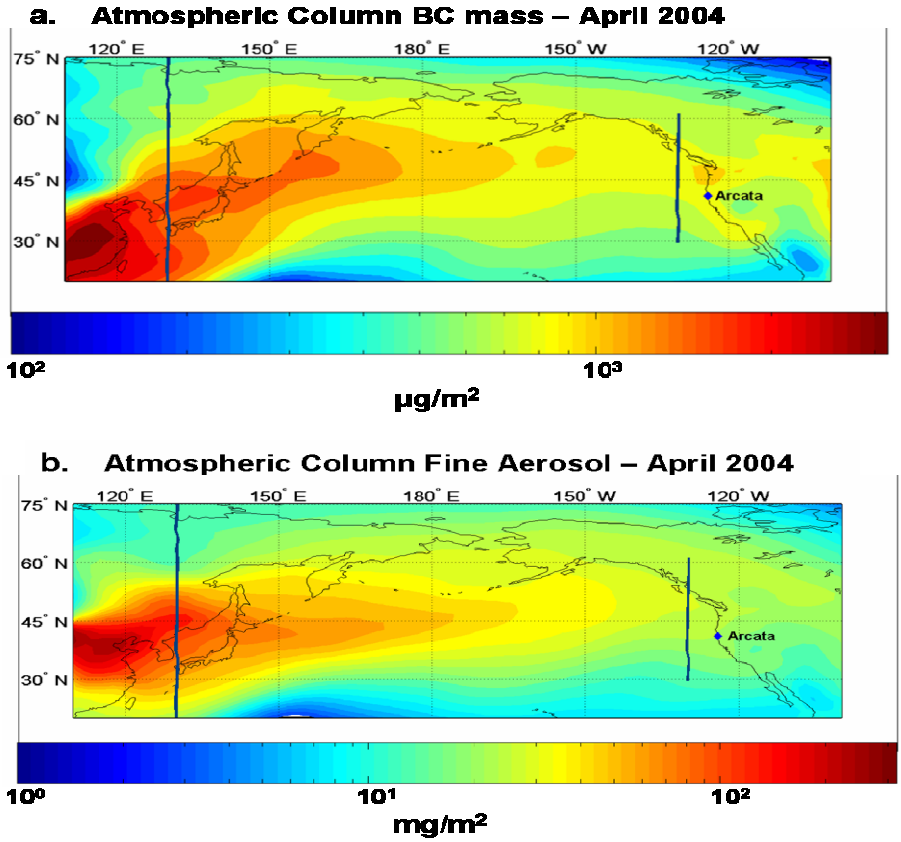

Figure 2.2. CFORS derived atmospheric column (a) BC and (b) fine mass, averaged from March 26 -April 26, 2004. White lines indicate the latitude range where transports were calculated.

CFORS couples observed meteorological fields (i.e, reanalysis fields) with surface emissions of pollutants to simulate three dimensional distribution of pollutant gases and chemical composition of aerosols [*Uno, et al.*, 2003]. The Trans-Pacific tracer domain extends from 15ºN to 80ºN and between 110ºE and 105ºW, with a horizontal resolution of 200 km. Vertical resolution of the CFORS atmosphere is given in 18 layers ranging in thickness from 50 meters at the surface to over 1000 meters at the top altitude of 15 km. Output variables include concentrations of BC,

sulfate, fine dust, and organic carbon, the sum of which we use as a measure of total aerosol mass. The model incorporates wet and dry removal parameters for dust, sulfate, OC, and SO_2 as well as first order oxidation conversion of SO_2 to sulfate [*Uno, et al.,* 2003]. A wet removal parameter for BC, equal to that of SO_2, was incorporated during this study [*Uno, et al.*, 2003]. In the CFORS model, wet removal affects only the atmospheric layers below cloud base, which is determined from the RAMS hydrometeor field [*Uno, et al.*, 2003].

Table 2.3. CFORS modeled anthropogenic sulfate, SO_2, dust and BC transport during CIFEX 2004 and ACE-Asia 2001

Aerosol	**ACE-Asia 130E 5 – 15 April, 2001 *(Seinfeld et al., 2001)***	**CIFEX - 130E 26 March – 25 April, 2004**	**CIFEX - 130W 26 March – 25 April, 2004**
Sulfate	36 Gg/day	11 Gg/day	9 Gg/day
SO_2	-	13 Gg/day	1 Gg/day
Dust	1.27 Tg/day	0.42 Tg/day	0.06 Tg/day

Spatial distributions of column integrated concentrations of BC and aerosol fine mass obtained from CFORS are shown in Figure 2.2 for April 2004. For comparison, Figure 2.3 shows aerosol visible optical depth (AOD) for April 2004 and 2001obtained from MODIS (Moderate Resolution Imaging Spectro-radiometer) [*Tanre, et al.*, 1997]. Figure 2.2 and Figure 2.3 reveal similar patterns of large values in eastern China with the pollution plume extending in the northeastern direction into North America. Eastward transport of dust, anthropogenic sulfur dioxide and sulfate across 130ºE between 15ºN and 75ºN (Figure 2.2 – solid black line at 130ºE) was calculated from CFORS output and compared with analogous CFORS calculations made during ACE-Asia (Table 2.3), April 2001 [*Seinfeld, et al.*, 2004]. Modeled daily

average transport of dust and sulfate across 130ºE between March 26 and April 25, 2004 equals only a third of the CFORS estimates for April 2001 (Table 2.3). MODIS retrievals of AODs for April 2001 and 2004 (Figure 2.3) also show reduced AODs for 2004 in the Eastern Pacific, thereby corroborating the reduced transport estimated by CFORS for 2004 compared to 2001.

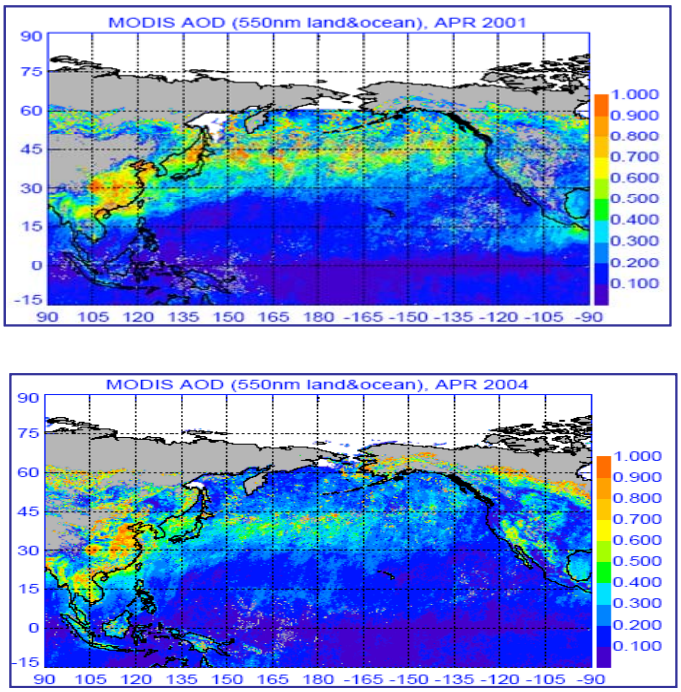

Figure 2.3. MODIS retrievals of average AOD (aerosol optical depth) in April 2001 and April 2004.

For the CIFEX campaign, CFORS used [*Streets, et al.*, 2003] for Asian emission inventories of sulfate, SO_2, OC and BC. US EPA inventory for 2001 supplied North American emissions for CFORS calculations. Surface wind speed, soil wetness and texture, and ground cover control surface dust emissions [*Uno et al.*,

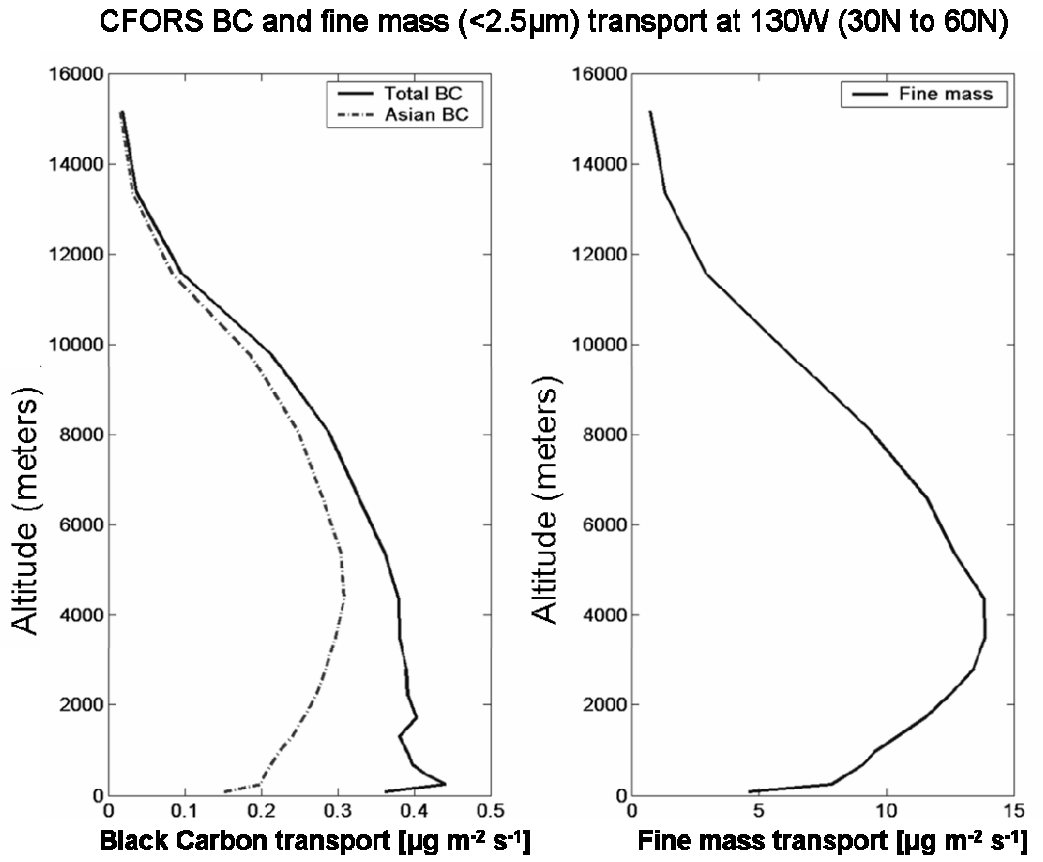

Figure 2.4 Average total BC, Asian BC, and fine mass transport across 130ºW (between 30ºN and 60ºN) from March 26 to April 25, relative to altitude.

2003] and the vertical temperature profile determines the dust uplift height. From March 26 through April 25, CFORS-derived BC net transport between 30ºN and 60ºN (Figure 2.2 - solid line) at 130ºW was 32 Gg, of which roughly 75% originates from Asian sources. This amounts to 77% of the estimated 41.5 (27 – 93) Gg of BC emitted monthly from North American sources [*Bond, et al.*, 2004]. The CFORS net fine aerosol mass transport for the period of March 26 to April 25 was 1100 Gg. Figure 4 shows the vertical profile of the average March 26 to April 25 CFORS BC, Asian BC and fine aerosol mass transport at 130ºW, between 30ºN and 60ºN. The temporally and spatially integrated transport between the surface and 2 km is 7 Gg of BC and the

rest, 25 Gg, is transported within the free troposphere above 2 km. For fine aerosol mass, the surface to 2 km layer transports 200 Gg and the region above, 900 Gg. Thus the dominant transport (78 % of BC and 82 % of fine aerosol mass) occurs above 2 km.

The accuracy of CFORS fine mass and BC transport is assessed next by considering the following observed properties: 1.) the vertical distribution of fine mass in the Eastern Pacific Ocean taken from aircraft data between 200 and 6500 meters and 2.) surface concentrations of EC, OC, SO_4, and fine dust and at elevations ranging from 15 to 2500 meters.

2.3 Vertical Profiles of Aerosol Mass Concentration from Aircraft

Out of the 24 research flights made, 8 provided data on the vertical and horizontal aerosol number distribution in the Eastern Pacific within a 400 km range of Trinidad Head, CA. These 8 flights were chosen because they provide both vertical aerosol profiles, as well as level flights of significant length that were free of cloud contamination. The remaining 16 flights were primarily dedicated to cloud analysis. The flight tracks are shown in Figure 2.1, right panel. These data include vertical aerosol profiles between 200 and 6500 meters (max altitude of the King Air) level, clear-sky, flight legs at varying altitudes, each lasting between 6 and 30 minutes.

Aerosol size distributions were obtained with a SMPS (Scanning Mobility Particle Sizer) for particles between 0.013 and 0.3 μm diameter, and a PCASP (Passive Cavity Aerosol Spectrometer probe) for particles between 0.1 and 2.5 μm

diameter. The PCASP was calibrated to a refractive index of 1.58 and PCASP sizes were corrected assuming a refractive index of 1.45 [*Stolzenburg, et al.*, 1998]. Diameter corrections were obtained from [*Liu and Daum*, 2000]. Combining the SMPS and PCASP spectra produced approximately one aerosol size spectrum per minute, for diameters ranging from 0.01 to 2.5 μm. There is a 10% (+/- 12%) discrepancy between integrated spectra and mean CPC (Condensation Particle Counter) concentrations for the same period. Mass concentration was calculated using an aerosol density of 1.9 g cm^{-3}. Uncertainty estimates were calculated from the standard deviation of number concentration in each size bin and the uncertainty in

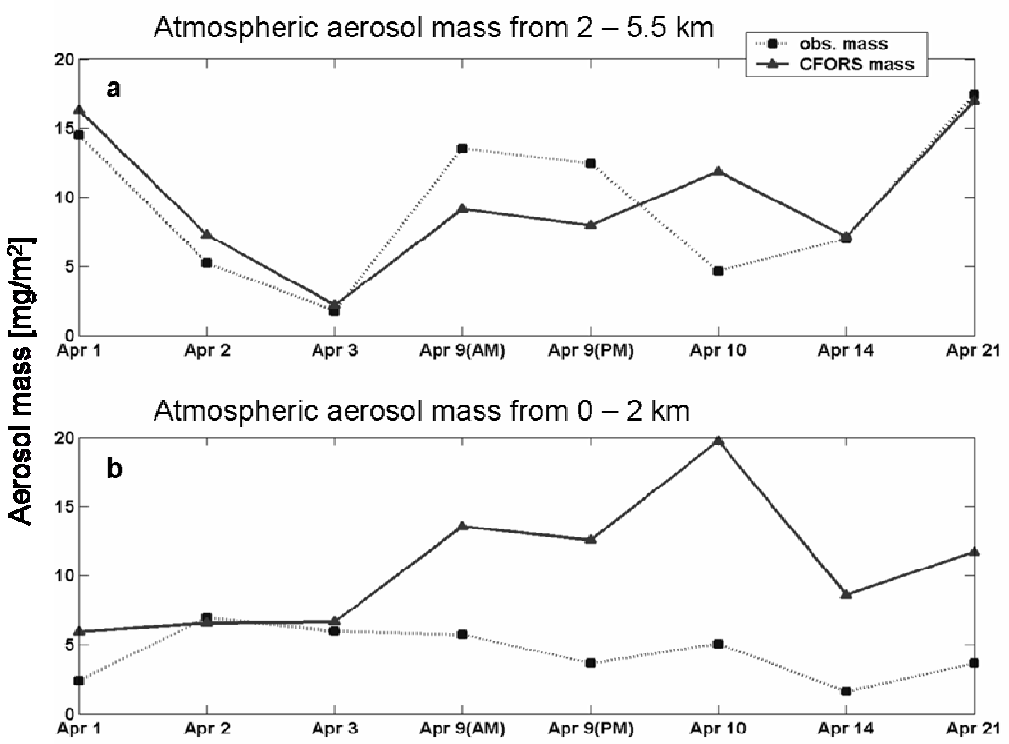

Figure 2.5. Modeled and calculated aerosol mass: a) between 2 km and 5 km and b) below 2 km. Aerosol mass was derived from observations of number concentration and size distribution on board the WY King Air.

aerosol density (+/-30%) [*Wittmaack*, 2002]. CFORS fine mass is defined as the sum of fine dust, sulfate, OC and BC mass concentration. Validation for this assumption is provided in section 4.0. The CFORS output includes the minimum and maximum aerosol mass concentration forecast by the model 12 hours prior and 12 hours following flight times as a measure of temporal sampling variability.

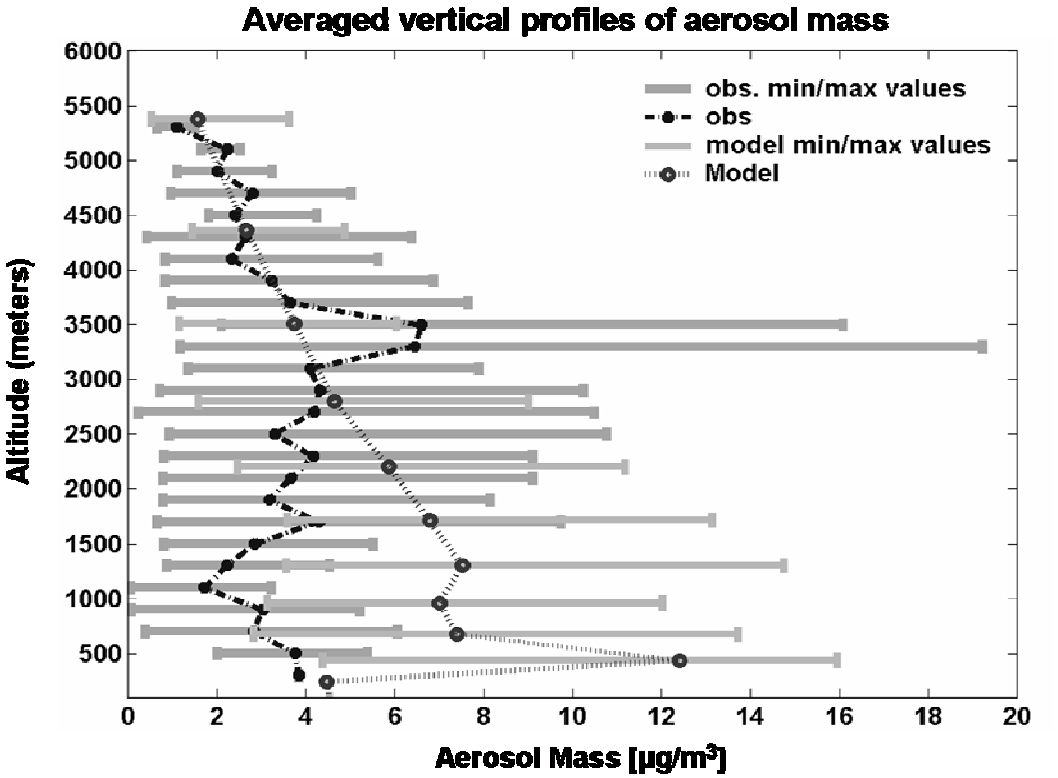

Figure 2.6. Comparison of vertical distribution of CFORS aerosol mass with derived aerosol mass from CIFEX flights. Uncertainties in measured mass reflect instrumental uncertainty as well as that of the assumed density of 1.9 + 0.57 g cm^{-3}.

Vertically integrated aerosol mass obtained from the data taken during the 8 clear-sky flight days agrees with the CFORS prediction for the middle troposphere

(2km to 5.5 km) within 3% (Figure 2.5a). However CFORS over predicts the fine mass in the lower (0 to 2 km) troposphere (Figure 2.5b) by 280 (+/-140) %. The mean, April 2004, aerosol mass vertical distribution, representing all level flights and vertical profiles collectively, compares similarly to the averaged April 2004 CFORS vertical mass distribution (Figure 6). CFORS predictions agree well with observations above the boundary layer, but over-predict aerosol mass near the surface 140% to 420%.

2.4 Comparison of CFORS with IMPROVE Network Data

IMPROVE network sites provided BC and fine mass (<2.5μm) aerosol data for March 28 through April 24, 2004 at 30 sites in Alaska, Washington, Oregon, California, and Hawaii (Figure 2.1). This study compares these data to the CFORS model outputs at each IMPROVE site location. Bulk aerosol samplers collected filter samples over a 24 hour period, midnight to midnight (local time) at each site. Elevation of the IMPROVE sites ranges from 15 to 2600 meters. Only CFORS output coincident with the time of IMPROVE sampling were used in the comparison.

The IMPROVE network provides bulk fine aerosol mass concentration, as well as chemical composition by mass. The filters were analyzed by DRI (Desert Research Institute). Fine mass was obtained from gravimetric measurements. The Thermal Optical Reflectance (TOR) method was used to retrieve EC and OC mass values [*Chow, et al.*, 2004]. One caveat to this method is that the values reported for OC and EC assume that all CO_2 evolved at temperatures less than 550ºC in the absence of O_2 is due to organics, as well as all CO_2 evolved before the filter reflectance returns to the

initial value. If these assumptions are incorrect, then the given OC may be 30 percent higher than the actual amount, and likewise the EC could be under-predicted.

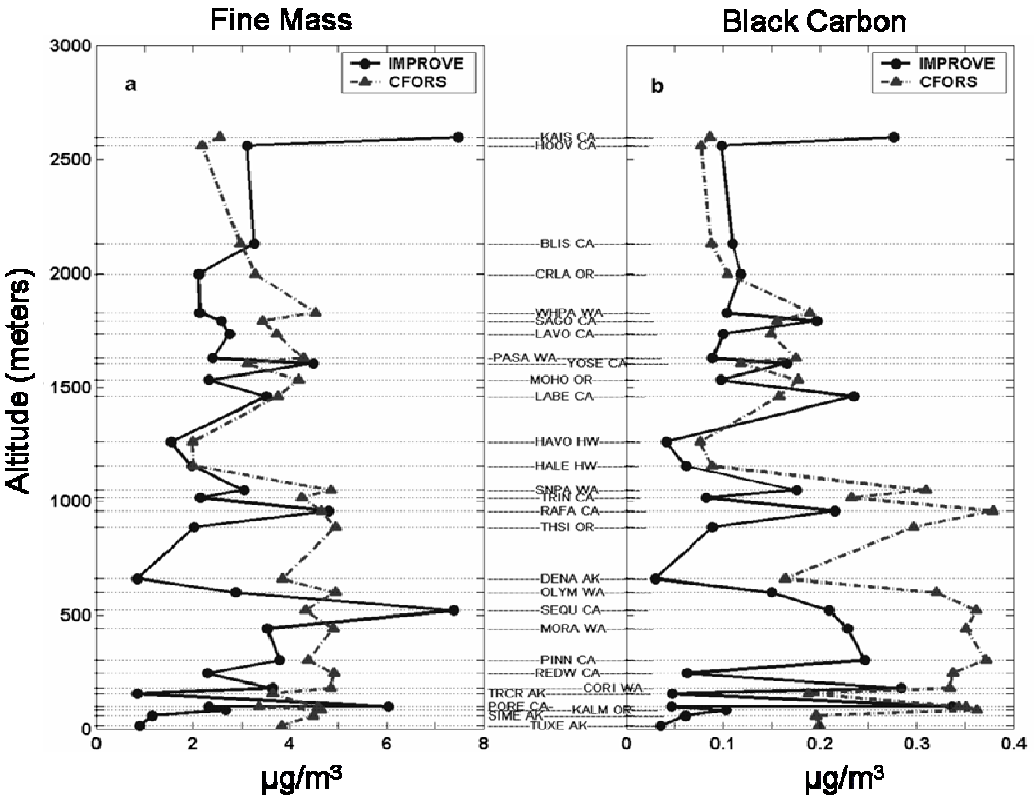

Figure 2.7. Comparison of vertical distribution of (a) CFORS and IMPROVE fine aerosol mass and (b) CFORS and IMPROVE BC. The IMPROVE fine aerosol represents the soil, organic carbon, elemental carbon, and sulfate contribution to the total aerosol mass, for comparison with the same species comprising the CFORS aerosol mass.

Soil(μgm^{-3}) is calculated using [*Eldred, et al.*, 1997]:

$$\text{Soil} = 2.20 * \text{Al} + 2.49 * \text{Si} + 1.63 * \text{Ca} + 2.42 * \text{Fe} + 1.94 * \text{Ti} . \qquad (2.1)$$

Ion chromatography is used to determine the sulfate concentration collected on fine nylon filters [*Eldred and Cahill*, 1997].

For this study the IMPROVE fine mass was calculated as the sum of the PM2.5 soil, sulfate, BC, and OC mass concentration. This corresponds to the

components summed in the CFORS model to represent total fine mass. On average these 4 species accounts for 70 (+/-10) % of the bulk, fine aerosol mass measured at each site. Other aerosol components not included in the model output and likely contributing to the observed mass are nitrates, sea salt, and the non-carbon fraction of organic mass.

Figure 2.7 compares the April 2004 averaged, vertical distribution of the CFORS output and the IMPROVE data for (a) the fine aerosol mass concentration and (b) the average black carbon mass concentration during the CIFEX campaign. The EC IMPROVE data are used as observed BC and IMPROVE soil data represents the observed fine dust. As with the CIFEX flight data comparisons, CFORS generally over predicts the fine mass at low altitudes, and is in closer agreement at higher elevations. The average percent difference of fine mass above 1000 meters is 47% compared to 155% for the lower elevations. Analogous to the fine mass comparisons, CFORS over-predicts the IMPROVE BC below 1000 meters on average by 214% while above 1000 meters the average percent difference between model and observations is 18%.

For both BC and fine mass, the largest differences between observations and the CFORS model occur below 1000 meters and decrease with altitude. The comparison between CFORS and the IMPROVE data, shown as a function of altitude is consistent with the CIFEX flight data presented in Figures 2.5 and 2.6, which show similar results in the altitude ranges of the IMPROVE sites. The best agreement between model and flight observation is above 2.5 km.

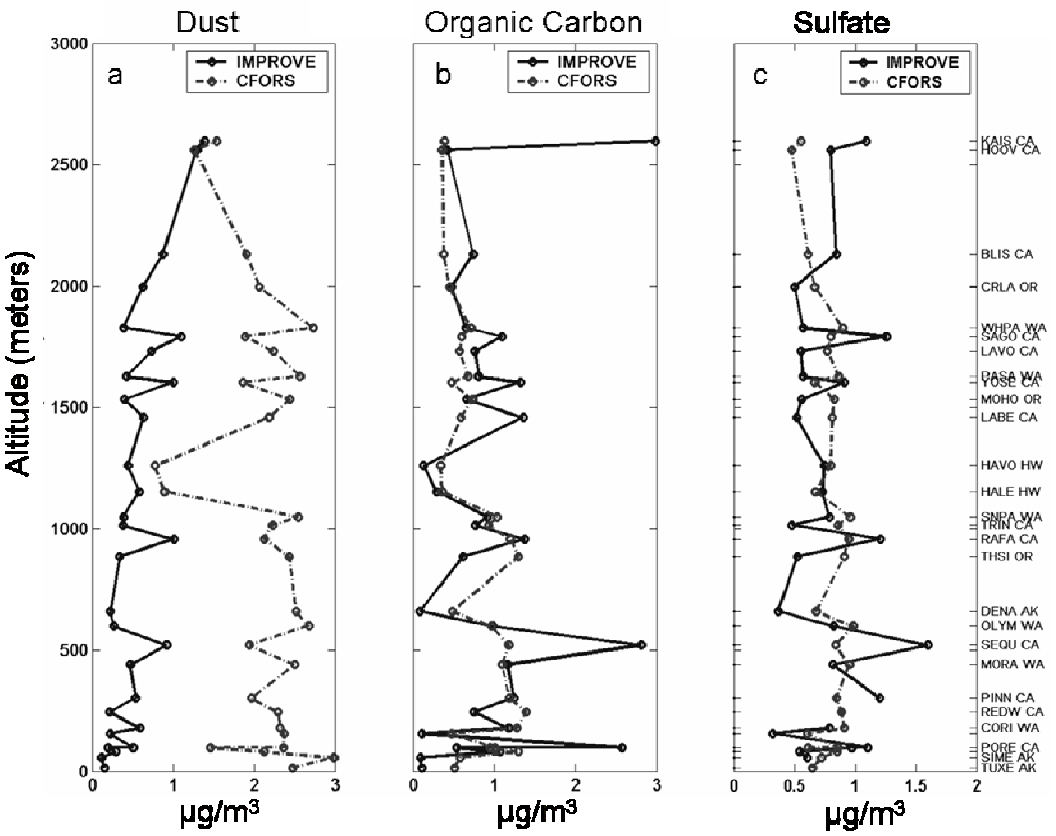

Figure 2.8. Comparison of IMPROVE and CFORS vertical distribution of (a) dust, (b) organic carbon, and (c) sulfate.

Figure 2.8 presents the IMPROVE and CFORS comparison for each of the remaining aerosol components individually: (a) fine dust/soil, (b) organic carbon, and (c) sulfate. These data clearly demonstrate that the largest discrepancy between model and observations lie in the fine dust prediction, where the only agreement coincides with the two highest elevation sites. Both organic carbon and sulfate appear to be well predicted at all elevations, with exceptions at a few sites. Above 1000 meters the average percent differences for OC, sulfate, and fine dust are respectively -13%, 8%, and 209% and 107%, 21%, and 746% below 1000 meters.

2.4.1 Factors contributing to the surface overestimation

Since the boundary layer transport represents a minor fraction of the long range transport of aerosols, we have not conducted a detailed analysis of the factors contributing to the large over estimation of BC and dust within the boundary layer, but offer the following speculations. CFORS simulated rainfall points to a potentially major factor contributing to the model deficiency in the near surface layers. Precipitation data, obtained from the NOAA NCEP CPC REGIONAL US_Mexico daily gridded archive[2], provide a means of evaluating the CFORS/RAMS precipitation output for all sites in Washington, Oregon and California. Results show that CFORS precipitation generally appears in the right place at the right time. Model and observations are correlated with an r^2 equal to 0.53 (Figure 2.9). However, the model regularly produces rain totals, which on average are only a third of the gridded rain data, and often misses a rain event entirely. A combination of inadequate wet removal parameters and insufficient precipitation throughout transport may help explain the over-prediction at low altitudes. [*Uno, et al.*, 2003] found that CFORS tended to over-predict both sulfate and EC during rain events, but that in general the model observation agreement at the surface was quite good in the Western Pacific Ocean. In addition, errors in North American dust and BC emissions likely contribute to the boundary layer over prediction observed over the west coast of North America. CFORS agreement with observations at higher altitudes compared with those at the surface show that although the model has difficulty forecasting locally generated

[2] http://ingrid.ldeo.columbia.edu/SOURCES/.NOAA/.NCEP/.CPC/.REGIONAL/.US_Mexico/.daily/.gridded/.archive/

pollutants and boundary layer processes, the predictions for long range transport of Asian aerosols and BC at high altitudes are reasonable estimates.

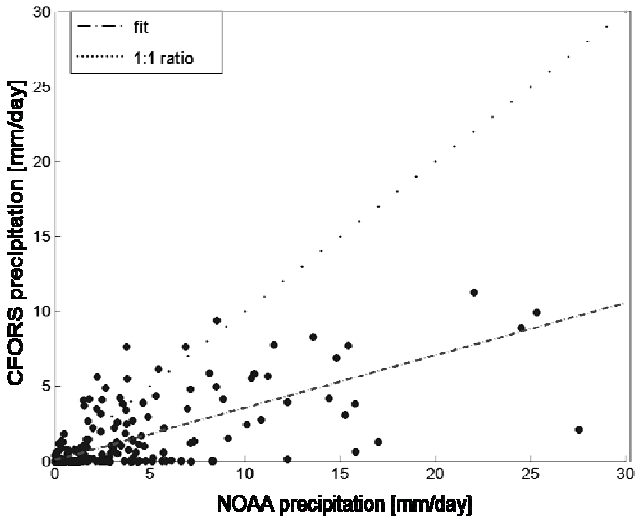

Figure 2.9. Scatter plot of CFORS precipitation vs. NOAA NCEP precipitation.

2.4.2 Asian tracers and air mass trajectories in CFORS and IMPROVE data

In the CIFEX flight regions, CFORS estimates that 78% of the BC transport above 2 km comes from Asia (Figure 2.10), with the remaining aerosol mass originating from the Arctic, (including Alaska) north of 60ºN, and recirculation from North America, south of 30ºN and Central America. CFORS isolates the Asian BC from the total BC as a separate variable using only BC emitted from Asian sources. A previous study comparing the CFORS modeled BC to observations in the Western Pacific showed that CFORS captures the continental outflow of Asian BC concentration within 25% between the surface [*Uno, et al.*, 2003] and 12000 meters [*Carmichael, et al.*, 2003]. At higher altitudes the CFORS model tended to under predict BC concentration, indicating that emission inventories used for Asian BC may

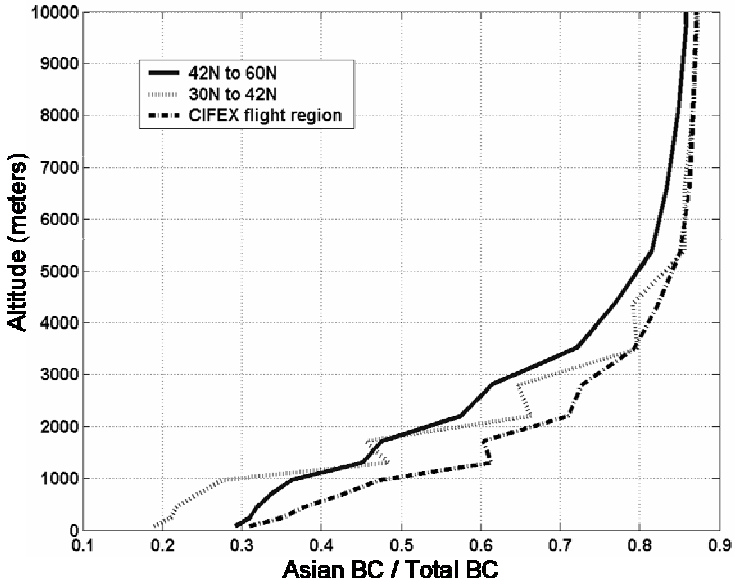

Figure 2.10. CFORS fraction of Asian BC to total BC as a function of altitude at 130ºW.

be too low [*Carmichael, et al.*, 2003].The CFORS Asian BC percentage represents the increasing Asian influence on total aerosol mass with altitude. This is consistent with analysis of the IMPROVE Pb (lead) data and the NOAA-HYSPLIT (Hybrid Single-Particle Lagrangian Integrated Trajectory) [*Draxler and Hess*, 1998] 10-day back trajectories discussed below.

A 4-year time series (2001 to 2004) of the average Pb to fine mass ratio for both high (>1600 meters) and low (<700 meters) IMPROVE sites in Washington, Oregon and California (Figure 2.11.a) displays a significant annual peak during winter and early spring at the high elevation sites, and a reduced signal and ratio at the lower elevations. The 4-year time series of absolute Pb concentration (Figure 2.11.b) indicate prominent peaks in spring and fall for both high and low elevation sites; however the springtime peaks dominate at high elevations. As Asia produces 3 times

more Pb per year than North America [*Pacyna and Pacyna*, 2001] and since both Pb concentrations in Taipei [*Hsu, et al.*, 2005] and IMPROVE Pb concentrations in Western North America are highest during the period of Asian transport, it makes a useful indicator of Asian influence on the aerosol measured at the IMPROVE sites. The Pb to fine mass ratio from the IMPROVE data correlates significantly, although not strongly, to the CFORS Asian BC fraction. The correlation coefficient is significant at 0.34. The 95% confidence limits are narrow between 0.21 and 0.45 and the probability that they are uncorrelated is $3x10^{-7}$. The correlation coefficient for the

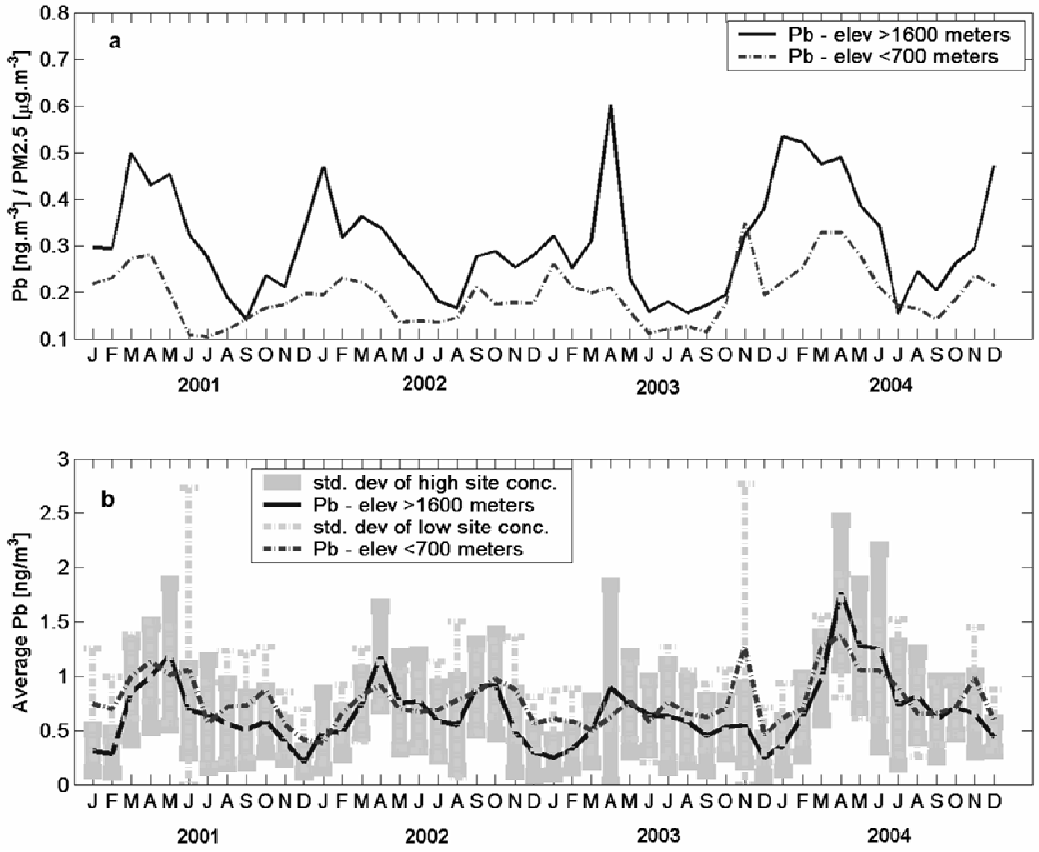

Figure 2.11. (a) 4 year time series of monthly averaged ratio of Pb to fine mass concentrations at high (>1600 meters, solid line) and low (<700 meters, dashed line) elevation IMPROVE sites in Washington, Oregon, and California and (b) a 4-year time series of the absolute monthly averaged Pb concentration at high and low elevation improve sites.

high elevation sites increases to r = 0.4 (0.16 – 0.59). The Pb ratio and Asian BC fraction are completely uncorrelated at r = 0.036 (-0.18 – 0.25) for sites below 700 meters. The correlation between Pb and EC in Hong Kong was found to be between 0.7 and 0.8 [*Zheng and Fang*, 2000]. Due to unique variability of local and Asian Pb and BC emissions, as well as errors in the CFORS boundary layer simulation, it is not surprising that the correlation is not higher. The significance, however, confirms the CFORS simulated increase in Asian BC fraction with altitude.

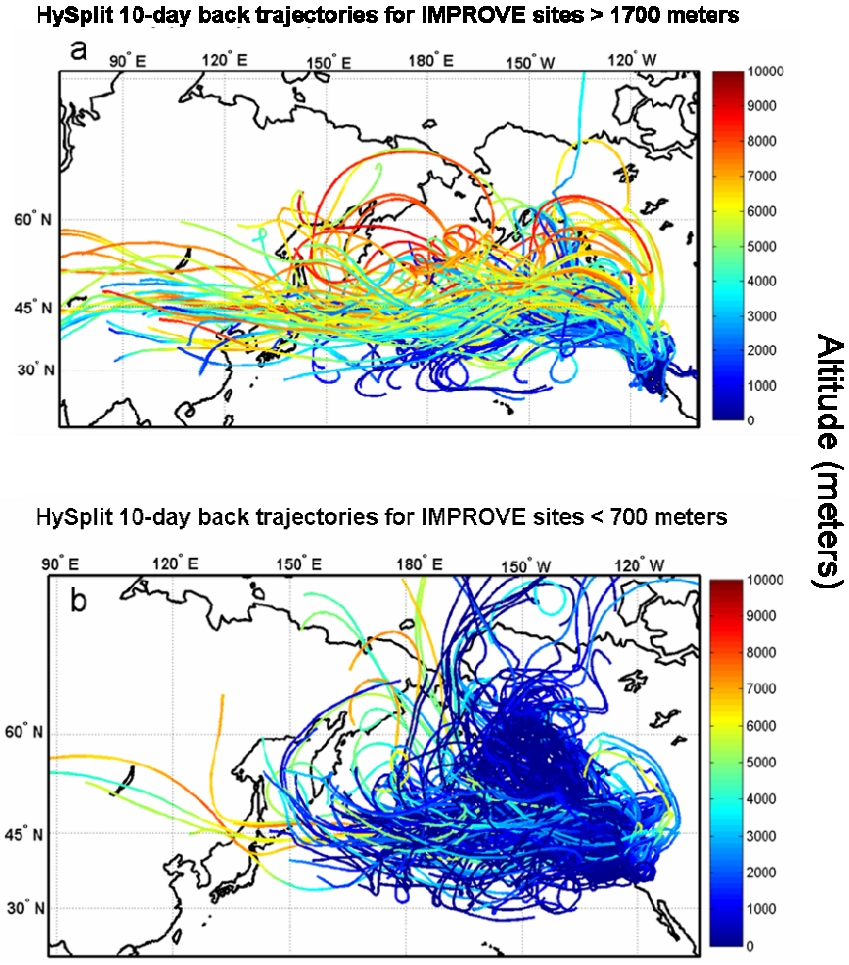

Figure 2.12. 10-day, HySplit back trajectories at (a) high (>1700 meters) elevation and (b) low (<700 meters) elevation IMPROVE sites in CA, WA, and OR.

In addition to the Pb data, a comparison of the HYSPLIT [*Draxler and Hess*, 1998] air mass 10-day back trajectories for a selection of high (>1700 meters) (Figure 2.12.a) and low (<700 meters) (Figure 2.12.b) elevation sites, coincident with the IMPROVE aerosol collection days, also indicates a more frequent and pronounced Asian influence on the air masses arriving at high elevation sites. Air masses arriving at the low elevation sites, although from the west, originate almost entirely from the Central Pacific, and the low altitudes of the trajectories point toward a predominantly marine aerosol. The back trajectories for all sites are consistent with this analysis, showing an increase in the percentage of days when air masses appear to originate in Asia or Eastern Europe as elevation increases (Figure 2.13).

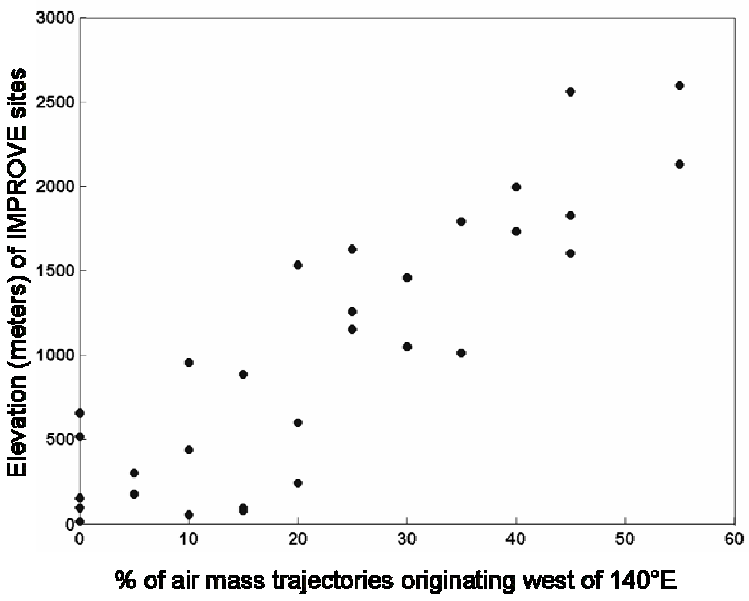

Figure 2.13. Scatter plot of IMPROVE elevation vs, percentage of air mass 10-day back trajectories with an end point west of 140ºE.

2.5 Implications to Radiation Budget and Climate

The simulated concentrations of BC between 1 and 3 km, as well as the measured BC concentrations, range from 0.1 $\mu g/m^3$ to 0.3 $\mu g/m^3$ (Figure 7(b)). Above 3 km CFORS BC exponentially decreases with altitude (Figure 2.14). Because of fast large-scale transport in the free troposphere above the boundary layer, BC and other aerosols once they enter the west coast, can be transported across North America in less than a week. There are several reasons why the transported BC can have important effects in regional radiation budget and climate.

First, BC in the atmosphere warms the atmosphere and cools the surface by absorbing incoming solar radiation and preventing it from reaching the surface. The direct radiative forcing due to the CFORS predicted BC is estimated using the Monte Carlo Aerosol-Cloud-Radiation (MACR) model developed by our group [*Podgorny, et al.*, 2000; *Podgorny and Ramanathan*, 2001; *Vogelmann, et al.*, 2001]. The BC profile applied in the MACR model simulation uses the CFORS model results above 1.5 km and assumes a well mixed boundary layer of BC below 1.5 km as shown in Figure 2.14. The vertical BC distribution corresponds to the mean April 2004 BC concentration (as predicted by CFORS) spatially averaged over a rectangle bound by 35ºN - 60ºN and 125ºW - 115ºW. To calculate the forcing due to the BC we run the radiation model first for a control case assuming purely scattering aerosol and then again after adding the CFORS BC in each atmospheric layer. Using a mass absorption efficiency of 10 m^2/g [*Hansen*, 2003], the calculated AOD (aerosol optical depth) for the BC alone is 0.007. The background AOD for the scattering aerosol is obtained by

subtracting the calculated BC AOD from the observed AOD of 0.124. The observed AOD is the mean April AOD measured at the AERONET site [*Holben, et al.*, 1998] located at Trinidad Head, CA (41.05ºN, 124.15ºW, 107 meters). The atmospheric column SSA (single scattering albedo), calculated as the purely scattering AOD divided by the observed AOD is 0.944 which compares well to SSA values obtained at AERONET sites in this region of 0.935.

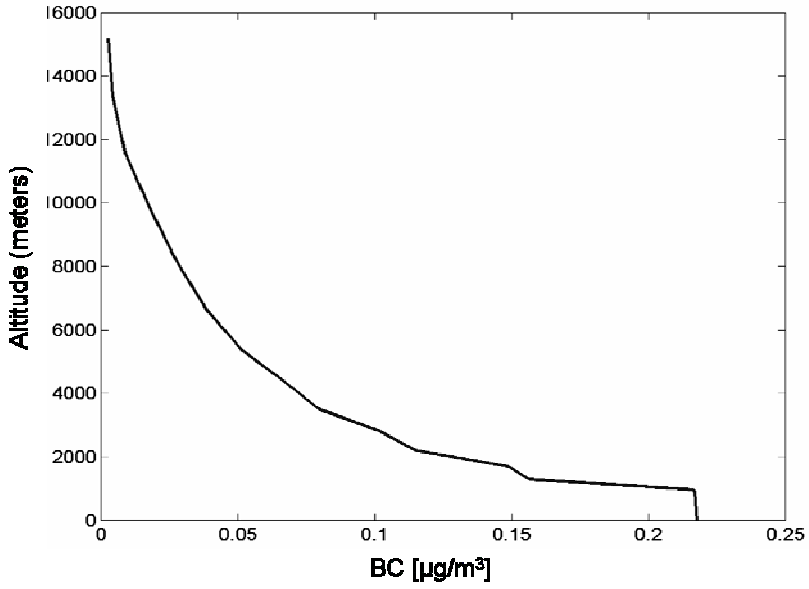

Figure 2.14. CFORS vertical profile of mean BC concentrations for April 2004, averaged over 30ºN to 60ºN and 125ºW to 115ºW. Below 1 km a well mixed boundary layer is assumed.

The calculated diurnal mean radiative forcing at TOA (top of the atmosphere), in the atmosphere, and at the surface is shown in Table 2.4. Under clear sky conditions, the forcing attributed to the BC is larger at TOA and in the atmosphere over a land surface compared to the ocean; however the surface dimming of -1.45

Wm^{-2} to -1.47 Wm^{-2} remains relatively unchanged. This reduction in solar radiation at the surface could account for 20% of the 7 Wm^{-2} dimming over the United States reported by [*Liepert and Tegen*, 2002]. The positive forcing at TOA and in the atmosphere for both cases indicates an enhancement of the greenhouse effect, while a cooling at the surface and warming in the atmosphere suggest the possibility of changes in the tropospheric lapse rate.

Inclusion of cloudy skies in the MACR model calculations decreases the magnitude of the overall forcing over both land and ocean. In the model, clouds reduce the negative surface forcing by 13%, the positive forcing in the atmosphere and at TOA by 27% and 61% respectively (Table 2.4) relative to the clear sky forcing. These calculations, however, assume BC and cloud droplets as external mixtures. If BC is internally mixed with cloud droplets (e.g, by serving as nuclei) it can enhance aerosol solar absorption (by factors of 2 to 3) and therefore enhance the surface dimming. This is because black carbon mixed with cloud drops or ice crystals have been shown to significantly enhance solar absorption [*Chylek and Hallett*, 1992; *Mikhailov, et al.*, 2006]. The effects of enhanced absorption within clouds are discussed in several papers [*Chylek and Hallett*, 1992; *Chylek, et al.*, 1984; *Conant, et al.*, 2002; *Jacobson*, 2006; *Kaufman and Koren*, 2006].

Lastly, BC and dust transported from Asia can impact upper troposphere clouds over North America through the so-called indirect effect [*Abbatt, et al.*, 2006; *Hendricks, et al.*, 2005; *Lohmann, et al.*, 2004; *Pruppacher and Klett*, 1997]. For example, using ground based lidar polarization data, [*Sassen, et al.*, 2003] indicate that

Asian aerosols influenced the formation and phase of ice clouds, leading to unusually warm cirrus ice clouds. Mid and upper troposphere clouds exert a strong greenhouse effect, in addition to increasing the planetary albedo. Particularly, over the Pacific Ocean long wave cloud forcing (i.e, greenhouse effect) is between 35 to 50 W m^{-2}, while the shortwave cloud forcing is -60 to -95 W m^{-2} [*Ramanathan, et al.*, 1989]. Thus a preferential increase in the greenhouse effect of a few W m^{-2} (e.g, due to an increase in thin cirrus cloud optical depth or life time due to increased IN) can amplify the greenhouse forcing. On the other hand, if the presence of BC with dust leads to warmer cirrus clouds, the greenhouse effect would be suppressed and the albedo effect would dominate and lead to a negative forcing.

Table 2.4. Radiative forcing in Wm^{-2} due to the CFORS modeled BC and calculated using the MACR model.

	TOA	ATM	SFC	Comments
OCEAN	0.59	2.04	-1.45	clear sky ocean (ocean diurnal mean albedo = .05)
	0.23	1.49	-1.26	Including regional mean cloud properties
LAND	1.08	2.55	-1.47	clear sky land (land albedo=0.23 from MODIS)
	0.66	1.91	-1.25	Including regional mean cloud properties

2.6 Conclusions

In summary this study points to a significant amount of Asian aerosol reaching North America during spring. Over 75% of the CFORS modeled BC transport at 130ºW originates in Asia and this transport amounts to approximately 77% of the published estimates of North American BC emissions. This finding is corroborated by results from the ITCT 2K2 campaign, which found strong evidence for long range

transport of biomass burning and fossil fuel chemical indicators [*de Gouw, et al.*, 2004], the two principal sources of BC. Ground based measurements at Trinidad Head, CA during ITCT 2K2 confirmed that Asian aerosols did reach the surface along the coast through downward mixing after passage of large frontal systems, but that on average, Asian pollution was concentrated at higher altitudes and impacted higher elevation sites year round [*VanCuren, et al.*, 2005]. [*Roberts, et al.*, 2006] observed that that the aged aerosol, characteristic of long-range transport, appeared exclusively above 2500 meters during the CIFEX flights. Comparison of CFORS to surface observations shows that the model accurately predicts concentration of BC, OC, and sulfate within 20% above 1 km. Flight data indicate that, within 3%, total fine mass is accurately simulated by CFORS above 2 km and 6.5 km. Although the CFORS comparison with the IMPROVE soil data also show agreement only above 2km, the IMPROVE sites do not reach high enough to make a proper comparison with the flight data.

Based on the comparisons of vertical profiles between the model and observations, we conclude that the CFORS predicted transport for fine mass and BC above 2 km should be a reasonable approximation to the actual transport. The estimated fine aerosol and BC transports above 2 km for the month of April 2004 are 900 Gg and 25 Gg respectively. The corresponding transports for the entire atmosphere (surface to top of the atmosphere) are 1100 Gg (fine aerosol) and 32 Gg (BC). Thus the surface to 2 km region contributes only 22% to BC transport and 20% to fine aerosol mass transport, and the poor agreement with observed concentrations of

BC and fine aerosol mass in the boundary layer should not overly impact the transport estimates. As a result we recommend the range of 25 Gg to 32 Gg for long range BC transport and 900 Gg to 1100 Gg for long range fine aerosol transport into and above North America. This black carbon transport, which includes a significant fraction from Asia, may impact regional climate over the both the Western United States and the Pacific Ocean. The MACR model shows that the BC concentration predicted by CFORS over Western North America absorbs an additional 2.04 to 2.55 W/m^2 in the atmosphere and causes a -1.45 to -1.47 W/m^2 dimming over land and ocean. Further implications of the transported BC and other Asian aerosol to regional radiation budget, cloudiness and climate should be studied.

Publication Acknowledgement

The text of Chapter 2, in full, is a reprint of a published paper, Hadley OL, Ramanathan V, Carmichael GR, , "Trans-Pacific Transport of black carbon and fine aerosols into North America" *Journal of Geophysical Research-Atm* 112 (D5): Art. No. D05309 MAR 14 2007. I was the primary researcher and author.

References

Abbatt, J., S. Benz, D. Cziczo, Z. Kanji, U. Lohmann, and O. Mohler (2006), Solid Ammonium Sulfate Aerosols as Ice Nuclei: A Pathway for Cirrus Cloud Formation, *Science*, *313*, 1770.

Bertschi, I. T., and D. A. Jaffe (2005), Long-range transport of ozone, carbon monoxide, and aerosols to the NE Pacific troposphere during the summer of 2003: Observations of smoke plumes from Asian boreal fires, *J Geophys Res-Atmos*, *110*, -.

Bey, I., D. J. Jacob, J. A. Logan, and R. M. Yantosca (2001), Asian chemical outflow to the Pacific in spring: Origins, pathways, and budgets, *J Geophys Res-Atmos*, *106*, 23097-23113.

Bond, T. C., D. G. Streets, K. F. Yarber, S. M. Nelson, J. H. Woo, and Z. Klimont (2004), A technology-based global inventory of black and organic carbon emissions from combustion, *J Geophys Res-Atmos*, *109*, D14203.

Carmichael, G. R., et al. (2003), Evaluating regional emission estimates using the TRACE-P observations, *J Geophys Res-Atmos*, *108*, -.

Chow, J. C., J. G. Watson, L. W. A. Chen, W. P. Arnott, and H. Moosmuller (2004), Equivalence of elemental carbon by thermal/optical reflectance and transmittance with different temperature protocols, *Environ Sci Technol*, *38*, 4414-4422.

Chylek, P., and J. Hallett (1992), Enhanced Absorption of Solar-Radiation by Cloud Droplets Containing Soot Particles in Their Surface, *Q J Roy Meteor Soc*, *118*, 167-172.

Chylek, P., V. Ramaswamy, and R. J. Cheng (1984), Effect of Graphitic Carbon on the Albedo of Clouds, *J Atmos Sci*, *41*, 3076-3084.

Conant, W. C., A. Nenes, and J. H. Seinfeld (2002), Black carbon radiative heating effects on cloud microphysics and implications for the aerosol indirect effect - 1. Extended Kohler theory, *J Geophys Res-Atmos*, *107*, -.

de Gouw, J. A., et al. (2004), Chemical composition of air masses transported from Asia to the U. S. West Coast during ITCT 2K2: Fossil fuel combustion versus biomass-burning signatures, *J Geophys Res*, *109*, D23S20.

Draxler, R. R., and G. D. Hess (1998), An overview of the HYSPLIT_4 modeling system for trajectories, dispersion, and deposition, *Australian Meteorological Magazine*, *47*, 295-308.

Eldred, R. A., and T. A. Cahill (1997), Sulfate sampling artifact from SO2 and alkaline soil, *Environ Sci Technol*, *31*, 1320-1324.

Eldred, R. A., T. A. Cahill, and R. G. Flocchini (1997), Composition of PM(2.5) and PM(10) aerosols in the IMPROVE network, *J Air Waste Manage*, *47*, 194-203.

Goldstein, A. H., et al. (2004), Impact of Asian emissions on observations at Trinidad Head, California, during ITCT 2K2, *J Geophys Res*, *109*, D23S17.

Hansen, A. D. A. (2003), *The Aethalometer*, Magee Scientific Company, Berkely CA.

Heald, C. L., D. J. Jacob, R. J. Park, B. Alexander, T. D. Fairlie, R. M. Yantosca, and D. A. Chu (2006), Transpacific transport of Asian anthropogenic aerosols and its impact on surface air quality in the United States, *J Geophys Res-Atmos*, *111*, -.

Hendricks, J., B. Karcher, U. Lohmann, and M. Ponater (2005), Do aircraft black carbon emissions affect cirrus clouds on the global scale? *Geophys Res Lett*, *32*, -.

Holben, B. N., et al. (1998), AERONET - A federated instrument network and data archive for aerosol characterization, *Remote Sens Environ*, *66*, 1-16.

Hsu, S. C., S. C. Liu, W. L. Jeng, F. J. Lin, Y. T. Huang, S. C. C. Lung, T. H. Liu, and J. Y. Tu (2005), Variations of Cd/Pb and Zn/Pb ratios in Taipei aerosols reflecting long-range transport or local pollution emissions, *Sci Total Environ*, *347*, 111-121.

Jacob, D. J., et al. (2003), Transport and Chemical Evolution over the Pacific (TRACE-P) aircraft mission: Design, execution, and first results, *J Geophys Res-Atmos*, *108*, 1-19.

Jacobson, M. Z. (2006), Effects of externally-through-internally-mixed soot inclusions within clouds and precipitation on global climate, *J Phys Chem A*, *110*, 6860-6873.

Jaffe, D., S. Tamura, and J. Harris (2005), Seasonal cycle and composition of background fine particles along the west coast of the US, *Atmos Environ*, *39*, 297-306.

Kaufman, Y. J., and I. Koren (2006), Smoke and pollution aerosol effect on cloud cover, *Science*, *313*, 655-658.

Liang, Q., L. Jaegle, D. A. Jaffe, P. Weiss-Penzias, A. Heckman, and J. A. Snow (2004), Long-range transport of Asian pollution to the northeast Pacific: Seasonal variations and transport pathways of carbon monoxide, *J Geophys Res-Atmos*, *109*, -.

Liepert, B., and I. Tegen (2002), Multidecadal solar radiation trends in the United States and Germany and direct tropospheric aerosol forcing, *J Geophys Res-Atmos*, *107*, -.

Liu, H. Y., D. J. Jacob, I. Bey, R. M. Yantosca, B. N. Duncan, and G. W. Sachse (2003), Transport pathways for Asian pollution outflow over the Pacific: Interannual and seasonal variations, *J Geophys Res-Atmos*, *108*, -.

Liu, Y. G., and P. H. Daum (2000), The effect of refractive index on size distributions and light scattering coefficients derived from optical particle counters, *J Aerosol Sci*, *31*, 945-957.

Lohmann, U., B. Karcher, and J. Hendricks (2004), Sensitivity studies of cirrus clouds formed by heterogeneous freezing in the ECHAM GCM, *J Geophys Res-Atmos*, *109*, -.

Mikhailov, E. F., S. S. Vlasenko, I. A. Podgorny, V. Ramanathan, and C. E. Corrigan (2006), Optical properties of soot-water drop agglomerates: An experimental study, *J Geophys Res-Atmos*, *111*, -.

Pacyna, J., and E. Pacyna (2001), An assessment of global and regional emissions of trace metals to the atmosphere from anthropogenic sources worldwide, *Environmental Reviews*, *9*, 269-298.

Park, R. J., et al. (2005), Export efficiency of black carbon aerosol in continental outflow: Global implications, *J Geophys Res-Atmos*, *110*, -.

Parrish, D. D., Y. Kondo, O. R. Cooper, C. A. Brock, D. A. Jaffe, M. Trainer, T. Ogawa, G. Hubler, and F. C. Fehsenfeld (2004), Intercontinental Transport and Chemical Transformation 2002 (ITCT 2K2) and Pacific Exploration of Asian Continental Emission (PEACE) experiments: An overview of the 2002 winter and spring intensives, *J Geophys Res-Atmos*, *109*, -.

Podgorny, I. A., W. Conant, V. Ramanathan, and S. K. Satheesh (2000), Aerosol modulation of atmospheric and surface solar heating over the tropical Indian Ocean, *Tellus B*, *52*, 947-958.

Podgorny, I. A., and V. Ramanathan (2001), A modeling study of the direct effect of aerosols over the tropical Indian Ocean, *J Geophys Res-Atmos*, *106*, 24097-24105.

Pruppacher, H. R., and J. D. Klett (1997), *Microphysics of Clouds and Precipitation*, 2nd ed., 954 pp., Kluwer Academic Publishers.

Ramanathan, V., B. R. Barkstrom, and E. F. Harrison (1989), Climate and the Earths Radiation Budget, *Phys Today*, *42*, 22-32.

Roberts, G., G. Mauger, O. Hadley, and V. Ramanathan (2006), North American and Asian aerosols over the eastern Pacific Ocean and their role in regulating cloud condensation nuclei, *J Geophys Res-Atmos*, *111*, -.

Sassen, K., P. J. DeMott, J. M. Prospero, and M. R. Poellot (2003), Saharan dust storms and indirect aerosol effects on clouds: CRYSTAL-FACE results, *Geophys Res Lett*, *30*, -.

Seinfeld, J. H., et al. (2004), ACE-ASIA - Regional climatic and atmospheric chemical effects of Asian dust and pollution, *B Am Meteorol Soc*, *85*, 367-+.

Stohl, A. (2001), A 1-year Lagrangian "climatology" of airstreams in the Northern Hemisphere troposphere and lowermost stratosphere, *J Geophys Res-Atmos*, *106*, 7263-7279.

Stolzenburg, M., N. Kreisberg, and S. Hering (1998), Atmospheric size distributions measured by differential mobility optical particle size spectrometry, *Aerosol Sci Tech*, *29*, 402-418.

Streets, D. G., et al. (2003), An inventory of gaseous and primary aerosol emissions in Asia in the year 2000, *J Geophys Res-Atmos*, *108*, 8809.

Tanre, D., Y. J. Kaufman, M. Herman, and S. Mattoo (1997), Remote sensing of aerosol properties over oceans using the MODIS/EOS spectral radiances, *J Geophys Res-Atmos*, *102*, 16971-16988.

Uno, I., et al. (2003), Regional chemical weather forecasting system CFORS: Model descriptions and analysis of surface observations at Japanese island stations during the ACE-Asia experiment, *J Geophys Res*, *108*, 8668.

VanCuren, R. A., and T. A. Cahill (2002), Asian aerosols in North America: Frequency and concentration of fine dust, *J Geophys Res-Atmos*, *107*, -.

VanCuren, R. A., S. S. Cliff, K. D. Perry, and M. Jimenez-Cruz (2005), Asian continental aerosol persistence above the marine boundary layer over the eastern North Pacific: Continuous aerosol measurements from Intercontinental Transport and Chemical Transformation 2002 (ITCT 2K2), *J Geophys Res*, *110*, D09S90.

Vogelmann, A. M., V. Ramanathan, and I. A. Podgorny (2001), Scale dependence of solar heating rates in convective cloud systems with implications to general circulation models, *J Climate*, *14*, 1738-1752.

Wittmaack, K. (2002), Advanced evaluation of size-differential distributions of aerosol particles, *J Aerosol Sci*, *33*, 1009-1025.

Yienger, J. J., M. Galanter, T. A. Holloway, M. J. Phadnis, S. K. Guttikunda, G. R. Carmichael, W. J. Moxim, and H. Levy (2000), The episodic nature of air pollution transport from Asia to North America, *J Geophys Res-Atmos*, *105*, 26931-26945.

Zheng, M., and M. Fang (2000), Correlations between organic and inorganic species in atmospheric aerosols, *Environ Sci Technol*, *34*, 2721-2726.

Chapter 3

Laboratory Development of a Modified Thermal-Optical Analysis Using Spectral Absorption Selectivity to Distinguish Black Carbon from Char in Filtered Precipitation Samples

3.1 Introduction

The results presented in Chapter 2 indicate that a significant mass of BC is transported to the Western United States during March and April. Furthermore, high elevation sites (>1700 meters) are most significantly impacted by these transport events and it is in these high elevations where a significant percentage of California's fresh water supply is stored in the mountain snow packs. Both field and modeling studies have shown that BC deposited onto snow and ice decreases the albedo of the surface and leads to faster melting of glaciers, polar ice, and mountain snow packs [*Chylek, et al.*, 1983; *Clarke and Noone*, 1985; *Conway, et al.*, 1996; *Flanner, et al.*, 2007; *Hansen and Nazarenko*, 2004; *Jacobson*, 2004; *Painter, et al.*, 2007; *Warren and Wiscombe*, 1980]. In order to understand the potential significance of the transported BC on California's snow pack, falling snow was collected and analyzed for BC concentration in two locations in the Sierra Nevada Mountains, as well as on the California coast, during the SUPRECIP II field experiment in February – April 2006. This chapter describes the method by which the rain and snow samples were filtered and analyzed for BC concentration. Results from this field study are discussed in Chapters 4 and 5.

Measuring BC concentration is challenging and often hampered by high uncertainties [*Arnott, et al.*, 2005; *Bond and Bergstrom*, 2006; *Chow, et al.*, 2001]. Analyzing BC filtered from water samples presented additional challenges, which included evaluating the filtration efficiency and accounting for increased interferences from organic carbon (OC) concentrated in the precipitation. This chapter outlines the laboratory methods used to evaluate and analyze filtered precipitation samples for BC concentration. This method includes modifications to a thermo-optical analysis (TOA) method that is often used to quantify BC collected on filters [*Kirchstetter and Novakov*, 2007; *Novakov and Corrigan*, 1995], but one that is also subject to significant artifacts from organics present in the sample that pyrolize or char during thermal analysis. The distinctive spectral absorption properties of BC and these charred organics were used to distinguish the BC mass on the filter. This analysis method was developed specifically to analyze these filtered precipitation samples, where the charred organic mass dominated the BC signal during TOA. This method is useful for any BC samples where pyrolysis of organics is a problem.

3.2 Laboratory evaluation of sample filtration

Prior to analyzing the samples, an evaluation of the filtration efficiency had to be completed. In order to do this, a laboratory standard of a known amount of soot suspended in water was needed. Following is a description of the BC standard preparation, filtration efficiency evaluation, and final modifications to the thermo-

optical analysis to account for organic and dust interference in field samples compared to the laboratory standard.

3.2.1 Preparing the laboratory standard

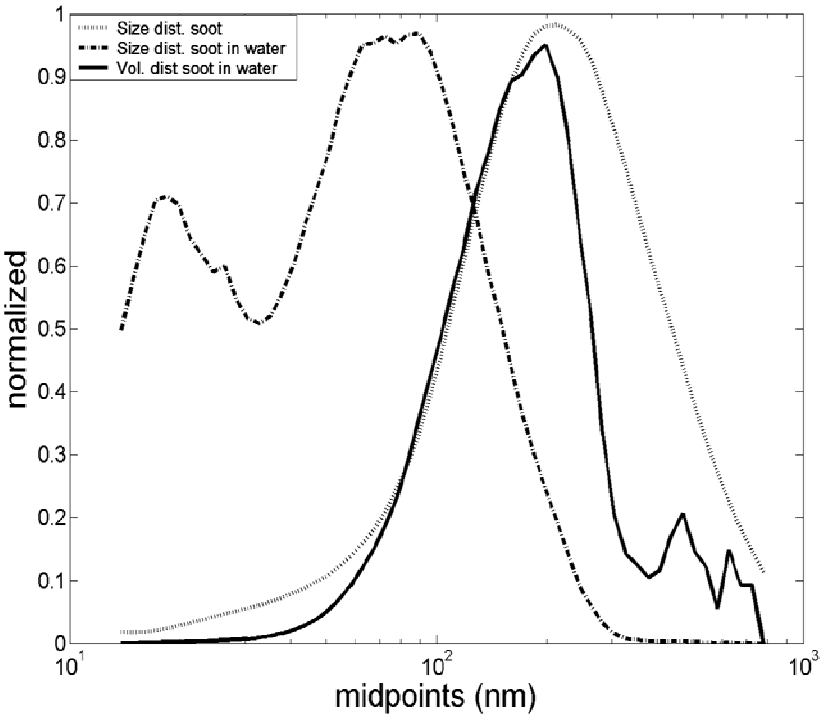

Figure 3.1. Size and volume distribution of laboratory generated soot.

The BC standard was prepared with soot generated from an inverted methane flame that produces nearly pure EGC particles with a log normal size distribution around 0.2 μm (Figure 3.1) and negligible organic interference [*Kirchstetter and Novakov*, 2007]. The soot collected for one hour on a 47 mm Teflon membrane filter. Immediately after collection, the soot was exposed for 15 minutes to ozone concentration in excess of 2.9×10^4 PPM. Without exposure to the ozone, the fresh

and extremely hydrophobic soot did not go into the water, but instead formed small tar balls at the surface. Studies have shown that fresh BC or soot only becomes wettable or hydrophilic after exposure to atmospheric oxidants of which ozone is one example [*Chughtai, et al.*, 1996; *Zuberi, et al.*, 2005]. Ozone oxidation of the soot crudely simulated aging of atmospheric BC before incorporation into precipitation, and served as a surrogate for chemical processing of the soot in actual field samples. This brief exposure to such a high concentration of ozone probably exceeded the extent of oxidation experienced by BC particles in the environment, but ensured that the soot particles mixed well in the water and thus functioned as a proper calibration standard.

After ozone exposure, the filter was placed under a polonium static eliminator bar to remove the static charge from the soot and prevent soot particles from flying off the weighing boat and out of the beaker. The soot was then scraped from the filter and weighed with a micro balance accurate to 10 μg. Standards were made by mixing soot masses between 0.5 and 1 mg with 100 mL of distilled water and sonicating until all of the soot was suspended and produced a uniform light grey solution. The duration of ozone exposure appeared to affect how readily the soot went into solution.

The size and volume distributions of the soot particles in solution were determined by nebulizing an extremely high concentration of this solution, approximately 10 μg mL^{-1}, with nitrogen gas and mixing with dry air to evaporate the solution droplets and re-form the soot particles, which were then passed through a DMA (Differential Mobility Analyzer) and CPC (Condensation Particle Counter). The number and volume ie mass distributions for soot in solution are shown in Figure 3.1.

Increases in ozone exposure appeared to shift the log normal number distribution from 0.1 to 0.08 μm, however shifts in the mass distribution were negligible. The log normal mass distribution centers at 0.2 microns, typical for aged BC in the atmosphere [*Clarke and Noone*, 1985; *Clarke, et al.*, 2004].

3.2.2. Filtration

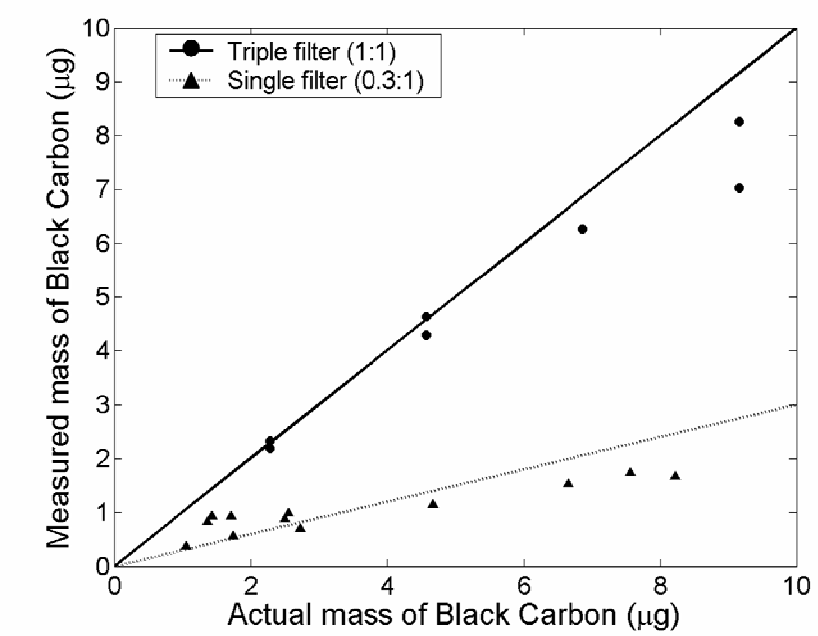

Figure 3.2 Filter efficiency test for single vs. triple filter efficiency

Consistent with previously measured concentrations of BC in precipitation [*Chylek, et al.*, 1999; *Clarke and Noone*, 1985; *Ducret and Cachier*, 1992], the standard was diluted into 200 mL samples ranging in soot concentrations from 11.45 μg L^{-1} to 45.8 μg L^{-1}. These concentrations resulted in total filter loadings ranging from 2.29 μg to 9.16 μg. A vacuum pump pulled the solution through a series of three, in-line, quartz fiber, 13mm filters, followed with a methanol rinse. Prior testing

showed that the methanol did not affect the mass of BC retained on the filters, but removed water and some organic residues from the loaded filter. Initial filter evaluation tests using only a single filter showed that the filtration efficiency decreased from 60% at low mass loadings (<3 μg) to less than 30% as the BC loading on the filter increased (Figure 3.2). BC mass recovery using 3 filters also showed a slight drop off as filter loading reached maximum values, however even at the highest loading (9 μg), 90% total recovery was observed (Figure 3.2). The average mass recovery for all concentrations was 92(±7) %, with the efficiency of the front filter increased by a factor of 2.5 relative to the single filter. The greater resistance, created by the additional filters, lowered the flow rate of the fluid through the front filter. Since small particle capture efficiency on a fibrous medium is controlled by colloidal force interactions between the particles and the filter fibers (ie London-van der Wahl, electrostatic, hydrophobic, steric, and hydration forces) [*Li and Park*, 1999], and force strength varies with proximity of the particles to the filter fibers, the longer contact time between the particles and the filter fibers, due to low flow velocity, increased removal efficiency by allowing more time for particles to diffuse to the collectors or fibers. Particle capture efficiency is proportional to K/U, where K is the particle to filter deposition rate and U is the flow velocity through the filter [*Li and Park*, 1999; *Spielman*, 1977]. Although a low flow rate could be used for the single filter set-up, additional BC capture on the second and third filters increased recovery by another 15 to 20%, and helped verify minimal losses through the first filter. On average the

amount of soot lost to surfaces or not captured by the filters during laboratory testing was less then 8%.

3.3 Measuring Black Carbon using Thermal-Optical Analysis

This section describes basic analysis methods for measuring BC and then discusses the modifications that were made to analyze the precipitation samples filtered using the procedure described in 3.2. The most commonly used methods for measuring atmospheric BC concentration involve optical or a combination of thermal and optical characterization of aerosol samples collected on filters. These methods are imperfect, in part due to the non-standardized definition of BC. Method inter-comparisons, for example, yield BC estimates that can differ by as much as a factor of 7 [*Currie, et al.*, 2002; *Watson, et al.*, 2005]. A brief description of BC measurement strategies is included below, although detailed reviews of techniques used to measure BC in aerosols may be found elsewhere [*Bond and Bergstrom*, 2006; *Chow, et al.*, 2004].

Filter-based optical methods determine the mass of BC on the filter from measured light absorption, or attenuation, using a modification of the Beer-Lambert law [*Weingartner, et al.*, 2003]:

$$BC = \frac{ATN * A}{MAE} \qquad (3.1)$$

In this application concentration times path length is redefined as mass of BC on the filter divided by the sample area on the filter (A). Molar absorptivity is converted to mass attenuation (absorption) efficiency (MAE) and has units of m^2g^{-1}. For filter based

measurements attenuation rather than absorption is often used because actual light absorption is enhanced due to multiple scattering by the filter [*Bond and Bergstrom*, 2006].

Experimentally determined values of MAE are influenced by several factors. The filter used to collect the BC particles can have the most significant impact. For example, a highly reflective quartz fiber filter, like that in the widely-used aethalometer [*Hansen*, 2003], scatters light to the particles and enhances approximately two-fold the amount of light absorbed by BC compared to that absorbed by the same mass of BC suspended in air [*Bodhaine*, 1995; *Weingartner, et al.*, 2003]. Thus, the distinction between the mass attenuation efficiency (MAE) of filter-bound BC and the mass specific *absorption cross-section* of atmospheric BC is important. Light-scattered away from the detector by non-absorbing particles can also lead to overestimation of the MAE [*Arnott, et al.*, 2005], whereas the apparent MAE may decrease as the filter loading of BC increases [*Kirchstetter and Novakov*, 2007]. The size and mixing state of BC particles influence the MAE of both filter-bound and atmospheric particles [*Bond and Bergstrom*, 2006; *Kirchstetter, et al.*, 2004; *Liousse, et al.*, 1993]. After applying corrections for filter-induced artifacts, the published range of MAE values for BC in air at 550 nm is 5 to 14 m^2g^{-1}, with a central value of 7.5+1.2 m^2g^{-1} [*Bond and Bergstrom*, 2006; *Liousse, et al.*, 1993]. For BC on a quartz fiber filter, an enhancement factor of 2 yields a range of MAE values of approximately 10 to 20 m^2g^{-1}.

The thermal-optical analysis (TOA) of carbonaceous particles provides a measure of the total carbon (TC) in the sample and an estimate of how much is organic carbon (OC) versus elemental carbon (EC) [*Chow, et al.*, 2004]. In most TOA methods, the sample is heated sequentially in inert (He) and oxidative (He/O_2 mixture) atmospheres, respectively, to volatilize and combust the sample carbon. Evolved carbonaceous material is oxidized to CO_2 or reduced to methane and quantified. Nominally, the carbon evolved during heating in the inert atmosphere is OC whereas the carbon evolved during heating in the oxidative atmosphere is EC. The challenge in TOA lies in differentiating the OC and EC. Early combustion of EC in the inert-phase and the formation of char (EC-like material that is refractory and light-absorbing) due to pyrolysis of OC can lead to large errors in the estimation of EC. Optical characterization of the sample either by measured transmission or reflectance of laser light is intended to monitor and correct for these sources of error. Several variations of TOA exist [*Chow, et al.*, 2004; *Lavanchy, et al.*, 1999; *Petzold and Niessner*, 1995], including the one employed in this study [*Kirchstetter, et al.*, 2004]. In this TOA method, the sample is heated in O_2 only (i.e, there is no inert phase) and light-transmission is used to distinguish between OC and BC. The light-absorbing, refractory carbon is referred to as BC instead of EC because optical absorbance, rather than the oxidative potential of the air in the sample chamber, is the primary indicator of carbon type. A new variation on the TOA method is the optical characterization of the sample over a broad spectral region, as opposed to at a single wavelength, in an attempt to improve the distinction between OC and BC.

3.3.1 Modifications to Thermo-optical analysis

Modifications were made to an existing TOA method (Figure 3.3) for the purpose of determining BC content on Tissuequartz fiber filters. The new method used in this study included broadband optical characterization of samples as they were heated during TOA. Differences in the spectral properties between BC and organic char were used to separate the absorption due to BC from that due to the char. Light transmission, from a white light emitting diode, over a spectral range of 400 to 900 nm wavelengths was measured with an Ocean Optics (model S2000) spectrometer. For this analysis, optical properties of the sample laden filter, combined with direct measurements of thermally evolved carbon, are used to determine the BC mass on the filter.

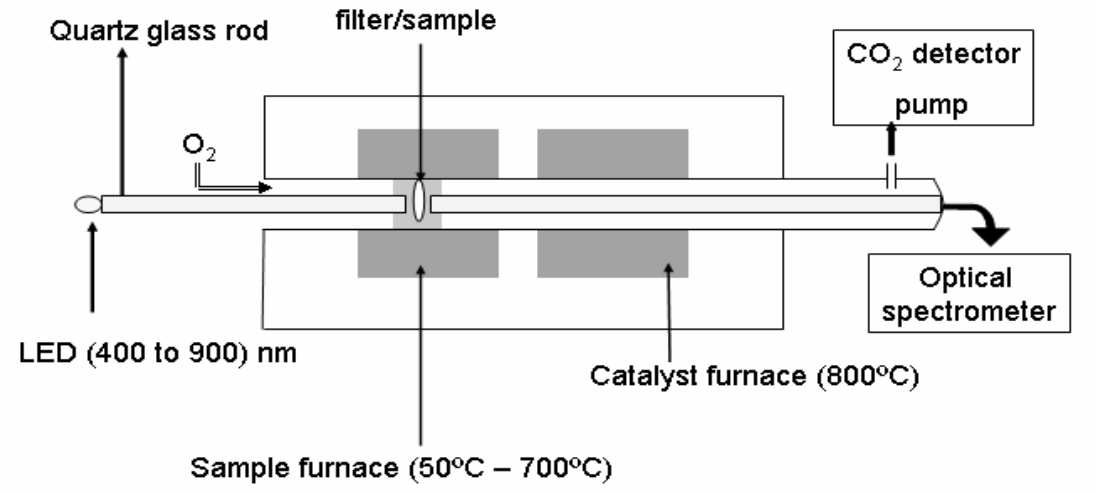

Figure 3.3. Block diagram of the thermal-optical analyzer.

The carbon mass (C_{mass}) removed from the filter as a function of temperature increase was computed directly by summing the concentrations of evolved carbon

atoms, calculated from measured moles of CO_2 per mole of O_2 (calculated from the oxygen carrier gas flow rate (0.2 L min^{-1})) and the sample temperature ramp rate (40º min^{-1}). The equation used to calculate C_{mass} is given in the Appendix A, equation A.1. The sampling interval was 1ºC over the analysis range 50ºC to 700ºC) [*Kirchstetter and Novakov*, 2007]. Plotting TC as a function of temperature yields the carbon thermogram (Figures 3.4 & 3.5, solid line). The peaks correspond to different forms of carbon evolving at different temperatures. Prior work suggests that most OC evolves between 50ºC and 450ºC, while BC generally evolves at temperatures between 400ºC and 700ºC [*Novakov and Corrigan*, 1995]. Estimating BC and OC solely on the basis of evolution temperature, however, is error-prone because the char formed from

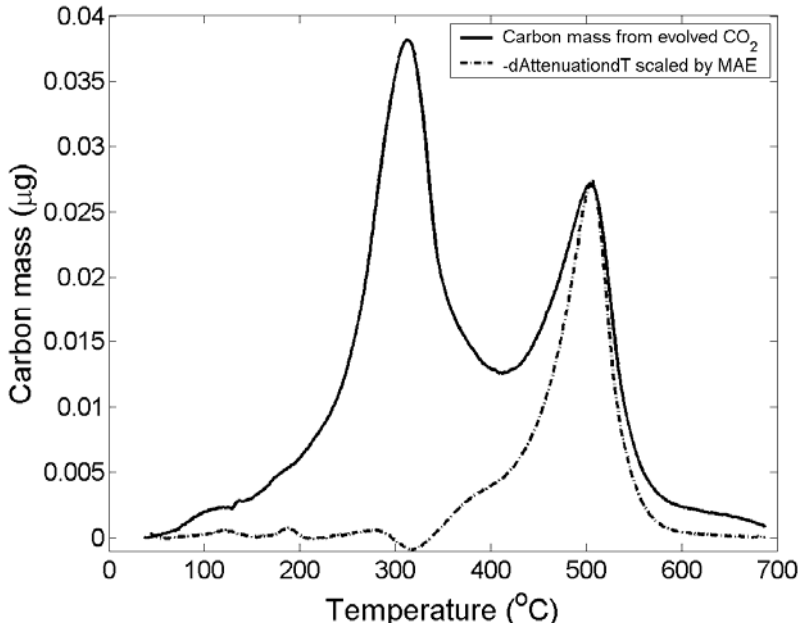

Figure 3.4. From laboratory standard, soot peak with organics. Change in attenuation is scaled to match the carbon (soot) peak at 500ºC.

pyrolyzed OC may co-evolve with the BC. In addition, BC may combust at lower temperatures if catalytic materials are present in the sample [*Mikhailov, et al.*, 2006; *Novakov and Corrigan*, 1995], thereby shifting the BC further into the region of the thermogram dominated by the OC.

Simultaneously measured changes in light attenuation (ATN) by the filter indicate the addition or removal of optically active carbon. ATN (T) is determined from the transmittance of light through the filter as:

$$ATN(T) = -\ln\left[\frac{I_s(T)}{I_o} * \frac{I_o}{I_r}\right] \qquad (3.2)$$

[*Kirchstetter, et al.*, 2004; *Weingartner, et al.*, 2003], where I_o is the intensity of light incident on the filter, $I_s(T)$ is the intensity of light measured on the other side of the loaded filter and is a function of temperature as light absorbing carbon is added and removed from the filter. I_r is the light intensity measured at T=700ºC, when all light absorbing carbon has been removed from the filter. A plot of the variation in ATN (i.e, the derivative of ATN with respect to temperature) versus temperature yields the optical thermogram (Figures 3.4 & 3.5, dashed line). When char formation is minimal and the sample does not darken during analysis (as evidenced by little or no decrease below baseline in the optical thermogram), the black carbon and ATN thermogram peaks overlap (Figure 3.4) and the optical thermogram can be used to estimate the BC content of the sample. Figure 3.4 shows carbon and optical thermograms for a sample of particles generated with the laboratory diffusion flame [*Kirchstetter and Novakov*,

2007], where the optical thermogram is scaled to the height of the carbon thermogram. The scaling factor is the MAE of the BC and it varies with sample.

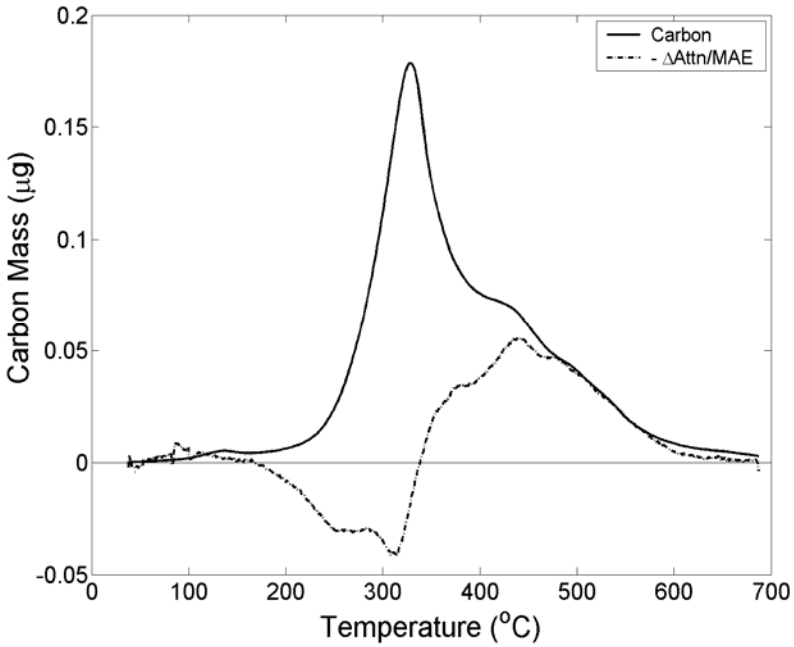

Figure 3.5. Carbon thermogram and attenuationl from a field sample of snow melt water. Change in attenuation is multiplied by -1 and scaled to match carbon mass. The scaling factor is the MAE of both the charred OC and the BC. Charred OC obscures the BC signal

For many atmospheric samples, the left side of the BC thermogram peak may be obscured by co-evolving carbonaceous material, such as refractory organics or char formed by pyrolysis of organics during analysis (Figure 3.5). When this occurs, it is unclear which region of the carbon thermogram to integrate for BC mass. Integrating the carbon thermogram after the attenuation (that initially increased due to charring organics) returns to its original value over-estimates the amount of BC in the sample. This is because a small amount of BC may evolve before attenuation returns to its initial value. As the measured MAE for char was typically much smaller than the

MAE than BC, the BC removal will have a much greater affect on reducing attenuation than the same amount of char. After attenuation returns to initial values, a significant mass of char still residing on the filter will be interpreted as BC in the thermogram. Spectral-optical characterization of the sample can be used to aid in the distinction between BC and co-evolving char, as described below.

3.3.2. Separating Pyrolyzed (charred) Organic Carbon from Black Carbon

The dependence of absorption, or in this case, attenuation, on wavelengths, λ, is often expressed as a power law [*Bergstrom, et al.*, 2007; *Kirchstetter, et al.*, 2004]:

$$ATN(\lambda) = c\lambda^{-k} \qquad (3.3)$$

where k is the absorption angstrom exponent (AAE) and c is the attenuation coefficient. Differences in the AAE values for pure BC, pure char and the mixture of BC and char allowed the relative contributions of BC and char to the light attenuation on the filter to be determined throughout thermal processing. Direct measurements of thermally evolved CO_2 were used to determine the MAE for both BC and char, as well as provide the uncertainty in the calculated mass of BC. A more complete description of the process and subsequent error analysis follows.

The transmitted intensity of light ($500<\lambda<600$ nm) through a sample filter was continuously monitored throughout thermal evolution. This spectral region was not extended to longer or shorter wavelengths due to insufficient LED output below 480 nm and contamination of the light signal from the furnace heat at wavelengths greater than 600 nm for temperatures greater than 500ºC. Char typically began forming at

T=200ºC. As the amount of char increased on the filter, light attenuation also increased (Figure 3.5), as did the spectral dependence of absorption or measured AAE value (Figure 3.6). The total amount of light attenuated by the char and BC on the filter may be approximated as the sum of the attenuation due to the pure BC and that due to the char. Thus equation 3.3 may be rewritten as:

$$ATN(\lambda,T) = c_1(T)\lambda^{-k_{BC}} + c_2(T)\lambda^{-k_{char}} \approx c(T)\lambda^{-k_m}, \text{ for } 500\text{nm} \le \lambda \le 600\text{nm} \qquad (3.4)$$

As the sum of two exponentials does not follow a simple power law, equation 3.4 is an approximation that is valid only over the specified region of the spectrum as shown by the shaded gray area in Figure 3.4. $\mathbf{k_{BC}}$, $\mathbf{k_{char}}$, and $\mathbf{k_m}$ are respectively, the absorption

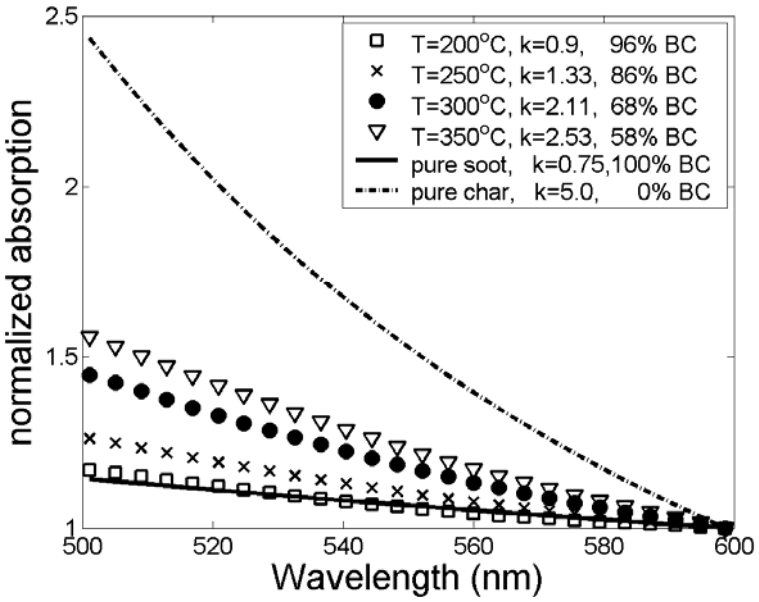

Figure 3.6. Spectral dependence of light absorption by soot and by char. The angstrom exponent, k, describes change in absorption as a function of wavelength (abs = λ^{-k}). Absorption is normalized to 600 nm. T refers to temperature.

angstrom exponents (AAE) of pure BC, pure char, and the measured LAC (light absorbing carbon), i.e. BC plus char on the filter. $\mathbf{k_{BC}}$, which is the AAE measured for laboratory soot between 500-600nm, was 0.75 +/- 0.02. The average AAE for BC in field samples was also 0.75, however the uncertainty was higher at +/-0.15. In equations 3.4 & 3.6, $\mathbf{k_{BC}}$ is the measured AAE of the sample prior to thermal processing. $\mathbf{k_{char}}$ was measured during TOA of the "back-up" filters from field sample filtration. These filters contained no BC, verified by optical measurements before and after TOA, and thus attenuation changes during thermal processing were due only to charring OC. $\mathbf{k_{char}}$ was 5+/-1. To determine the AAE value of the combined BC and char, or $\mathbf{k_m}$, linear regression is used to find the slope of the log of measured attenuation with respect to the log of wavelength between 500 and 600 nm and at each temperature (Equation 3.5).

$$k_m(T) = -\frac{\Delta \ln(ATN(\lambda, T))}{\Delta \ln(\lambda)} \tag{5}$$

The attenuation constant, c, which is solved for equation 4 once k_m is known, depends directly on the mass of light absorbing carbon on the filter and is therefore a function of temperature. Finally, solutions for c1 and c2 may be determined using two different values of lamda near 550 nm (λ_1= 530 nm and λ_2 = 570 nm). Thus equation 3.4 can be made into two equations, and the two unknown constants (c_1 and c_2) may be solved for algebraically (see Appendix A, equations A.3 – A.5).

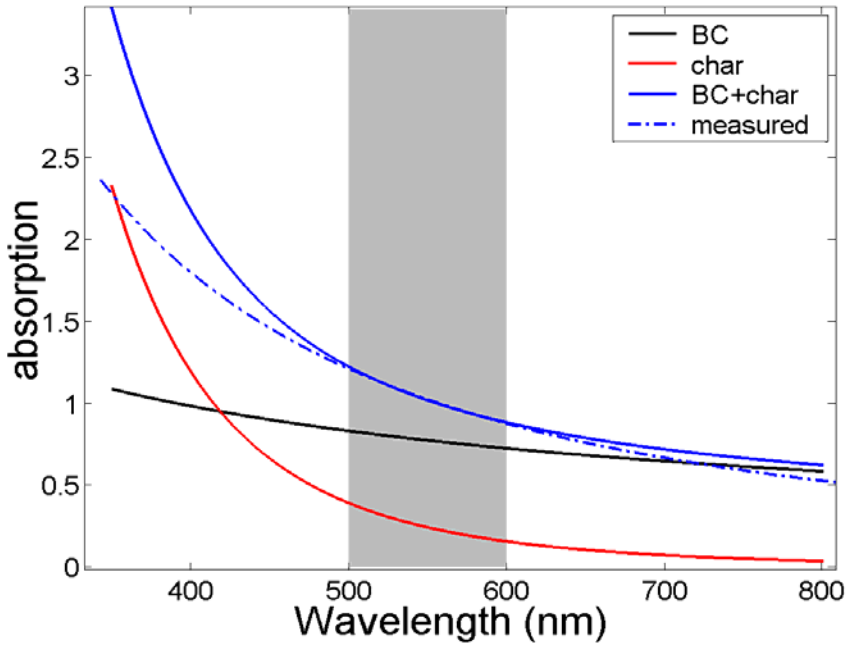

Figure 3.7. The black and red lines are the spectral absorption of pure BC and char respectively and follow the equation: abs = $\mathbf{A}\lambda^{-k}$, where k for BC is 0.75 and k for char is 5. **A** is determined uniquely for BC and char. The blue solid line is the summation of BC and char (red and black lines). The blue dashed line is created from the measured values for k and A between 500 and 600 nm (the shaded region).

Figure 3.7 illustrates how solutions for c_1 and c_2 are applicable over the specified spectral region, but under-predict the absorption at shorter wavelengths. This phenomenon has been previously observed in field measurements of soot and organic carbon mixtures [*Bergstrom, et al.*, 2007; *Kirchstetter, et al.*, 2004]. These equations further imply that derived AAE values for field samples, which would typically be a mix of absorbers, are valid only over the spectral region measured and extrapolating absorption at longer or shorter wavelengths may not be appropriate. The fraction of attenuation change at 550 nm due to BC (**a**) and that due to char (1-**a**) at each temperature during thermal optical analysis, was calculated from equation 4 as:

$$a(\lambda_{550nm}, T) = \frac{c_1(T)\lambda_{550nm}^{-k_{BC}}}{c(T)\lambda_{550nm}^{-k_m}} \qquad (3.6)$$

Assuming that all of the carbon evolved at temperatures greater than 480ºC was absorbing and comprised of the original BC and the char, MAE values for BC and char were determined using a best fit to the direct carbon measurement at temperatures greater than 480ºC. An iterative routine was used to find MAE_{BC} and MAE_{char}, such that when the BC and char attenuation components were individually scaled by these values and summed, the reconstructed curve matched the direct measurement of carbon mass remaining on the filter at temperatures greater than 480ºC (Figure 3.8). The equation for calculating carbon mass remaining on the filter as a function of temperature is given in the supporting information.

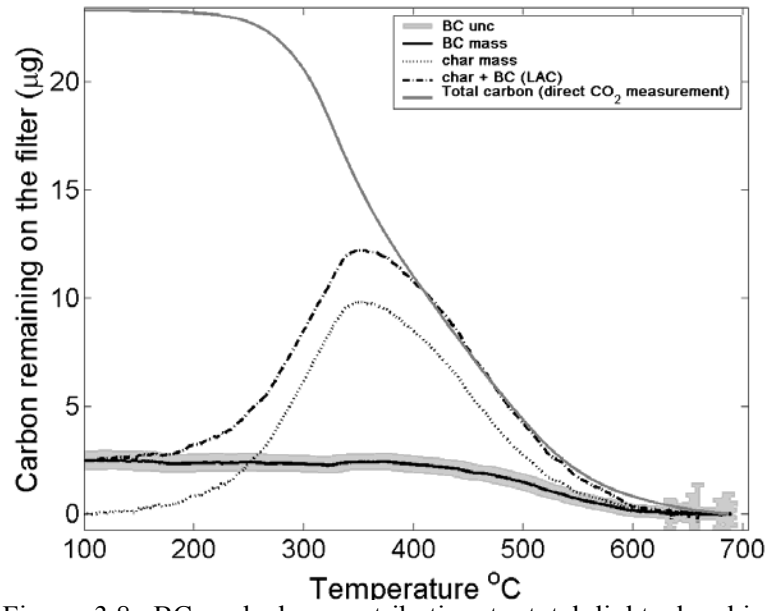

Figure 3.8. BC and char contribution to total light absorbing carbon. Total carbon is the total amount of carbon remaining on the filter and was derived from the direct measurement of evolved CO_2 as a function of temperature.

The range of previously published MAE values for BC on quartz fiber filters constrained the values for MAE_{BC} between 10 and 20 m^2/g. The range of values for MAE_{char}, 0.5 to 7 m^2/g, was found using the same field sample back-up filters used to find $\mathbf{k_{char}}$. The fitting algorithm cycled through the range of MAE values at increasing increments of 0.05 m^2g^{-1} and found those values corresponding to the minimum RMS (root mean square) difference between the measured carbon mass and the reconstructed sum of BC and char mass. BC mass remaining on the filter during TOA was determined by combining the Beer-Lambert law as shown in equation 3.1 with the derived fraction of attenuation due to BC calculated using equation 6 and the MAE_{BC} value corresponding to the best fit with the directly measured carbon mass.

$$BC(T) = \frac{a_{550nm}(T) * ATN_{550nm}(T) * A}{MAE_{BC}} \tag{7}$$

The average calculated mass attenuation efficiency for the BC filtered from 29 precipitation samples was 13.97 +/- 4.2 m^2g^{-1}. This wide range of MAE values is likely due to variability in source, chemical structure, and size of the BC particles. Absorption enhancement due to coating of the BC particles by sulfates and organics [*Liousse, et al.*, 1993] would not apply here as the water soluble coating should be removed by the water sample. This may also explain why the MAE values tend to be on the lower end of published values for BC MAE. The average calculated MAE of char was 3.1 +/- 2.3 m^2g^{-1}.

3.3.3 Calculating Uncertainties

A root mean square (RMS) difference was calculated from the closeness of the fit between the reconstructed LAC (BC plus char) mass and the direct measurement of total carbon mass from evolved CO_2 at temperatures greater than 480ºC. The RMS difference, which represents the uncertainty in BC mass, was assumed to be entirely due to the uncertainty in the MAE_{BC}, as opposed to uncertainties in the carbon measurement or the MAE of char. The uncertainty in the MAE_{BC} for each sample can be expressed as a simple calculation:

$$\sigma_{MAE_{BC}} = \left| \frac{dMAE_{BC}}{dBC} \right| * RMS \tag{8}$$

The uncertainty in **a**, calculated from the uncertainties in the derived values for $\mathbf{k_{BC}}$, $\mathbf{k_{char}}$, and $\mathbf{k_m}$, along with the uncertainty in measured attenuation (+3) and MAE_{BC} are propagated through equation 7 and give an uncertainty of BC mass at each temperature. The overall uncertainty in the final calculation for BC mass is the sum of the standard deviation from the retrieved BC mass between T=100ºC and T=300ºC and the average calculated uncertainty over the same temperature range. Figure 3.9 shows the percent uncertainty plotted as a function of total BC mass on the filter. The lower detection limit for this method is approximately 0.35 μg of BC. For BC mass greater than 1.0 μg, the percent uncertainty approaches 20%. The overall uncertainty is unique for each sample and ranges from 12% to 100%, depending on BC concentration, char, and dust content.

During thermal processing, some inorganic material may still contribute to changes in the light transmission. For example, oxidation of metals in the dust, such

as Fe(II) to Fe(III), may affect light absorption measurements at visible wavelengths, however the MAE of dust is a factor of one hundred less than the MAE of BC [*Clarke, et al.*, 2004]. Consequently the signal interference of oxidizing metals on BC should be negligible in most field samples. If the field sample does contain a high enough concentration of metals relative to the BC concentration, the oxidation of these metals at high temperatures could significantly increase the absorption of visible wavelengths at temperatures greater than 500°C and contaminate the reference transmission, as well as obscure the AAE measurements. This effect was observed to varying degrees in a few of the field samples used in this study, which were subsequently removed from this analysis. Comparing the transmission measurement of a dust laden sample prior to and after thermal processing, revealed that enhanced absorption in the visible wavelengths did not extend past 800 nm. Thus, for cases where dust contamination is

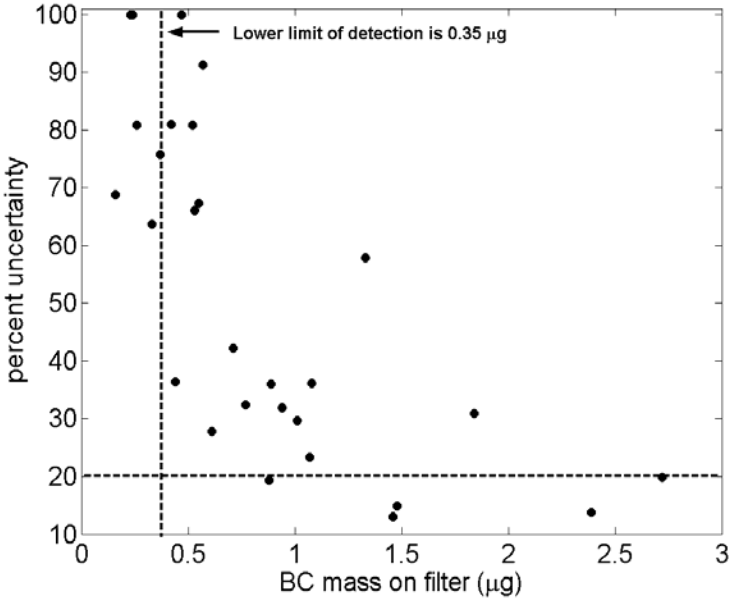

Figure 3.9. Percent uncertainty for field samples, vs filter loading. Dashed lines indicates that uncertainty approaches a constant value of 20% for BC mass above 1.0 μg and that the lower limit of detection is 0.35 μg of BC.

severe, the change in attenuation at 880 nm may still be used to estimate BC mass using the optical method alone.

3.4 Conclusions

Although there is still significant error associated with the BC measurements, this new BC analysis method provides a way to separate the BC signal from the charring signal of organics, a significant source of error in TOA of precipitation filtrate. Furthermore, errors less than 20% are at the lower end for previously published uncertainties in BC mass measured in snow and rain water, between 30% and 50% [*Chow, et al.*, 2004; *Chow, et al.*, 2001; *Clarke and Noone*, 1985]. This approach also provides a way to characterize measurement dependent uncertainties for each discrete sample, rather than assigning an uncertainty estimate to an entire analytical procedure. The MAE used for BC and for char result in mass calculations, that when summed, are consistent with the direct measure of total carbon mass obtained from the thermo-optical analyzer.

Relative to TOA of BC in atmospheric aerosols, the charring of organics from precipitation samples presented much higher signal interference in both the thermally dependent direct measurement of carbon and the optically inferred calculation. An analysis of light attenuation over a specific spectral region, rather than at a single wavelength, has led to a method for separating BC mass from organic char using individual absorption angstrom exponent values. Applying direct carbon

measurements from evolved CO_2 helped constrain and validate the MAE values obtained and used to find the BC concentration for each individual sample.

The techniques described above may also be applied to measurements of BC in ambient aerosol analysis. Further development of this method may allow for determining relative source contributions to BC aerosol from biomass burning and urban processes. Previous work has shown that the spectral dependence of absorption by BC particles generated by these processes differ similarly to BC and char. Soot generated from fossil fuel burning and urban processes have AAE values very close to that of the pure laboratory BC, while biomass burning produces soot containing spectral characteristics analogous to that of the char [*Bergstrom, et al.*, 2007; *Kirchstetter, et al.*, 2004]. Careful examination of the AAE values for soot generated by varying methods could potentially allow more accurate source apportionment for light absorbing aerosol.

3.5 Appendix

Carbon mass is derived from the measured CO_2 as it is evolved from the filter. Equation A.1 converts the partial pressure of CO_2 into carbon mass. Oxygen is the carrier gas for the CO_2 and moles of O_2 are calculated from the concentration and flow rate. Finally the mass is divided by the temperature ramp rate, to obtain a carbon mass for each degree increase in temperature. The total amount of carbon on the filter is the sum of all carbon evolved between 50°C and 70°C.

$$C_{mass}(T) = \frac{\left(\frac{\mu molesCO_2}{moles\ O_2}\right)\left(\frac{12g\ C}{mol\ C}\right) * \left(\frac{0.0409 mol\ O_2}{L\ O_2}\right) * \left(\frac{0.2L\ O_2}{\min}\right)}{\left(\frac{40°C}{\min}\right)} \quad \text{A.1}$$

The carbon mass remaining on the filter as a function of temperature is determined using equation A.1 as shown inA.2. The first term represents the total amount of carbon evolved from the filter and the second term is the amount of carbon evolved between 50°C and each 1°C temperature increase.

$$C(T)_{filter} = \sum_{T=50}^{700} C_{mass} - \sum_{i=50}^{T} C_{mass}(i) \quad \text{A.2}$$

Equations A.4 and A.5 are the solutions obtained for the coefficient of attenuation for char (c_2) and the coefficient of attenuation for BC (c_1).

$$c_1(T)\lambda^{-k_{BC}} + c_2(T)\lambda^{-k_{char}} \approx c(T)\lambda^{-k_m}, \text{ for } 500nm \le \lambda \le 600nm \quad \text{A.3}$$

Equation A.4 is obtained by rewriting equation A.3 (in main text as equation 3.3) to solve for c_2.

$$c_2 = \frac{c\lambda^{-k_m} - c_1\lambda^{-k_{BC}}}{\lambda^{-k_{char}}} \quad \text{A.4}$$

139

After substituting A.4 into A.3 and forming two equations with different values of lamda, the solution for c_1 is shown below.

$$c_1 = \frac{c\left(\lambda_2^{-k_m} - \lambda_1^{(-k_m+k_{char})}\lambda_2^{-k_{char}}\right)}{\left(\lambda_2^{-k_{BC}} - \lambda_1^{(-k_{BC}+k_{char})}\lambda_2^{-k_{char}}\right)}, \quad \begin{matrix}\lambda_1=530nm \\ \lambda_2=570nm\end{matrix} \qquad \text{A.5}$$

Publication Acknowledgement

A large segment of the text of Chapter 3 was submitted to Environmental Science and Technology in February 2008. In addition to myself, the primary author, co-authors on this paper are Dr. Craig E. Corrigan and Dr. Thomas W. Kirchstetter.

References

Arnott, W. P., K. Hamasha, H. Moosmuller, P. J. Sheridan, and J. A. Ogren (2005), Towards aerosol light-absorption measurements with a 7-wavelength Aethalometer: Evaluation with a photoacoustic instrument and 3-wavelength nephelometer, *Aerosol Sci Tech*, *39*, 17-29.

Bergstrom, R. W., P. Pilewskie, P. B. Russell, J. Redemann, T. C. Bond, P. K. Quinn, and B. Sierau (2007), Spectral Absorption Properties of Atmospheric Aerosols, *Atmos Chem Phys*, *Discuss., 7*, 10669-10686.

Bodhaine, B. A. (1995), Aerosol Absorption-Measurements at Barrow, Mauna-Loa and the South-Pole, *J Geophys Res-Atmos*, *100*, 8967-8975.

Bond, T. C., and R. W. Bergstrom (2006), Light absorption by carbonaceous particles: An investigative review, *Aerosol Sci Tech*, *40*, 27-67.

Chow, J. C., J. G. Watson, L. W. A. Chen, W. P. Arnott, and H. Moosmuller (2004), Equivalence of elemental carbon by thermal/optical reflectance and transmittance with different temperature protocols, *Environ Sci Technol*, *38*, 4414-4422.

Chow, J. C., J. G. Watson, D. Crow, D. H. Lowenthal, and T. Merrifield (2001), Comparison of IMPROVE and NIOSH carbon measurements, *Aerosol Sci Tech*, *34*, 23-34.

Chughtai, A. R., M. E. Brooks, and D. M. Smith (1996), Hydration of black carbon, *J Geophys Res-Atmos*, *101*, 19505-19514.

Chylek, P., L. Kou, B. Johnson, F. Boudala, and G. Lesins (1999), Black carbon concentrations in precipitation and near surface air in and near Halifax, Nova Scotia, *Atmos Environ*, *33*, 2269-2277.

Chylek, P., V. Ramaswamy, and V. Srivastava (1983), Albedo of Soot-Contaminated Snow, *J Geophys Res-Oc Atm*, *88*, 837-843.

Clarke, A. D., and K. J. Noone (1985), Soot in the Arctic Snowpack - a Cause for Perturbations in Radiative-Transfer, *Atmos Environ*, *19*, 2045-2053.

Clarke, A. D., et al. (2004), Size distributions and mixtures of dust and black carbon aerosol in Asian outflow: Physiochemistry and optical properties, *J Geophys Res-Atmos*, *109*, D15S09, doi:10.1029/2003JD004378.

Conway, H., A. Gades, and C. F. Raymond (1996), Albedo of dirty snow during conditions of melt, *Water Resour Res*, *32*, 1713-1718.

Currie, L. A., et al. (2002), A critical evaluation of interlaboratory data on total, elemental, and isotopic carbon in the carbonaceous particle reference material, NIST SRM 1649a, *J Res Natl Inst Stan*, *107*, 279-298.

Ducret, J., and H. Cachier (1992), Particulate carbon in rain at various termperate and tropical locations, *Journal of Atmospheric Chemistry*, *15*, 55-67.

Flanner, M. G., C. S. Zender, J. T. Randerson, and P. J. Rasch (2007), Present-day climate forcing and response from black carbon in snow, *J Geophys Res-Atmos*, *112*, -.

Hansen, A. D. A. (2003), *The Aethalometer*, Magee Scientific Company, Berkely CA.

Hansen, J., and L. Nazarenko (2004), Soot climate forcing via snow and ice albedos, *P Natl Acad Sci USA*, *101*, 423-428.

Jacobson, M. Z. (2004), Climate response of fossil fuel and biofuel soot, accounting for soot's feedback to snow and sea ice albedo and emissivity, *J Geophys Res-Atmos*, *109*, D21201, doi:21210.21029/22004JD004945.

Kirchstetter, T. W., and T. Novakov (2007), Controlled generation of black carbon particles from a diffusion flame and applications in evaluating black carbon measurement methods, *Atmos Environ*, *41*, 1874-1888.

Kirchstetter, T. W., T. Novakov, and P. V. Hobbs (2004), Evidence that the spectral dependence of light absorption by aerosols is affected by organic carbon, *J Geophys Res-Atmos*, *109*, D21208, doi:21210.21029/22004JD004999.

Lavanchy, V. M. H., H. W. Gaggeler, S. Nyeki, and U. Baltensperger (1999), Elemental carbon (EC) and black carbon (BC) measurements with a thermal method

and an aethalometer at the high-alpine research station Jungfraujoch, *Atmos Environ*, *33*, 2759-2769.

Li, Y. C., and C. W. Park (1999), A predictive model for the removal of colloidal particles in fibrous filter media, *Chem Eng Sci*, *54*, 633-644.

Liousse, C., H. Cachier, and S. G. Jennings (1993), Optical and Thermal Measurements of Black Carbon Aerosol Content in Different Environments - Variation of the Specific Attenuation Cross-Section, Sigma (Sigma), *Atmos Environ a-Gen*, *27*, 1203-1211.

Mikhailov, E. F., S. S. Vlasenko, I. A. Podgorny, V. Ramanathan, and C. E. Corrigan (2006), Optical properties of soot-water drop agglomerates: An experimental study, *J Geophys Res-Atmos*, *111*, (D7), D07209 doi:07210.01029/02005JD006389.

Novakov, T., and C. E. Corrigan (1995), Thermal Characterization of Biomass Smoke Particles, *Mikrochim Acta*, *119*, 157-166.

Painter, T. H., A. P. Barrett, C. C. Landry, J. C. Neff, M. Cassidy, C. R. Lawrence, K. E. McBride, and G. L. Farmer (2007), Impact of disturbed desert soils on duration of mountain snow cover, *Geophys Res Lett*, *34*, L12502, doi:12510.11029/12007GL030284.

Petzold, A., and R. Niessner (1995), Method Comparison Study on Soot-Selective Techniques, *Mikrochim Acta*, *117*, 215-237.

Spielman, L. A. (1977), Particle Capture from Low-Speed Laminar Flows, *Annu Rev Fluid Mech*, *9*, 297-319.

Warren, S. G., and W. J. Wiscombe (1980), A Model for the Spectral Albedo of Snow.2. Snow Containing Atmospheric Aerosols, *J Atmos Sci*, *37*, 2734-2745.

Watson, J. G., J. Chow, and L. W. A. Chen (2005), Summary of Organic and Elemental Carbon/Black Carbon Analysis Methods and Intercomparisons, *Aerosol and Air Quality Research*, *5*, 65-102.

Weingartner, E., H. Saathoff, M. Schnaiter, N. Streit, B. Bitnar, and U. Baltensperger (2003), Absorption of light by soot particles: determination of the absorption coefficient by means of aethalometers, *J Aerosol Sci*, *34*, 1445-1463.

Zuberi, B., K. S. Johnson, G. K. Aleks, L. T. Molina, and A. Laskin (2005), Hydrophilic properties of aged soot, *Geophys Res Lett*, *32*, L01807, doi:01810.01029/02004GL021496.

Chapter 4

Measurements of BC in Snow and Rain in Northern California

4.1 Introduction

Several field studies, including CIFEX (the Cloud Indirect Effects Experiment) described in Chapter 2, have shown that trans-Pacific transport of pollution from Asia to North America can be significant in the late winter and early spring [*Bertschi and Jaffe*, 2005; *Bey, et al.*, 2001; *de Gouw, et al.*, 2004; *Goldstein, et al.*, 2004; *Hadley, et al.*, 2007; *Heald, et al.*, 2006; *Park, et al.*, 2005; *Parrish, et al.*, 2004]. This well documented, enhanced springtime transport of pollution is due to an increase in the number of cold fronts passing over inner Mongolia and the Taklimakan desert regions, which lift and carry aerosols to about 6 km in altitude where they are transported great distances across the Pacific Ocean by the mid latitude westerlies [*Liu, et al.*, 2003; *Stohl*, 2001]. Not only does the timing of this transport coincide with the onset of spring melt, but has the greatest impact at high elevation sites [*Hadley, et al.*, 2007; *VanCuren, et al.*, 2005], and therefore occurs at a time when the potential to affect mountain snow packs in the Western United States is the greatest.

Recent modeling studies have predicted that snow surface albedo can be reduced by as much as 1% per 10 nanograms of black carbon (BC) per gram of equivalent snow water [*Clarke and Noone*, 1985; *Flanner, et al.*, 2007; *Grenfell, et al.*, 2002; *Hansen and Nazarenko*, 2004; *Jacobson*, 2007]. This relationship applies to internally mixed BC in fresh snow crystals with an effective radius of approximately

100 μm. As the snow ages, melts, and refreezes the crystals grow larger and amplify the effect of the BC inclusions by more than a factor of three. BC particles that are externally mixed with the snow crystals cause a much smaller albedo reduction [*Chylek, et al.*, 1983; *Conway, et al.*, 1996; *Warren and Wiscombe*, 1980]. Changes to the snow albedo directly affect snow pack melt rate, especially in spring when ambient temperatures are near 0°C [*Painter, et al.*, 2007]. Solar radiation on snow surfaces drives snow pack melt rates when ambient temperatures approach 0°C, as evidenced by comparison of snow cover and depth on north facing versus south facing slopes during spring melt. Snow packs in the Sierra Nevadas and the Southern Cascades are a crucial source of fresh water for California's massive agricultural production, as well as for densely populated urban and sub-urban centers. Measurements of actual BC concentration in the snow are necessary to place these modeled effects into a context relevant to the state of California.

During the SUPRECIP-2 (Suppression of Precipitation) experiment, automated precipitation collectors were installed in Northern California for the purpose of collecting and analyzing snow and rain for BC concentration. The goal of this study was to determine the possible impact of BC aerosols on snowpack melt rates in California mountain ranges, as well as to determine relative contributions from regional sources vs. long range transport. Over 55 precipitation samples were collected between late February and mid April of 2006. Ambient aerosol measurements extended into mid-May, although no samples were collected due to a lack of precipitation. Of the samples collected, 29 contained a sufficient volume of water for

BC analysis. The rest were analyzed for Fe (iron), Ca (calcium), Al (aluminum) and K (potassium) using x-ray fluorescence spectroscopy (XRF). These additional aerosol species helped identify possible source region and type for the aerosols, including the BC, found in the precipitation.

4.2 Experimental Methods

Snow and rain samples were collected in the Sierra Nevadas and southern Cascades and rain samples were collected on the Northern California coast throughout February, March, and early April, 2006. The precipitation samples were filtered and analyzed for BC mass concentration using a modified version of TOA (thermal optical analysis) described in detail in Chapter 3. Lastly, smaller precipitation samples were filtered and analyzed for Fe, Ca, Al, and K using XRF (X-ray Fluorescence spectroscopy).

4.2.1 Field site locations

Three EcoTech automated rain water samplers (RWS) were installed at three sites in Northern California (Figure 4.1). Two of the sites were located in the Sierra Nevada and Cascade mountain ranges and one on the California coast. Site choice was based both on the scientific relevance of the location, as well as installation logistics, i.e. accessibility, available power, and availability of meteorological and other ambient aerosol data. Precipitation collected at the coastal site was expected to be influenced the least by North American emissions. Contrasting mountain locations

were chosen such that one site was located in a rural, relatively pristine area and thus representative of remote mountain locations. The other site was selected to represent mountain regions that are heavily influenced by pollution from industrial and urban processes.

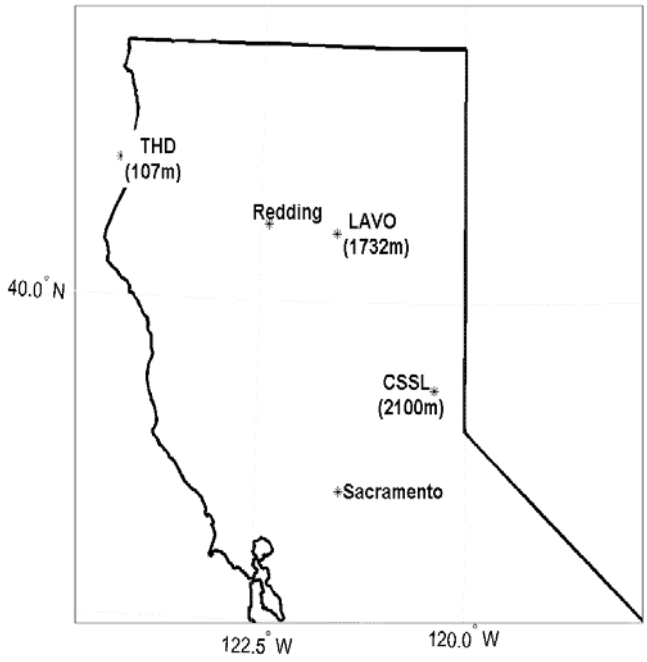

Figure 4.1. Map of sample collection sites. The elevation is shown in parenthesis

The CMDL (Climate Monitoring and Diagnostics Lab) station at Trinidad Head (THD), the coastal site, was an ideal choice for collecting precipitation samples with limited North American continental influence. THD is located on a small point that juts out away from the mainland. The largest local source of urban pollution is from Eureka, south of THD. Although prevailing winter storms generally arrive at

THD from the northwest; the cyclonic rotation of winds under low pressure systems may have picked up some continental pollution from the south.

The "clean" mountain location, also the IMPROVE (Interagency Monitoring of Protected Visual Environments) site at Mt. Lassen Volcano National Park (LAVO), is removed from any local (<100 km) major urban centers. Meteorological data, as well as aerosol data from the IMPROVE monitoring network, were already available here, making this an ideal spot for snow collection. Additionally, an aethalometer [*Hansen*, 2003], used to measure ambient BC concentration, and a nephelometer, which measures light scatter as a proxy for total ambient aerosol concentration, were installed at this site. The nephelometer data were used primarily to correct the aethalometer BC data for scattering artifacts [*Arnott, et al.*, 2005]. Lastly, UC Davis installed three-hour interval, continuous aerosol analyzers for the duration of the SUPRECIP-II campaign. The aerosol measurements included mass concentrations for over 26 elements, however only the aforementioned Fe, Ca, Al and K were used for this study. Size distributions for the mass concentration of each element were separated into eight size bins: 10-5, 5-2.5, 2.5-1.15, 1.15-0.75, 0.75-0.56, 0.56-0.34, 0.34-0.26, and 0.26-0.09 microns.

In contrast to LAVO, the third site, CSSL (Central Sierra Snow Laboratory, UC Berkeley), was chosen as the snow collection site likely to be dominated by regional pollution from both San Francisco and Sacramento, as well as by local pollutants from nearby I-80, residences, and trains on the nearby Southern Pacific Rail. Meteorological data, as well as aerosol measurements made by the UC Davis

team, were also available here. Ambient BC concentration and light scatter data were not available at this site due to the limited number of instruments available.

4.2.2 Sample Collection

The RWS (rain water sampler), automated, wet only, snow and rain collectors were installed at all three sites and operated for up to one week without the need for an on site technician (Figure 4.2). An external, tipping bucket gauge sensed when a precipitation event began, and signaled the RWS lid to open and begin collecting. When the event ended, the collector lid closed and the samples were protected from contamination by dry deposition. Samples were separated by days rather than by event, such that for each day of rain or snow, one sample was collected. An overflow

Figure 4.2. Rain and snow collection at Mt. Lassen Volcano Natl. Park

valve protected the samples in the event of extreme precipitation events. Each sampler held eight sample bottles with a 400 mL capacity. A computer data logger tracked the date, time, and intensity of each event. Two of the collectors installed at Central Sierra Snow Lab and Lassen Volcano National Park were modified for snow collection. Both the external tipping bucket and collection funnels were heated and melted the snow as it fell on the surface. The temperature inside these collectors was held constant at 10ºC. Samples from all three sites were collected weekly and frozen until the analysis, described in Chapter 3, could be performed.

4.2.3. XRF (X-ray fluorescence spectroscopy) analysis of aerosols in the precipitation

In addition to the analysis for BC mass, X-ray fluorescence spectroscopy (XRF) was used to measure mass concentration of over 26 elements in the precipitation samples. Samples were filtered through Watcom, Nuclepore (0.4 micron pore size) filters. The filters were mounted and analyzed using XRF spectroscopy [*VanCuren, et al.*, 2005] at the ALS (Advanced Light Source Facility) at Lawrence Berkeley National Laboratory. The beam size was 500 X 500 microns, and five points were measured on each filter to evaluate surface loading variability on the filter. Blanks using filtered, distilled water gave clean results for Fe, Ca, Al, and K, which are the elements used in this analysis.

4.3 Results and Discussion

A minimum BC mass loading on the filter of 0.4 μg was essential to obtaining a valid measurement, and therefore at least 100 mL, and preferably 200 mL, of accrued precipitation was needed. A total of 55 precipitation samples were collected during this field experiment, 29 of which contained a sufficient volume of water to make a BC measurement. Nearly half of these were collected at THD, where the average BC concentration in rainwater per day was determined for 14 different days. At LAVO and CSSL, 7 and 8 samples, respectively, were analyzed for BC. The remaining smaller samples were analyzed for Fe, Ca, and K concentrations. Combined with air mass back trajectory calculations, and measurements of the elemental composition of ambient aerosols, these elemental species yield valuable clues to the sources of aerosol found in California precipitation. Results from this analysis are discussed in Chapter 5.

4.3.1 BC mass concentration in precipitation

The average BC concentrations in rain at THD, and in snow at CSSL and LAVO, were respectively 4.99 ng/g, 6.7 ng/g, and 6.97 ng/g (Figure 4.3). Although the differences in average BC concentrations between each site were not radically different, the relative amounts followed what was expected. Rainwater at THD, which sits 100 meters above sea-level on the Northern California coast, contained on average the lowest concentration of BC. Although rain collected at THD was the least subject of all the sites to North American influences, directly south and less than 30 miles

from THD are several major industrial facilities, including saw mills and power plants. Due to typical cyclonic rotation of winds during rain events, which tend to approach THD from the southwest, it was possible that emissions from these facilities may have been observed in the rainwater here. LAVO, which sits approximately 60 miles due east of Redding, CA at an elevation of 1732 meters, is both inland and far from major urban or industrial centers. The BC concentration measured in snow and rain at LAVO was slightly higher, but not statistically different, given the variability, from THD or CSSL. Of the three sites, measurements made at LAVO should have most closely represented remote California snow pack. Variability found in the BC concentration at LAVO was much lower than at the other two sites and probably more characteristic of average background concentrations in the California mountain ranges. Uncertainties measured at LAVO were also higher than the other two sites. This was because the average volume of water used for the BC analysis was about half that of THD and CSSL. Therefore the BC mass retrieved from these smaller volumes of water tended to be low and subject to higher uncertainty. CSSL, at an elevation of 2100 meters, is located directly downwind of Sacramento and San Francisco, as well as just a few miles from I-80, a primary trucking route across the Sierra Nevada, and was therefore expected to be heavily influenced by these regional and local pollution sources. Several houses and a small ski resort were also located nearby. Surprisingly, the average BC concentrations measured in the snow at CSSL, although higher than at the other two sites, was also not statistically different when compared to sample concentration variability.

Due to the preferential sampling of rain and snow from heavy (>10 mm/day) precipitation events, the average BC concentration measured in snow during this study may have underestimated the true concentration of BC in the mountain snow pack. In short, for a given amount of BC in the atmosphere, more precipitation will result in a lower concentration. BC analysis was limited only to samples from these large events, because they provided the sample size needed to make a valid measurement. The effect of daily precipitation amount and ambient concentrations on BC and other aerosol species measured in snow and rain is discussed below.

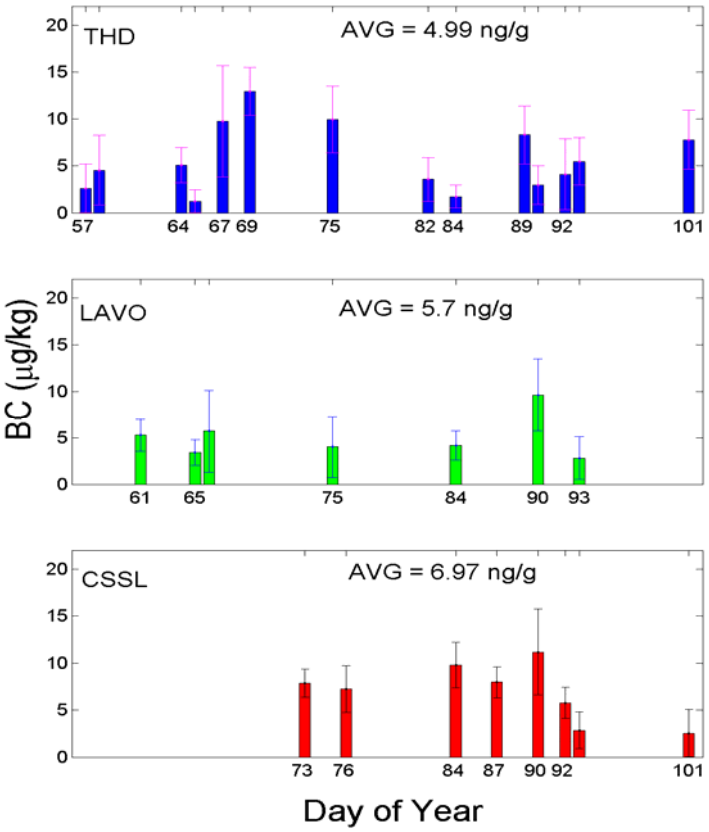

Figure 4.3. Measured concentration of BC at THD, LAVO, and CSSL in March and April, 2006.

4.3.2 Factors Controlling BC Concentration in Precipitation

In the mountains, precipitation primarily forms from two different mechanisms: forced orographic lift and synoptic or meso scale storm systems, and often a combination of both. Orographic lift can occur on a variety of spatial scales, but put most simply, it is the result of low-level air masses encountering the mountains slope and being forced upward by the topography (Figure 4.4a). Air cools as it rises and water condenses on the available particles. If there is enough moisture for the drops/crystals to reach a sufficient size, rain or snow will fall. In this type of event, the aerosols that comprise the cloud condensation nuclei (CCN), those below the cloud, and those measured at the ground are likely to be the same. Precipitating clouds caused by synoptic and meso scale disturbances are initially fed by lifting air parcels in the warm sector in front of an approaching cold front (Figure 4.4b). Therefore the most likely source for the CCN forming these clouds is downstream of the system. The precipitation that forms along the boundary between the warm and the cold front; however, must fall through the cold dry layer behind the cold front, which is the source of aerosols removed by below cloud scavenging. Therefore the aerosols comprising the CCN and those below the clouds are not as likely to be the same. Typically in March and April, LAVO and CSSL are impacted by passing cold fronts, while the warm fronts pass far north of the sites [*Neiman, et al.*, 2005]. Interaction between the frontal system and the mountains often results in orographically forced lift of the cold front, significantly enhancing precipitation [*Kingsmill, et al.*, 2006].

Orographic enhancement of precipitation was more prevalent at CSSL than at LAVO, where snowfall during this experiment was twice that measured at LAVO.

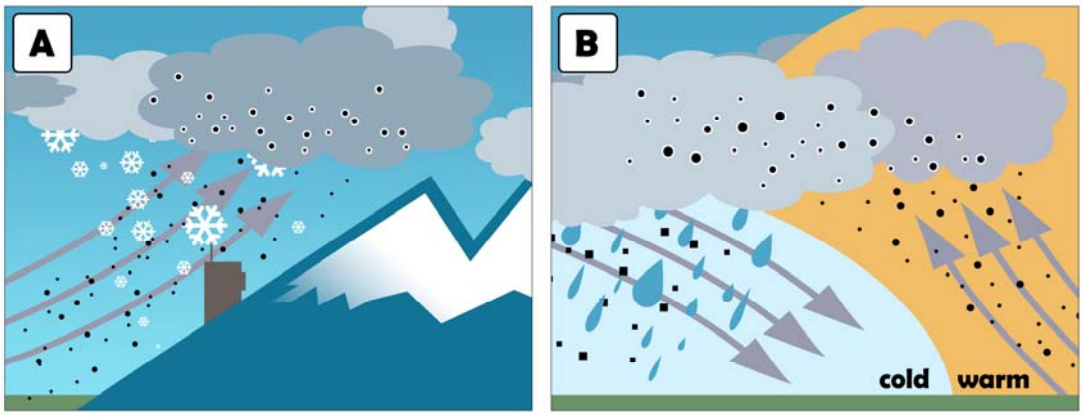

Figure 4.4.Clouds and precipitation formed by (a) orographic lift and (b) frontal lifting.

Two primary variables control BC concentration (or any aerosol species) in precipitation. First, the concentration of BC particles in the CCN and below the clouds restricts the total BC mass available for wet removal. BC particles in CCN are subject to "rain out", while particles below the cloud may be scavenged, or "washed out" by falling snow or rain. Depending on the meteorology, the BC particles in the CCN and those below the cloud may or may not originate from the same source. The second variable affecting BC concentration in rain or snow is the amount of precipitation diluting the concentration, i.e. a heavy rain or snowfall would result in a lower concentration for the same amount of BC. Determining which effect dominates is challenging as the two variables are not independent of each other. This is clearly demonstrated by Figure 4.5, which shows that ambient concentrations for all aerosol species tend to be lower during intense precipitation events than for lighter events.

This is not surprising as precipitation is the primary method for clearing the atmosphere of aerosols, i.e. the more rain or snow, the cleaner the air.

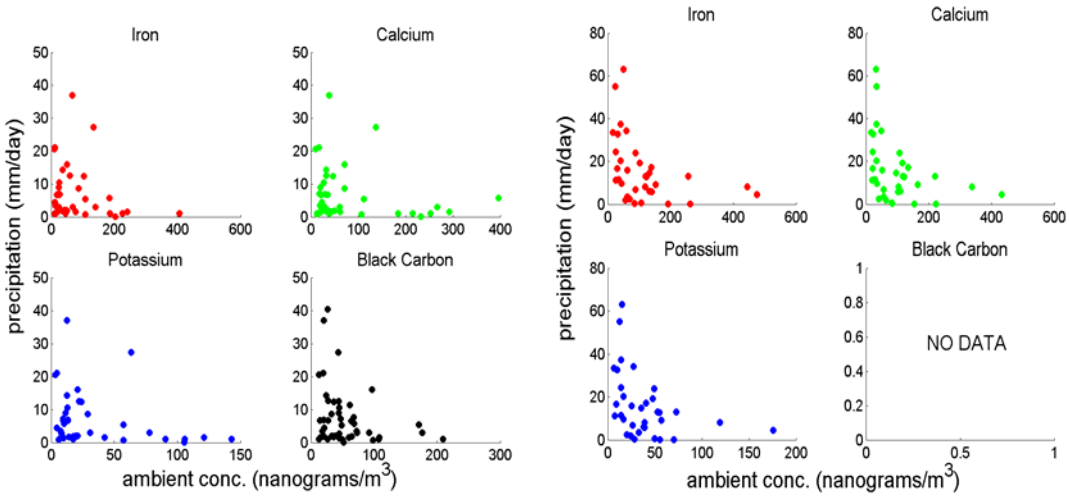

a. LAVO b. CSSL

Figure 4.5 Precipitation daily amounts vs. ambient concentrations at (a) LAVO and at (b) CSSL. Points are only plotted for days during which precipitation was detected.

4.3.3 Comparing BC removed in snow to ambient BC mass concentrations at LAVO

Although the concentration of BC in snow is of primary interest when looking at radiative impacts on melt rate, it is of little use to compare precipitation concentration to air concentration as the dilution effect could obscure the relationship. In the subsequent analysis, the dilution effect is removed by calculating total mass removed (M_d) from the atmosphere in each precipitation event (Equation 4.1).

$$M_d = M_c * P \tag{4.1}$$

M_d is the mass of aerosol deposited over a given area during the day for which a sample was collected. For conversion simplicity the area is given in cm^2 and P is the total measured precipitation for a given sample day(s) in cm such that area times amount fallen equals total grams of precipitation. For scaling purposes, as well as a comparison with ambient concentrations (ng/m^3), this area is expanded to m^2 in figures 4.6 and 4.7. M_c is the measured mass concentration of a given aerosol component in ng/cm^3 (or grams) of snow or rain water.

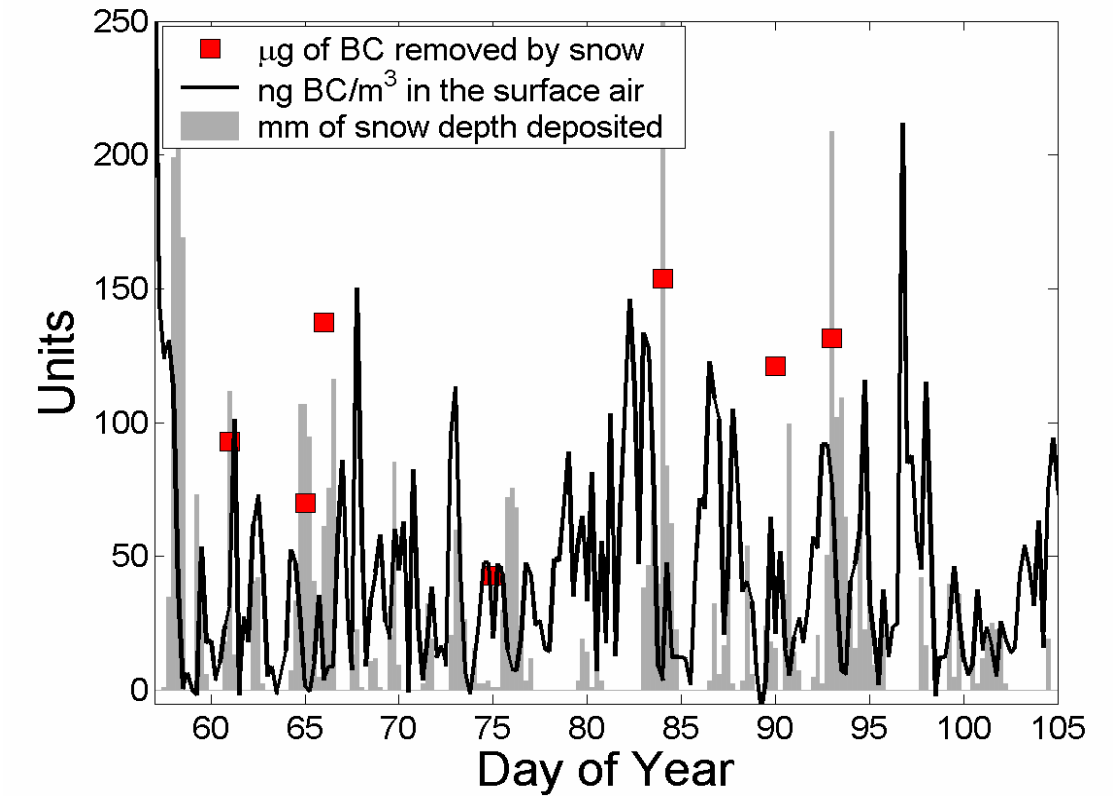

Figure 4.6. BC/m3 in the surface air in 6 hour time intervals (red line), mm of snow depth accumulated in 6 hour increments (light blue bars), total BC/m^2 deposited by the falling snow during a 24 to 48 hour period depending on timing of the snowfall (black squares). Snow depth is parameterized as precipitation * 10. Data are for LAVO.

In order to have a large enough sample volume for a BC measurement, precipitation from multiple days, but belonging to the same system, were combined for days: 61 and 62, 66 and 67, 74 and 75, 83 and 84, 92 and 93. Snow water from day 65 and 90 were not mixed with any others. Figure 4.6 shows a time series of ambient BC mass concentration in the surface air and the total mass of BC removed during the indicated snow days. As previously mentioned, BC measurements were only made for the heaviest precipitation days.

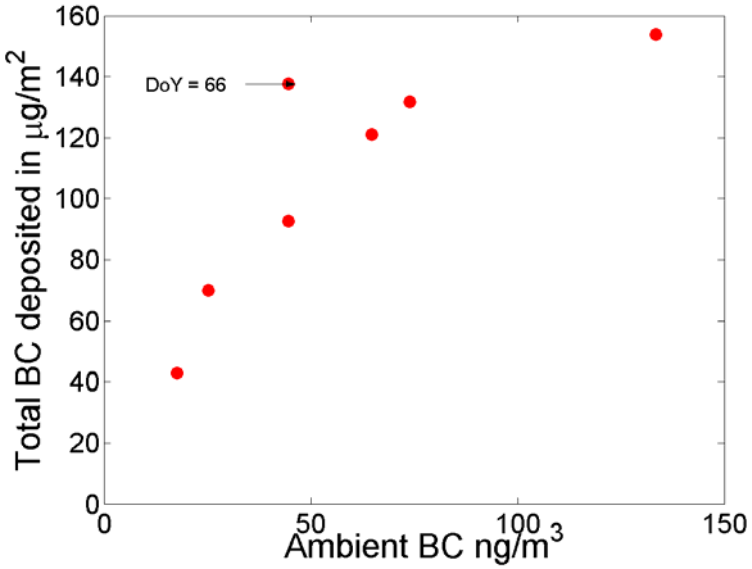

Figure 4.7 Correlation of BC removed in a precipitation event to average ambient concentrations 6 hours prior to the event. R^2 = 0.66.

A comparison of total BC deposited in a given precipitation event to the ambient BC concentration at LAVO on the same day showed no correlation; however the average, ambient concentrations of BC in the six hours just prior to the commencement of the precipitation were highly correlated (R^2 = 0.66) to the total amount of BC deposited during the subsequent event (Figures 4.7). This indicates that

below cloud scavenging was the dominant source of BC in snow at LAVO. The drop in ambient BC concentration during heavier precipitation events to levels near or below the aethalometer lower limit of detection, roughly 15 ng/m^3 (figure 4.7), suggested that nearly all the BC in the air is removed by the snow. Although it was possible that the aerosols observed at the surface were the same as those nucleating the cloud, if cloud drop nucleation was the dominant source of BC in precipitation, than the concentration of BC in the snow or rain water, rather than the total amount removed, should have had a higher correlation with the surface aerosols. Each rain drop or snow flake would, on average, have contained the same amount of BC. Similar analyses for Central Sierra Snow Lab and Trinidad Head were not possible due to a lack of continuous BC measurements available for these sites; however ambient measurements of Ca, Fe, and K mass concentrations in air, as well as in precipitation, were made at both LAVO and CSSL and are discussed in the following section.

4.3.4 Ca, Fe, and K mass concentration in snow and in surface air at LAVO and CSSL

Measurements of Ca, Fe, and K (primarily found in soil dust) mass concentration in snow water, as well as continuous ambient surface concentrations in 3 hour intervals, were available at both LAVO and CSSL. Precipitation samples from LAVO and CSSL, for which less than 75 mL were collected (all larger samples were used for BC analysis), were filtered through 0.45 micron Nuclepore filters and

analyzed for Ca, Fe, and K using X-ray fluorescence spectroscopy (XRF). The time series of ambient PM2.5 and PM10 surface concentrations, precipitation, and total amount of each element removed for both LAVO and CSSL are shown in Figures 4. 8 & 4.9 respectively.

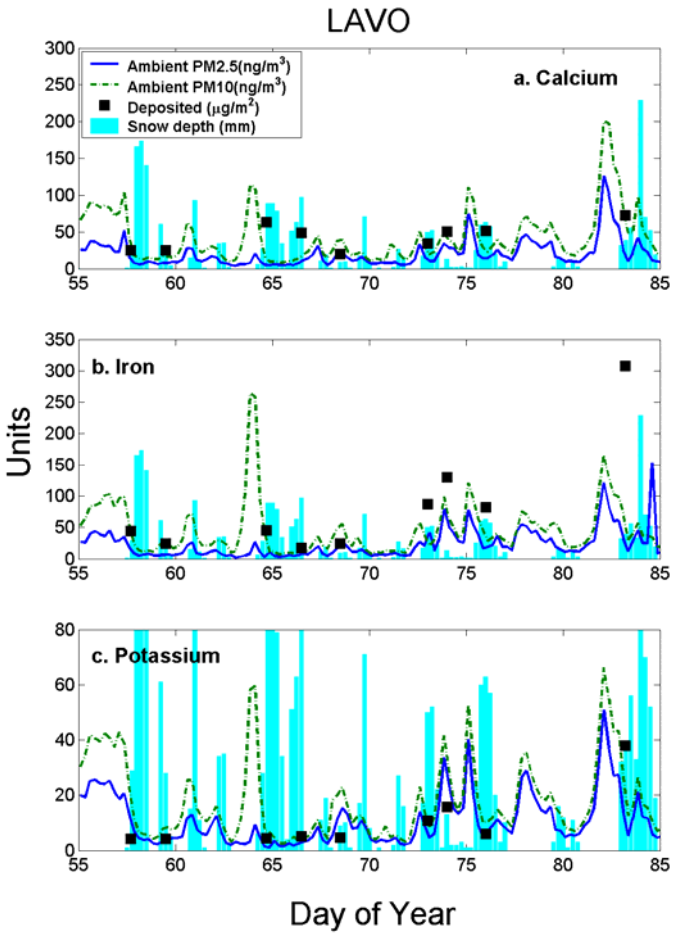

Figure 4.8. Time series of surface concentrations (solid line) and amount removed (squares) of: a.) Ca, b.) Fe and c.) K.

The comparison of the Ca, Fe, and K mass concentration (equation 4.1) removed per event to that measured at the surface produced slightly different results

than the equivalent BC comparison described previously. Ambient surface concentration of PM10 Ca mass at LAVO was weakly, but significantly, correlated to the total amount removed in the precipitation (Figure 4.10 a) at $R^2 = 0.33$. The ambient PM2.5 Ca was not significantly correlated with the precipitation Ca. In contrast, the PM2.5 Fe and K, and not the PM10, correlated significantly with the amounts removed by precipitation, with $R^2 = 0.76$ and 0.49 respectively (Figure 4.10 b&c). The ambient PM10 for Fe and K were not significantly correlated with

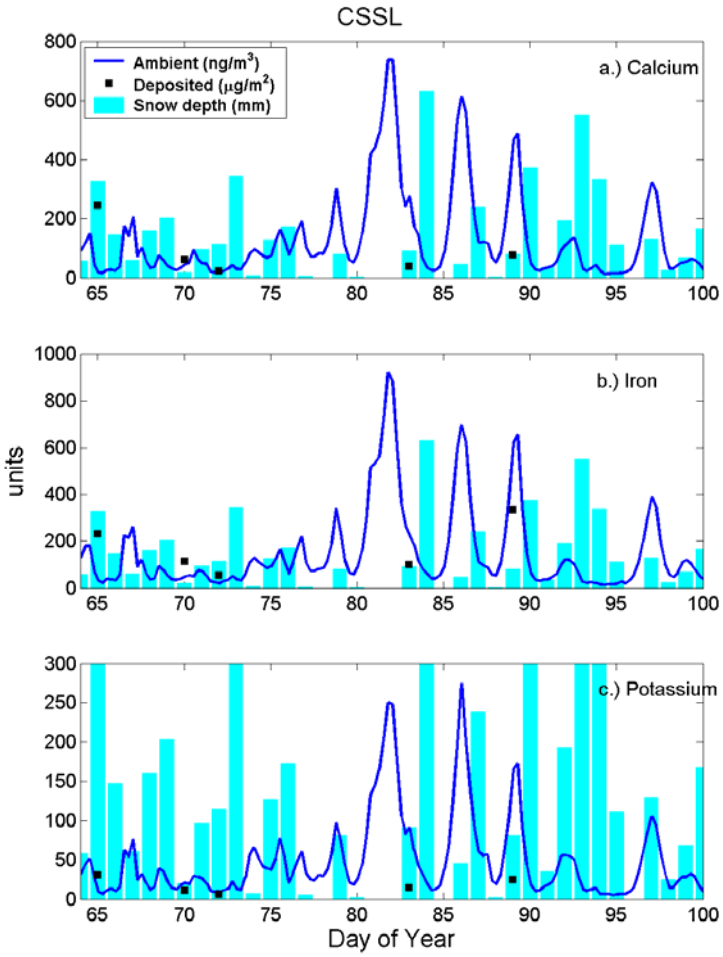

Figure 4.9. Time series of surface concentrations (solid line) and amounts removed (squares) of: a.) Ca, b.) Fe and c.) K at CSSL.

precipitation mass at LAVO. The calculated R-squared values for the XRF data are similar to the value determined for BC concentrations in the previous section. The same analysis for Central Sierra Snow Laboratory (CSSL) produced comparable results to that of LAVO; however with only five data points (Figure 4.10 d, e, & f), the significance of any correlation values was lost. The ambient concentrations used for these calculations were the average, ambient concentrations 6 hours prior to the precipitation event.

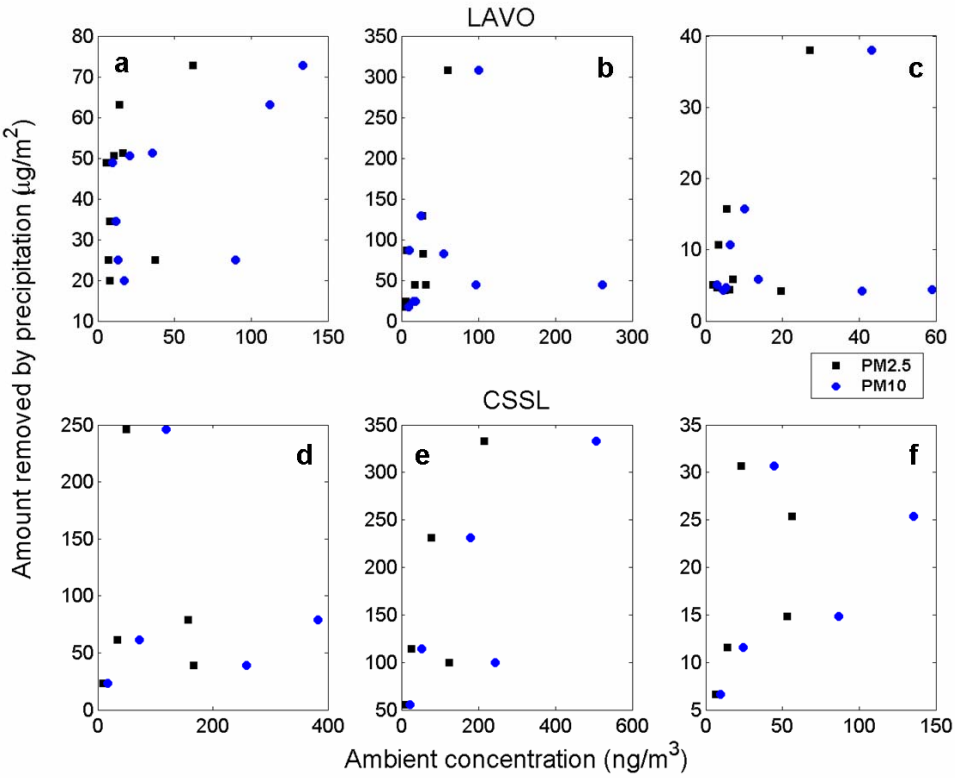

Figure 4.10. Ambient surface concentrations of Ca (a & d), Fe (b & e), & K (c & f) compared to total amount removed in a precipitation event for LAVO (a, b, & c) and CSSL (d, e, & f).

The comparison of Fe, Ca, and K in ambient surface air to the amount removed in the precipitation at LAVO indicated that the dust aerosols observed in the surface air were not as representative of the total atmospheric dust, susceptible to wet removal, as for the BC. For example, locally generated dust aerosol may be observed near the surface in both the fine and coarse mode, while the concentration of fine mode dust transported a greater distance and from a completely separate source may dominate at smaller sizes and at higher elevations. Despite the uncertain homogeneity of the observed ambient aerosols throughout the atmospheric column, the significant positive correlation between the surface and the precipitation aerosols supports the previous conclusion; wet scavenging was the dominant source of impurities in the snow at LAVO. Using the XRF data to fingerprint dust from different sources and isolate signatures of long range transport will be discussed further in Chapter 5.

The major difference between dust and BC emissions is that during times of persistent snow or rain, as observed in Northern California at the time of this study, dust emissions are greatly reduced, while BC emissions remain unchanged. Therefore, although a percentage of dust aerosols observed at LAVO and CSSL in March 2006 were probably transported long distances from dryer regions, the observed BC aerosol was likely a product of local and regional sources combined with an unknown contribution from long range transport. As the ambient BC aerosol observed at LAVO was strongly tied to the amount observed in the snow, sources of the ambient BC are relevant to the snow pack and are therefore examined in the next section.

4.3.5. Sources of BC

A high correlation between the BC removed by the snow and the ambient mass concentration prior to the onset of precipitation strongly indicated that washout of below cloud aerosols was a dominant source of BC in the snow water; therefore it is of interest to determine the origins of the ambient BC. The two primary sources for atmospheric BC are biomass burning and fossil fuel burning. Previous studies have shown that biomass burning generates excess fine potassium (K_{exc}), while fossil fuel (petroleum, diesel, and coal) combustion produces almost none [*Andreae*, 1983; *Coles, et al.*, 1979]. Therefore, both the correlation and overall ratio of K_{exc} to BC may be used as an indicator of BC source type. Since the primary source of potassium in atmospheric aerosols is from dust or soil, the soil fraction of fine potassium must be subtracted from total fine potassium (equation 4.2) to provide a value of K_{exc}.

$$K_{exc} = K_{fine}\left(D < 1\mu m\right) - \left(\frac{K}{Al}\right) * Al_{fine}\left(D < 1\mu m\right) \qquad (4.2)$$

Equation 4.2 is similar to the calculations used by Andreae [1983] and Yang [2005] to determine K_{exc}. The difference here is that Andreae [1983] used the fraction, K/Ca, and Yang [2005] used K/Fe to determine the soil fraction of fine potassium. The ratio of potassium to aluminum (Al) was chosen for this study for two reasons: 1) the total (coarse + fine) potassium mass concentration was more highly correlated with Al, at $R^2 = 0.96$, than with either Ca or Fe, and 2.) dust aerosols observed at LAVO may be enriched in either Ca or Fe depending on the source [*VanCuren, et al.*, 2005]. The average ratio of the total mass of potassium to the total mass of aluminum (Al)

measured at LAVO during this experiment was 0.23+/-0.05 and represents the soil or dust fraction of potassium. The calculation assumes that the ratio of soil potassium to Al remains constant at all sizes [*Andreae*, 1982] and that the potassium produced during biomass burning is confined to submicron particles [*Turn, et al.*, 1997].

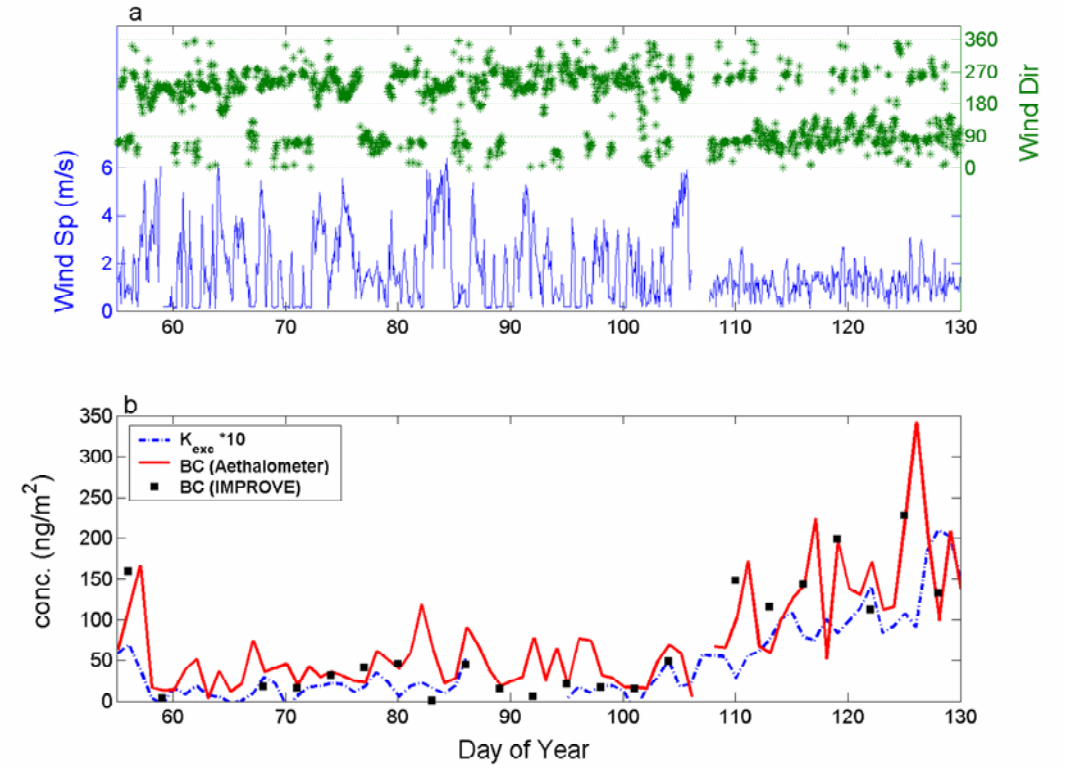

Figure 4.11. a.) Hourly wind speed and wind direction. b.) Daily BC mass concentration and excess fine (D<1 micron) potassium (K_{exc}). Elemental carbon (daily average for every third day) from the IMPROVE [*Chow, et al.*, 2001] data showed generally good agreement with the aethalometer BC data. K_{exc} was multiplied by 10 for scaling purposes.

A comparison of the K_{exc} with the ambient BC concentration revealed a significant correlation (Figure 4.11b) at $R^2 = 0.51$. The average ratio of K_{exc} to BC is approximately 0.07 +/-0.06, consistent with previous ratios reported for the United States and Northern Europe. The ratio of K_{exc} to BC for different bio-fuels has been

quantified at values averaging 0.21+/-0.06 for wood fuels (ash, almond, walnut, pine, etc…) and 0.88 for herbaceous fuels (rice, corn, grass, etc…) [*Fine, et al.*, 2002; *Turn, et al.*, 1997]. Assuming that the majority of the biomass fuel contributing to BC observed at LAVO is from wood and that a ratio of K_{exc} to BC equal to 0.21+/-0.06 represents 100% BC from biomass combustion; the fractional contribution of biomass combustion (F_{BM}) to the BC observed at LAVO in the spring may be roughly estimated at 33% and is simply the observed ratio, 0.07, divided by 0.21.

The increase in mass concentration of BC and K_{exc} in the latter half of April and in early May was marked by a systematic shift in wind direction from predominantly south/southwesterly to easterly (Figure 4.11a). Coincident with the shift in wind direction, the average wind speeds dropped below 2 m/s, whereas in March and early April, hourly averaged windspeeds from 4 to 6 m/s occurred frequently (Figure 4.11a). This marked a switch from a predominantly stormy, cyclonic rotation in March and early April to more of an anticyclonic, high pressure regime in late April and May. This shift coincided not only with an increase in BC aerosol, but also saw nearly a doubling in the average fraction of BC from biomass combustion.

The average ratio of K_{exc} to BC during March and early April was 0.05, but rose to 0.1 after April 15th (doy = 105), corresponding to an increase from 24% to 48% in the overall fractional contribution of biomass BC to total BC. This is consistent with the change observed in the 10-day air mass back trajectories computed from NOAA's HYSPLIT model (Figure 4.12) [*Draxler and Hess*, 1998]. Back trajectories

were plotted for every third day over the relative periods of interest. On some days, two trajectories separated by 6 hours were generated to look at small scale temporal variability.

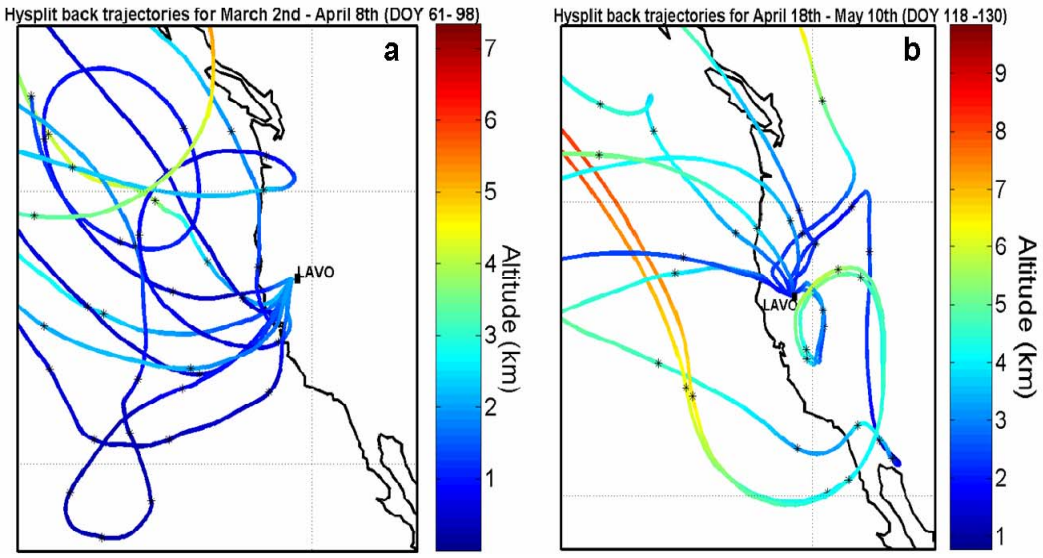

Figure 4.12. NOAA HYSPLIT back trajectories for Lassen Volcano National Park for a.) March 2 – April 8, 2006 and b.) April 18 – May 10, 2006. The source region for the aerosols in the early part of the study are predominantly southwest of LAVO, while in late April and early May, air masses predominantly originate from the north, northwest, and northeast of LAVO. Black dots represent 24 hour intervals.

Based both on the surface wind direction and the general trend in back-trajectories for the two periods, it is clear that the overall aerosol source region changed after April 15th. In March and early April, the back trajectories indicated that the regional aerosols impacting LAVO were strongly influenced by urban and industrial pollution from the San Francisco Bay Area and the I-5 corridor to the southwest of LAVO. For the later period, source regions were predominantly north, northeast, and northwest of LAVO where no significant source of urban pollution is located. As these air masses were arriving from significantly colder locales to the

north, it is possible that an increase in biomass burning from heating, as well as a decrease in urban pollution, would account for the apparent fractional increase in BC produced by biomass combustion. The general increase in ambient BC concentration during the latter part of the study was likely a result of dry weather, i.e. no rain or snow was periodically cleaning the air, combined with persistent stability (low wind speed), that allowed aerosol concentrations to rise at LAVO.

4.4 Radiative Impacts of BC in Snow

As previously mentioned, the concentration of BC in snow lowers the albedo of the snow pack, increases the amount of solar radiation absorbed in the surface layer, and possibly speeds the melt rate of snow. The key to understanding the link between BC concentration in snow and melt rate of snow is the sensitivity of the albedo to the BC. This is very difficult to measure. Previously mentioned radiation models [*Clarke and Noone*, 1985; *Flanner, et al.*, 2007; *Grenfell, et al.*, 2002; *Hansen and Nazarenko*, 2004; *Jacobson*, 2004] indicate that for fresh snow (snow crystal diameter ≈ 100 μm), albedo is reduced by approximately 1% for every 10 ng BC/g of snow (Figure 4.12). The average concentrations of BC measured in snow at LAVO and CSSL were 5.7 ng/g and 6.97 ng/g respectively, and ranged from 2.5 to 12 ng/g. Thus in order to detect the BC influence on albedo, measurements of snow albedo accurate to less than 1% would be required. A compilation of these model results places the BC measurements into context (Figure 4.13) and provides an estimate of potential impacts of BC in snow in the Southern Cascades and Sierra Nevada mountains.

The BC concentrations found in snow in the Sierras are sufficient to cause an initial albedo reduction between 0.3 and 1.2 %. The four model studies used in this analysis employed a similar snow crystal size (diameter ≈ 100 μm) and assumed either an internal mixture of BC and snow [*Hansen and Nazarenko*, 2004]; i.e. the BC particles are embedded inside the ice crystals rather than in between them, or a combination of internally and externally mixed BC [*Jacobson*, 2004]. Internal mixtures reduce albedo nearly twice as much as external mixtures [*Clarke and Noone*, 1985; *Hansen and Nazarenko*, 2004; *Jacobson*, 2004].

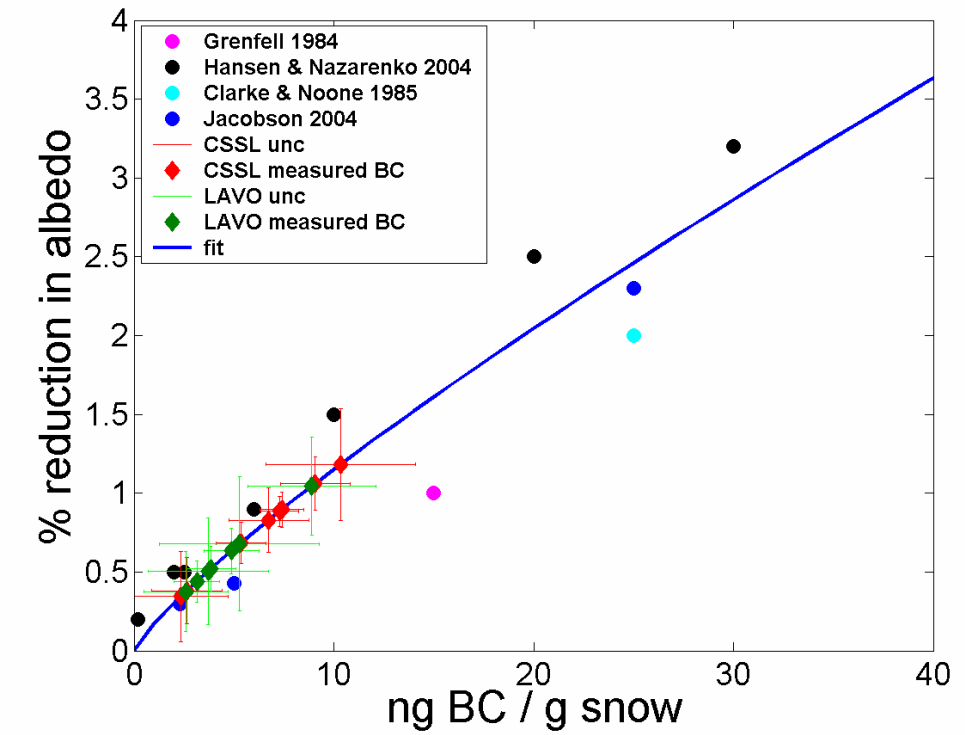

Figure 4.13. Measured BC concentration in snow at LAVO and CSSL are placed in context with the results from several modeling studies estimating the effect on snow surface albedo at $\lambda < 700$ nm.

Although there are many uncertainties associated with the effect of BC on snow albedo, these modeling studies provide a general estimate of how the measured

BC in the Sierra Nevada may potentially effect the snow melt. Employing the NCAR Column Radiation Model (CRM) , the hypothetical changes in albedo for $\lambda < 700$ nm are used to calculate the difference in absorbed short-wave radiation at the surface of the snow pack under clear skies and at latitude = 40°N and for March 24. Model results indicate that BC in snow has a negligible effect on albedo for wavelengths longer than 900 nm [*Jacobson*, 2004; *Warren and Wiscombe*, 1980]. The diurnally averaged shortwave solar radiation flux at the surface is approximately 292 W/m^2. The albedo for pure snow is prescribed at 0.97 [*Warren and Wiscombe*, 1980]. For reductions in albedo of 0.3% and 1.2%, the snow pack absorbs an additional 37 kJ/m^2 and 236 kJ/m^2, respectively, at the surface during one day. The latent heat of fusion for water is 334 J/g; thus the extra energy absorbed by the snow pack due to the presence of BC has the potential to melt an additional 110.8 mL to 706.2 mL per m^2 per day. This calculation represents a very rough estimate and does not take into account cloudy days, angle of snow surface to the incident radiation, differences in snow crystal size, uneven surfaces, and potential feedbacks. For example as the snow ages, the effective radius of the ice crystals grow and can amplify the BC absorption efficiency by a factor of three [*Flanner, et al.*, 2007; *Hansen and Nazarenko*, 2004; *Warren and Wiscombe*, 1980]. Furthermore, it has been suggested that BC may be left behind in the surface snow as the snow pack melts, effectively increasing the concentration and acting as a positive feedback in the melting process; however no observations of this phenomenon have been made available.

4.5 Conclusions

The average concentrations of BC in snow at the mountain sites were 5.7 ng/g at LAVO and 6.97 ng/g at CSSL, slightly higher than the average concentration of BC in rain water collected at Trinidad Head, 4.99 ng/g of water. The difference in BC concentration in snow between LAVO and CSSL was much smaller than expected based on their relative proximity to major sources. There are two explanations for this. First, during precipitation events, the predominant winds at LAVO are from the southwest and carry considerable pollution from the Central Valley, Sacramento, and San Francisco toward LAVO. Secondly, the total amount of precipitation falling at CSSL during March 2006 was about twice that at LAVO. When the dilution effect of heavy precipitation systems are taken into account, the total amount of BC removed from the atmosphere by snow at CSSL was on average 2.5 times greater than what was measured at LAVO. Similar measurements made by Chylek et al [1999] near Halifax, Nova Scotia showed that BC concentration in snow in rural Nova Scotia averaged 1.7 ± 0.83 ng/g, while urban snow near Halifax averaged 11 ± 7.7 ng/g of BC. The concentrations of BC found in the snow falling on the Sierra Nevadas and southern Cascades were therefore more typical of an urban environment, although very few measurements of this kind exist for comparison. The results from this study are based on 6 weeks of measurements taken at three sites in California. They suggest that BC has the potential to noticeably impact the snow pack; however more complete information about BC effects on California's snow pack will require a broader network of observation stations and longer time series of data.

A comparison between the BC concentration in snow water and the BC concentration in the air revealed no relationship; however when the total amount of BC mass removed by a precipitation event was compared with ambient BC concentration prior to the onset of the event, they correlated significantly with an R-squared value of 0.66. During precipitation events exceeding 10 mm, the atmospheric BC concentration dropped below the detection limit of the aethalometer. These two observations led to the conclusion that atmospheric BC is efficiently removed by snow and further, below cloud scavenging was the primary source for the BC in the snow sample water at LAVO during this study.

The observed ratio of excess fine potassium to BC indicates that approximately 76% of the BC found in the snow collected at LAVO during March, 2006 was from fossil fuel burning and the remaining 24% produced during biomass combustion, most likely residential heating. The predominantly southwesterly surface winds and the air mass back trajectories, pointed to Sacramento and San Francisco Bay area as a likely source of BC observed at LAVO. If the observed BC were produced locally (<100 km), the fractional contribution of biomass burning to BC should have been higher. In late April, when the winds shift and the back trajectories indicate regions to the north and east as dominant source locales for the observed aerosol, the BC from biomass burning nearly doubles to 48%. The gradual increase in observed ambient BC concentration is most likely due to the absence of wet removal, stable conditions, and low wind speeds.

Based on the results of several modeling studies, the BC concentration found in the snow at the mountain sites would lead to a reduction in surface albedo for fresh snow between 0.35 and 1.2% for wavelengths between 400 - 900 nm, assuming a snow crystal effective radius of 100 microns [*Flanner, et al.*, 2007; *Hansen and Nazarenko*, 2004]. This change in albedo leads to an additional 37 to 236 kJ/m^2 absorbed over one day by the snow pack for clear skies at this location and time of year. This result assumes that most of the BC particles are internally mixed in the ice crystals. All model results show that for larger snow crystals and aged snow the effectiveness of BC at reducing albedo and absorbing solar radiation increases dramatically. This could lead to a strong positive feedback in early springtime snow melt. Lastly, the effect of BC on snow in the Sierra Nevadas may be underestimated in this study due to dilution effect. Only the heaviest precipitation days provided a large enough sample to filter for BC. Lighter snow falls may contain higher concentrations of BC, which would be just as effective at lowering surface snow albedo as a heavy storm.

Previous studies [*Zhu, et al.*, 2007] have shown that the trans-Pacific transport of Asian pollutants, including significant amount of transported BC [*Hadley, et al.*, 2007], peaks in March and April. Dry deposition of BC during periods of atmospheric subsidence, when high altitude pollutants are more effectively transported to the surface may also play a role in reducing snow pack albedo. There are no chemical tracers that may be used to differentiate between combustion aerosols generated in North America, Asia, or any other region, so it is difficult to make any statements

regarding the influence of trans-Pacific transport of BC on mountain snow in California. Elemental fingerprints have been used to isolate soil dust from various regions around the globe [*Chow, et al.*, 2003; *Holmes and Zoller*, 1996; *Hsu, et al.*, 2005; *Labban, et al.*, 2004; *Shen, et al.*, 2007; *VanCuren, et al.*, 2005]. An analysis of the concentration of various crustal elements in precipitation water and the ambient atmosphere at the LAVO and CSSL sampling sites provided insight into the potential influence of long-range transport on mountain snow. Results from this analysis are discussed in Chapter 5.

References

Andreae, M. O. (1982), Marine Aerosol Chemistry at Cape Grim, Tasmania, and Townsville, Queensland, *Journal of Geophysical Research - Oceans and Atmospheres*, *87*, 8875-8885.

Andreae, M. O. (1983), Soot Carbon and Excess Fine Potassium - Long-Range Transport of Combustion-Derived Aerosols, *Science*, *220*, 1148-1151.

Arnott, W. P., K. Hamasha, H. Moosmuller, P. J. Sheridan, and J. A. Ogren (2005), Towards aerosol light-absorption measurements with a 7-wavelength Aethalometer: Evaluation with a photoacoustic instrument and 3-wavelength nephelometer, *Aerosol Sci Tech*, *39*, 17-29.

Bertschi, I. T., and D. A. Jaffe (2005), Long-range transport of ozone, carbon monoxide, and aerosols to the NE Pacific troposphere during the summer of 2003: Observations of smoke plumes from Asian boreal fires, *J Geophys Res-Atmos*, *110*, doi:10.1029/2004JD005135.

Bey, I., D. J. Jacob, J. A. Logan, and R. M. Yantosca (2001), Asian chemical outflow to the Pacific in spring: Origins, pathways, and budgets, *J Geophys Res-Atmos*, *106*, 23097-23113.

Chow, J., J. Watson, L. Ashbaugh, and K. Magliano (2003), Similarities and differences in PM10 chemical source profiles for geological dust from the San Joaquin Valley, California, *Atmos Environ a-Gen*, *37*, 1317-1340.

Chow, J. C., J. G. Watson, D. Crow, D. H. Lowenthal, and T. Merrifield (2001), Comparison of IMPROVE and NIOSH carbon measurements, *Aerosol Sci Tech*, *34*, 23-34.

Chylek, P., V. Ramaswamy, and V. Srivastava (1983), Albedo of Soot-Contaminated Snow, *J Geophys Res-Oc Atm*, *88*, 837-843.

Clarke, A. D., and K. J. Noone (1985), Soot in the Arctic Snowpack - a Cause for Perturbations in Radiative-Transfer, *Atmos Environ*, *19*, 2045-2053.

Coles, D. G., R. C. Ragaini, J. M. Ondov, G. L. Fisher, D. Silberman, and B. A. Prentice (1979), Chemical Studies of Stack Fly Ash from a Coal-Fired Power Plant, *Environ Sci Technol*, *13*, 455-459.

Conway, H., A. Gades, and C. F. Raymond (1996), Albedo of dirty snow during conditions of melt, *Water Resour Res*, *32*, 1713-1718.

de Gouw, J. A., et al. (2004), Chemical composition of air masses transported from Asia to the U. S. West Coast during ITCT 2K2: Fossil fuel combustion versus biomass-burning signatures, *J Geophys Res*, *109*, D23S20, doi:10.1029/2003JD004202.

Draxler, R. R., and G. D. Hess (1998), An overview of the HYSPLIT_4 modeling system for trajectories, dispersion, and deposition, *Australian Meteorological Magazine*, *47*, 295-308.

Fine, P. M., G. R. Cass, and B. R. T. Simoneit (2002), Chemical characterization of fine particle emissions from the fireplace combustion of woods grown in the southern United States, *Environ Sci Technol*, *36*, 1442-1451.

Flanner, M. G., C. S. Zender, J. T. Randerson, and P. J. Rasch (2007), Present-day climate forcing and response from black carbon in snow, *J Geophys Res-Atmos*, *112*, -.

Goldstein, A. H., et al. (2004), Impact of Asian emissions on observations at Trinidad Head, California, during ITCT 2K2, *J Geophys Res*, *109*, D23S17, doi:10.1029/2003JD004406.

Grenfell, T. C., B. Light, and M. Sturm (2002), Spatial distribution and radiative effects of soot in the snow and sea ice during the SHEBA experiment, *J Geophys Res-Oceans*, *107*, 8031, doi:8010.1029/2000JC000414.

Hadley, O. L., V. Ramanathan, G. R. Carmichael, Y. Tang, C. E. Corrigan, G. C. Roberts, and G. S. Mauger (2007), Trans-Pacific transport of black carbon and fine aerosols (D < 2.5 mu m) into North America, *J Geophys Res-Atmos*, *112*, D05309, doi:05310.01029/02006JD007632.

Hansen, A. D. A. (2003), *The Aethalometer*, Magee Scientific Company, Berkely CA.

Hansen, J., and L. Nazarenko (2004), Soot climate forcing via snow and ice albedos, *P Natl Acad Sci USA*, *101*, 423-428.

Heald, C. L., D. J. Jacob, R. J. Park, B. Alexander, T. D. Fairlie, R. M. Yantosca, and D. A. Chu (2006), Transpacific transport of Asian anthropogenic aerosols and its impact on surface air quality in the United States, *J Geophys Res-Atmos*, *111*, D14310, doi:14310.11029/12005JD006847.

Holmes, J., and W. Zoller (1996), The elemental signature of transported Asian dust at Mauna Loa observatory, *Tellus B*, *48*, 83-92.

Hsu, S. C., S. C. Liu, W. L. Jeng, F. J. Lin, Y. T. Huang, S. C. C. Lung, T. H. Liu, and J. Y. Tu (2005), Variations of Cd/Pb and Zn/Pb ratios in Taipei aerosols reflecting long-range transport or local pollution emissions, *Sci Total Environ*, *347*, 111-121.

Jacobson, M. Z. (2004), Climate response of fossil fuel and biofuel soot, accounting for soot's feedback to snow and sea ice albedo and emissivity, *J Geophys Res-Atmos*, *109*, D21201, doi:21210.21029/22004JD004945.

Jacobson, M. Z. (2007), The Effects of Agriculture and Snow Impurities on Climate and Air Pollution in California, edited, California Energy Commission.

Kingsmill, D. E., P. J. Neiman, F. M. Ralph, and A. B. White (2006), Synoptic and topographic variability of northern California precipitation characteristics in landfalling winter storms observed during CALJET, *Monthly Weather Review*, *134*, 2072-2094.

Labban, R., J. M. Veranth, J. C. Chow, J. L. P. Engelbrecht, and J. G. Watson (2004), Size and geographical variation in PM1, PM2.5 and PM10: Source profiles from soils in the western United States, *Water Air and Soil Pollution*, *157*, 13-31.

Liu, H. Y., D. J. Jacob, I. Bey, R. M. Yantosca, B. N. Duncan, and G. W. Sachse (2003), Transport pathways for Asian pollution outflow over the Pacific: Interannual and seasonal variations, *J Geophys Res-Atmos*, *108*, (D20), 8786, doi:8710.1029/2002JD003102.

Neiman, P. J., G. A. Wick, F. M. Ralph, B. E. Martner, A. B. White, and D. E. Kingsmill (2005), Wintertime nonbrightband rain in California and Oregon during CALJET and PACJET: Geographic, interannual, and synoptic variability, *Monthly Weather Review*, *133*, 1199-1223.

Painter, T. H., A. P. Barrett, C. C. Landry, J. C. Neff, M. Cassidy, C. R. Lawrence, K. E. McBride, and G. L. Farmer (2007), Impact of disturbed desert soils on duration of

mountain snow cover, *Geophys Res Lett*, *34*, L12502, doi:12510.11029/12007GL030284.

Park, R. J., et al. (2005), Export efficiency of black carbon aerosol in continental outflow: Global implications, *J Geophys Res-Atmos*, *110*, D11205, doi:11210.11029/12004JD005432.

Parrish, D. D., Y. Kondo, O. R. Cooper, C. A. Brock, D. A. Jaffe, M. Trainer, T. Ogawa, G. Hubler, and F. C. Fehsenfeld (2004), Intercontinental Transport and Chemical Transformation 2002 (ITCT 2K2) and Pacific Exploration of Asian Continental Emission (PEACE) experiments: An overview of the 2002 winter and spring intensives, *J Geophys Res-Atmos*, *109 (D23)*, D23S01, doi:10.1029/2004JD004980.

Shen, Z. X., J. J. Cao, R. Arimoto, R. J. Zhang, D. M. Jie, S. X. Liu, and C. S. Zhu (2007), Chemical composition and source characterization of spring aerosol over Horqin sand land in northeastern China, *J Geophys Res-Atmos*, *112*, doi:10.1029/2006JD007991.

Stohl, A. (2001), A 1-year Lagrangian "climatology" of airstreams in the Northern Hemisphere troposphere and lowermost stratosphere, *J Geophys Res-Atmos*, *106*, 7263-7279.

Turn, S. Q., B. M. Jenkins, J. C. Chow, L. C. Pritchett, D. Campbell, T. Cahill, and S. A. Whalen (1997), Elemental characterization of particulate matter emitted from biomass burning: Wind tunnel derived source profiles for herbaceous and wood fuels, *J Geophys Res-Atmos*, *102*, 3683-3699.

VanCuren, R. A., S. S. Cliff, K. D. Perry, and M. Jimenez-Cruz (2005), Asian continental aerosol persistence above the marine boundary layer over the eastern North Pacific: Continuous aerosol measurements from Intercontinental Transport and Chemical Transformation 2002 (ITCT 2K2), *J Geophys Res*, *110*, D09S90, doi:10.1029/2004JD004973.

Warren, S. G., and W. J. Wiscombe (1980), A Model for the Spectral Albedo of Snow.2. Snow Containing Atmospheric Aerosols, *J Atmos Sci*, *37*, 2734-2745.

Zhu, A., V. Ramanathan, F. Li, and D. Kim (2007), Dust plumes over the Pacific, Indian, and Atlantic oceans: Climatology and radiative impact, *J Geophys Res-Atmos*, *112*, D16208.

Chapter 5

Evidence of trans-Pacific Transport of Pollutants in Snow at Lassen Volcano National Park and Central Sierra Snow Laboratory

5.1 Introduction

Conclusions from the analysis completed during CIFEX (Cloud Indirect Forcing Experiment) and presented in Chapter 2 indicated that a significant amount of black carbon aerosol (BC) was transported from Asia to North America in March and April, 2004. At 2 km amsl (above mean sea level), the approximate elevation of LAVO (Lassen Volcano National Park) and CSSL (Central Sierra Snow Laboratory), the modeled fractional contribution of Asian BC to total BC mass was on average about 40 to 50% [*Hadley, et al.*, 2007]. BC measurements from IMPROVE (Interagency Monitoring for Protected Visual Environments) aerosol observatories located at elevations above 1000 km compared well with the modeled BC mass [*Hadley, et al.*, 2007]. Numerous studies have shown that typical meteorological conditions in the spring, along with a peak in Asian dust storms, enhances trans-Pacific transport of dust and pollutants from Asia to North America [*Bertschi and Jaffe*, 2005; *Bey, et al.*, 2001; *de Gouw, et al.*, 2004; *Goldstein, et al.*, 2004; *Heald, et al.*, 2006; *Jaffe, et al.*, 2005; *Liang, et al.*, 2004; *Liu, et al.*, 2003]. The timing of this enhanced transport occurs when the melt rate of the California snow pack is most sensitive to albedo reductions from BC in snow. Earlier in the year, the temperatures in the mountains are cold enough that the additional energy absorbed by the snow,

because of the lower albedo, is not sufficient to overcome the thermal barrier to cause melt. Later in the spring, warm ambient temperatures dominate the melt rate, and the increase in absorbed short wave radiation ($\lambda < 900$ nm) due to the BC will be negligible compared to absorbed long wave radiation ($\lambda > 900$ nm). Water, in any form, is an efficient absorber of infrared radiation.

Results from Chapter 4 showed that below cloud scavenging during snow or rain events was the dominant source of BC measured in the snow collected at LAVO. Nearly all precipitation events were associated with cyclonic rotation, characterized by winds from the southwest, which point to Sacramento and the San Francisco Bay Area as a likely source of regional, anthropogenic aerosol in the snow at LAVO, as well as at CSSL. Determining the relative contribution from trans-Pacific transport of Asian dust and BC mass to the total observed mass at LAVO in March and April 2006 was accomplished using the relative mass of Fe (iron) to Ca (calcium).

A previous study showed that the mass ratio of Fe to Ca observed in aerosols on the west coast of North America is an excellent indicator of North American vs. Asian dust [*VanCuren, et al.*, 2005]. VanCuren et al., [2005] found that dust samples in which the PM2.5 Ca mass was equal to or exceeded the Fe mass characterized Asian dust well (Figure 5.1). In North American dust, the Fe mass fraction of the PM2.5 tended to be twice that of Ca or higher. Results from several elemental Asian dust characterization studies showed that the mass ratio of Fe to Ca ranges from 0.5 to 1 in Asian dust and pollution aerosols measured in China, Korea, and Hawaii [*Holmes and Zoller*, 1996; *Krueger, et al.*, 2004; *Park, et al.*, 2007; *Shen, et al.*, 2007; *Sun, et*

al., 2005]. The highest ratios of Fe/Ca in Asian dust were measured near the Horquin Sand Land in China and in Northern Mongolia [*Shen, et al.*, 2007; *Sun, et al.*, 2005], where the average Fe/Ca was approximately equal to 1. Compared with other dust sources in China, particles generated from cold fronts moving across the Taklimakan Desert have been identified as those most frequently lofted to altitudes where they are transported through the free troposphere to the Western United States [*Sun, et al.*,

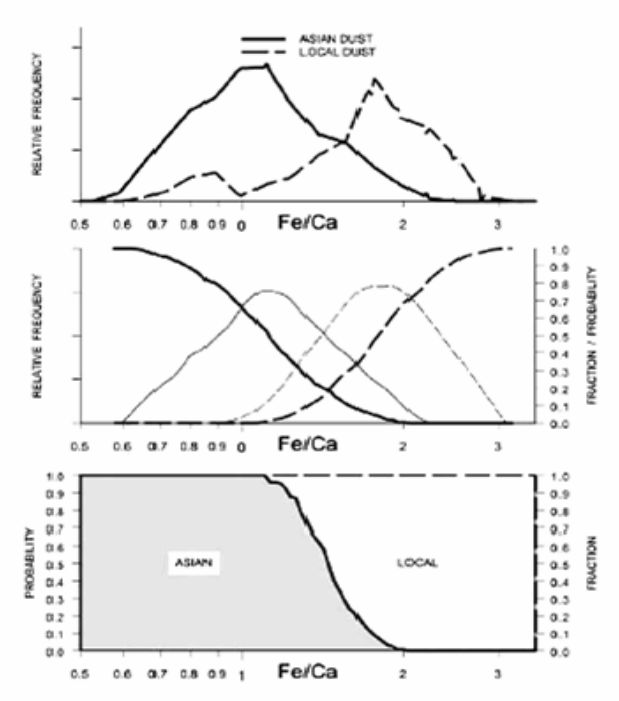

Figure 5.1. *"Bayesian mixing model for Asian and local dust. (top) Curves of frequency distributions for Fe/Ca ratios for 501 Asian dust events (solid line) and 100 local dust samples (dashed line); area under both curves equals 100%.Frequency distributions smoothed and adjusted for cross-contamination plotted with resulting cumulative frequency curves. (bottom) Bayesian probability that a sample having a particular Fe/Ca ratio is part of the Asian or local distribution (left y axis); the mixing model interprets the relative probabilities at each Fe/Ca value as fractional contributions from the two populations (right y axis)."* Taken from VanCuren et. al. [2005].

2001]. The ratio of Fe to Ca in dust from the Taklimakan desert is roughly 0.5 [*Sun, et al.*, 2005]. A dust characterization study for the San Joaquin Valley, California revealed that the Fe to Ca ratio is around 2 for agricultural dust, 0.9 for dust produced by dairy and cattle farms, and 1.3 for paved and unpaved roads [*Chow, et al.*, 2003]. These sources represent the major regional contribution to dust generation west of LAVO. South and east of LAVO there are several large dry lake beds and deserts that produce dust aerosol with a Ca content about 4 times greater than Fe [*Chow, et al.*, 2003; *Labban, et al.*, 2004]. Based on predominant surface winds and calculated back trajectories, dust from these regions rarely impact LAVO and the western slopes of the Sierra Nevada in the spring months. Furthermore, the annual Fe/Ca observed in the PM2.5 fluctuated around a value of 1 in the winter and spring when local and regional dust emissions were very low; however in July through September when local and

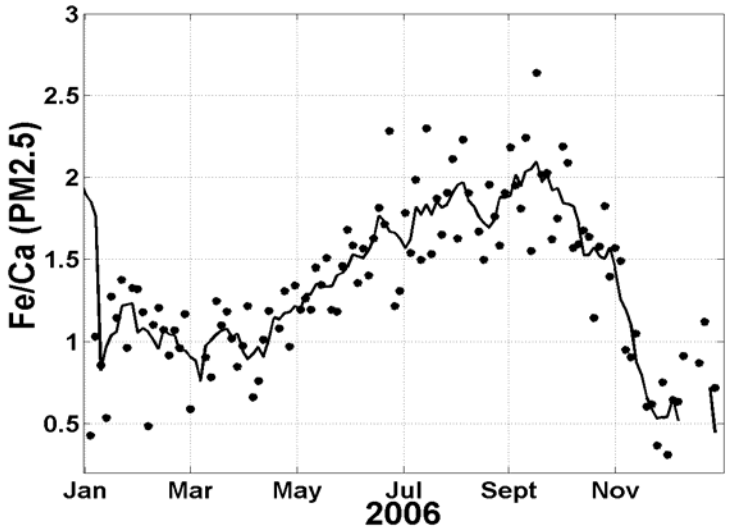

Figure 5.2 Annual cycle of the Fe/Ca ratio observed at LAVO taken from the IMPROVE data network. Solid line is a 5 point running average.

regional dust emissions were highest the Fe/Ca ratios were generally much closer to 2 (Figure 5.2). This annual signal combined with previous measurements of elemental composition of dust in both Asia and North America validated use of the PM2.5 Fe/Ca ratio as a qualitative fingerprint for Asian dust.

This chapter presents the results of an analysis of the elemental aerosol and precipitation composition at CSSL and LAVO, where evidence of trans-Pacific transport was observed in both the surface aerosols and in the collected snow samples. In addition, the fractional contribution from transported Asian dust and BC aerosol mass to the aerosol observed at LAVO was estimated for March and early April. The elemental composition of the observed aerosol, the aerosol mass distribution vs. particle diameter, air mass back trajectories, and local meteorology together allowed aerosol sources to be identified despite complications due to mixing of aerosols from multiple sources. In addition to the general analysis of the data from both LAVO and CSSL, three periods at LAVO were identified as having unique elemental partitioning at different size modes and were therefore examined in greater detail and presented as case studies.

5.2 Results

In April and May of 2002, as part of the ITCT 2K2 (Intercontinental Transport and Chemical Transformation 2002) experiment, Van Curen et al., [2005] found that for trans-Pacific transport of dust from Asia to North America, the ratio of Fe to Ca for PM2.5 aerosols was below one. When the Fe to Ca ratio exceeded two, the dust was

identified as exclusively North American. Observations at LAVO during the ITCT 2K2 study showed that most of the time the PM2.5 ratio of Fe to Ca, fell between 1 and 2, indicating of a mixture of local and Asian dust sources [*VanCuren, et al.*, 2005]. The analysis presented here, used the same approach as VanCuren et al. [2005] to separate Asian dust from regionally produced dust. Air mass back trajectories, calculated with the NOAA HYSPLIT (HYbrid Single-Particle Lagrangian Integrated Trajectory) model [*Draxler and Hess*, 1998], and surface winds were used to identify times when Ca rich dust sources east of the measurement sites may have impacted the observation sites. The assumption was made that the largest fraction of regional dust observed in the mountains was from agricultural soils. This was based on two factors: 1.) precipitation in Northern and Central California was record breaking in March 2006 and therefore passive dust emissions from dry roads and cattle farms would have been greatly reduced and 2.) an increase of agricultural plowing in March and April, as farmers prepared to plant crops, would have tended to generate more agricultural dust relative to passive generation (as observed by the author during the field collection phase).

5.2.1 General Analysis and Results from LAVO and CSSL

XRF (X-ray fluorescence spectroscopy) analysis of aerosols collected at LAVO and CSSL in the spring of 2006 (Chapter 4) produced similar results to those from the ITCT 2K2 study. The PM2.5 Fe to Ca ratio usually between 1 and 2 (Figure 5.1 shaded regions), indicating mixed Asian and North American dust, with exception

to the period between February 20th and March 11th (DoY 58 – 70), when the PM2.5 Fe/Ca at LAVO was near or below one, indicating that the background dust aerosol was almost entirely transported from Asia. The Fe/Ca ratio observed in the PM10, PM2.5 and PM1.0 size fractions at LAVO were often very different from one another (Figure 5.1a) and since the elemental composition of dust from a unique source is generally consistent for all size modes [*Andreae*, 1983; *Holmes and Zoller*, 1996; *Labban, et al.*, 2004; *Mori, et al.*, 2003], the size segregated elemental composition of crustal aerosols observed at LAVO represented a mixture of dust from multiple sources. The elemental composition of the aerosol found in the snow samples were indicative of the aerosol composition at higher altitudes and generally compared well with the PM2.5 and PM1.0 Fe/Ca ratios (Figure 5.3 & 5.4). This is consistent with

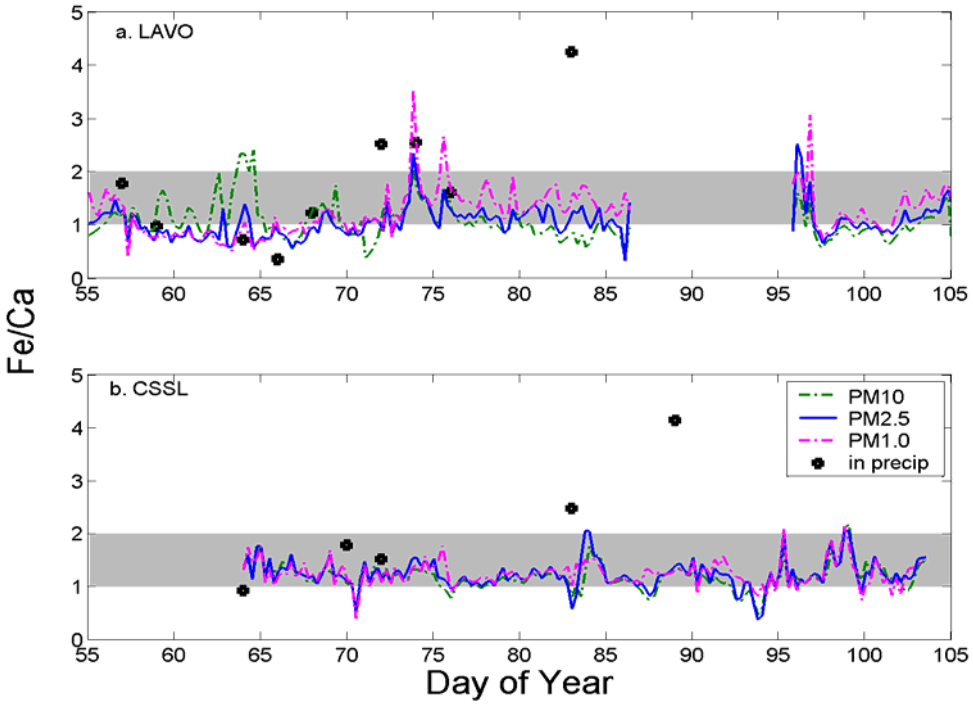

Figure 5.3 Fe/Ca ratios for PM10, PM2.5, PM1.0 ambient aerosols, as well as in the precipitation, at a.) LAVO and b.) CSSL

aerosol physics, as gravitational settling tends to confine the largest particles to the lowest atmospheric layers. Although soil dust is generally the primary source of both Ca and Fe, fine particulate Fe may also be found in biomass burning aerosol, as well as from certain fossil fuel combustion processes [*Luo, et al.*, 2008]. Marine generated aerosol are an alternate source for Ca, which accounts for about 1% of the total sea salt mass [*White*, 2008].

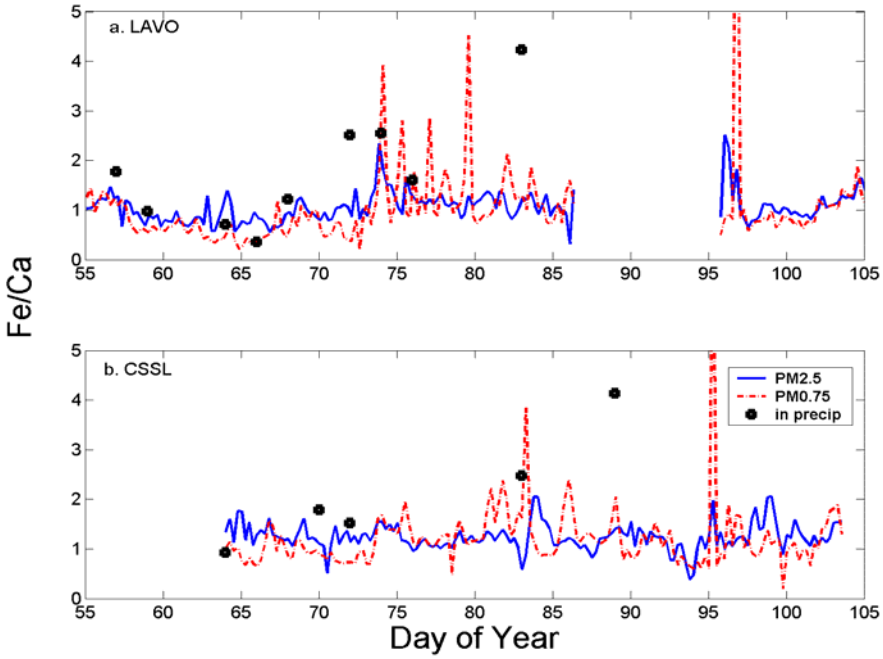

Figure 5.4 Ratio of Fe/Ca in PM2.5 and PM0.75 at a.) LAVO and b.) CSSL

The same analysis for CSSL revealed a different picture. Unlike at LAVO, the ratio of Fe to Ca was consistent between the different size modes for the entire study period (Figure 5.3b), and was rarely below one or greater than two. If, for example, the high Fe concentration, periodically observed in the LAVO PM1.0 aerosol (Figure 5.3a), was due to mixing with urban pollution or biomass burning plumes, then fine

mode aerosols at CSSL should also have been enriched in Fe, as HYSPLIT back trajectories indicated that this site was likely impacted by pollution from the same urban regions as LAVO. The considerable amount of residential burning observed near the CSSL site would have contributed Fe rich particles from biomass burning emissions as well. Enrichment in the PM1.0 Fe, relative to Ca, was not evident in the data (Figure 5.3 b). A plausible explanation for this discrepancy lies in the relative aerosol mass concentration in the different size modes at LAVO and CSSL. The ambient PM2.5 mass concentrations for Fe and Ca were about 4.5 times greater, on average, at CSSL than at LAVO. In comparison the PM0.75 Fe and Ca was only 2.5 and 2 times greater, respectively, at CSSL. The ratio of Fe to Ca for PM0.75 aerosols for LAVO and CSSL are shown in Figure 5.4 (a&b). Significant, episodic, enrichment in PM0.75 Fe was observed at both sites after March 15th (DoY = 74). The higher concentration of dust aerosol swamped the contribution of fine mode Fe from sources other than dust at CSSL (compared to LAVO). Peaks in the PM1.0 and PM0.75 Fe/Ca ratios, reaching values as high as 3 or 4, were observed periodically at both CSSL and LAVO (Figure 5.4). Throughout March and April, the PM0.75 Fe was significantly correlated to the excess fine potassium[1]: R^2 = 0.47 at LAVO and R^2 = 0.3 at CSSL, indicating that biomass burning was a likely contributor to the episodic enhancement of Fe concentration in the fine mode (Figure 5.5).

[1] The excess fine potassium and its relevance to biomass burning were described in Chapter 4.

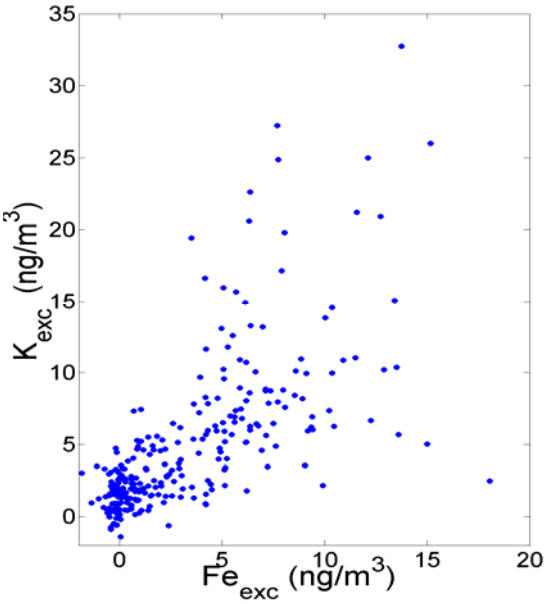

Figure 5.5. The excess fine Fe vs. the excess fine K.

Both the PM10 and PM1.0 Fe and Ca mass were highly correlated with one another at each site, although less so at LAVO, which confirming that nearly all of the Fe and Ca observed at both of these sites was from soil dust [*Eldred, et al.*, 1997]. The day to day PM10 and PM1.0 Fe and Ca concentrations between LAVO and CSSL were also significantly correlated at R^2 values ranging from 0.25 to 0.37. (Figure 5.6). Although a correlation between aerosol mass concentrations separated by hundreds of km can be indicative of long range transport [*VanCuren and Cahill*, 2002], it is more likely in this case, that the same regional meteorology controlled aerosol variability at CSSL and LAVO. The daily precipitation at both locations was highly correlated; R^2 = 0.64 (Figure 5.7), which more than accounts for the similar variability observed at the two sites. Furthermore, the ratio of Fe/Ca at both sites showed no correlation at all, which would be expected if both sites were impacted by the same aerosol.

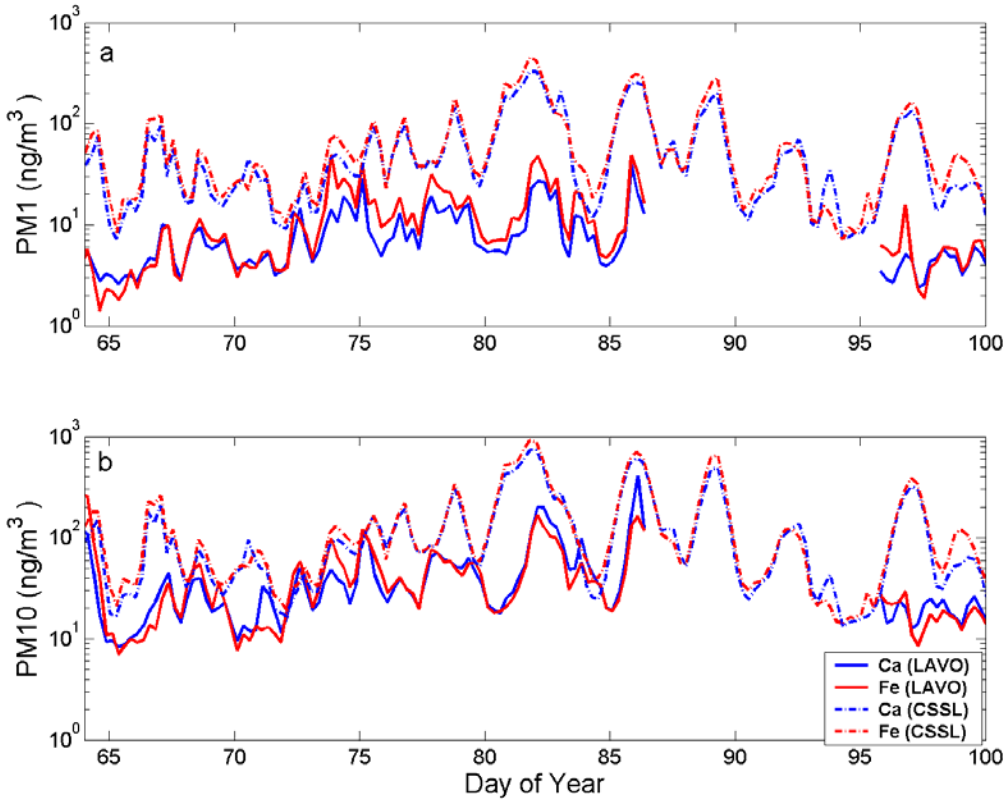

Figure 5.6. Total mass concentration for a.) PM1.0 and b.) PM10 at LAVO (solid line) and CSSL (dashed line).

In general, the Fe and Ca fractional composition of aerosol at LAVO and CSSL indicated that the observed dust in the mountains during this study was predominantly Asian combined with a smaller fraction of regional dust. This was based on two observations: 1.) the PM2.5 ratio of Fe/Ca, while often greater than one, was still usually quite low (< 1.5), indicating an Asian dust signature and 2.) compared to Asian dust emissions, the persistent rain and snow in Northern California during this study would have almost entirely suppressed regional dust emissions. Mixing with Fe from industrial emissions or biomass burning may have periodically enhanced the Fe PM0.75 mass at both sites. The abrupt and short lived duration of the fine mode Fe enhancement, suggested that the source of the excess fine Fe was local or regional.

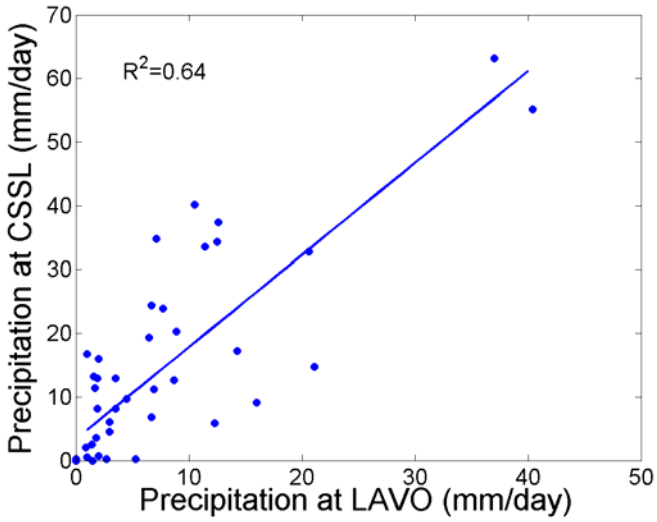

Figure 5.7 Scatter plot of precipitation at CSSL vs. LAVO.

Based on the Fe/Ca ratio observed in the aerosol at LAVO and CSSL, an estimate of relative contribution of East Asian PM2.5 dust to the total observed PM2.5 dust was established. The total PM2.5 soil mass was calculated using the XRF elemental data and equation 2.1 [Eldred, et al., 1997]. The Asian dust fraction was assessed using the following assumptions: when the Fe/Ca ratio was greater than or equal to 2, the fractional contribution was zero, when the Fe/Ca ratio was less than or equal to 1, the fractional contribution was 1, finally when Fe/Ca ratio was between 1 and 2, the fractional contribution was scaled linearly [*VanCuren, et al.*, 2005], i.e, a Fe/Ca ratio of 1.3 corresponds to a fractional contribution of Asian dust equal to 0.7. Previous aerosol analysis of the relative composition of aerosols exported from Asia showed that the average BC, or EC, mass in the spring was approximately equal to 8 to 10% of the PM2.5 soil dust mass [*Shen, et al.*, 2007; *Yang, et al.*, 2005]. Assuming that a proportionate amount of Asian BC is transported along with the dust, a rough

estimate of the relative contribution of Asian BC to the total observed BC was made at LAVO during March and early April (Figure 5.8). This analysis was not extended to later dates, as wind direction and back trajectory analysis indicated a strong potential for Ca rich North American dust sources (Chapter 4), thereby invalidating the calculation. The estimated average Asian BC contribution to total average observed BC for the period shown was 33 – 40%, slightly lower than the CFORS model estimated contribution at this altitude and location in the spring of 2004 (Chapter 2) [*Hadley, et al.*, 2007], which was 40 to 50%. The average contribution of Asian dust to the total dust during this same time period was on average, 87% +/- 18%.

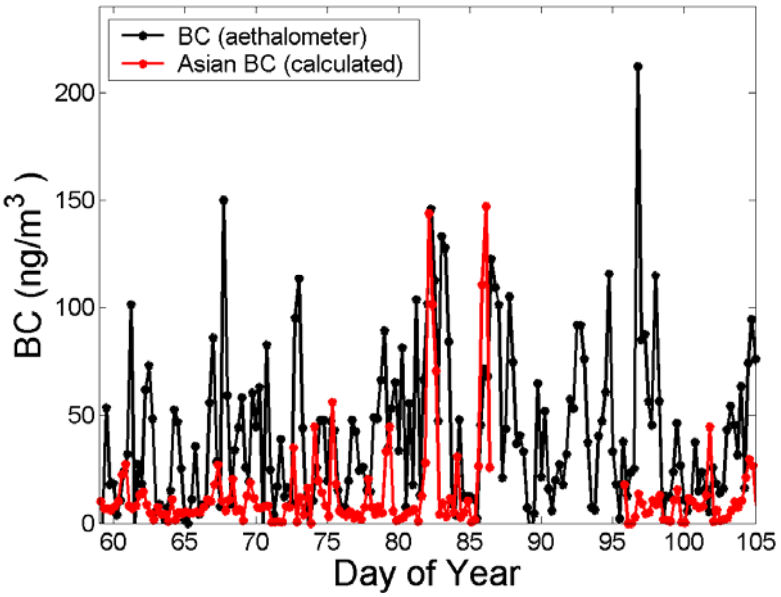

Figure 5.8 Estimate of the Asian BC compared to total BC observed at LAVO, using an Asian BC/dust ratio equal to 0.1.

Three case studies, each spanning two days, examine aerosol and meteorological observations at LAVO in the following section. The dates for each of

the case studies were chosen based on the following criteria: an XRF analysis of a precipitation sample was available, the fractional elemental composition of PM10 and PM1.0 exhibited unique characteristics, and lastly, PM10 mass concentration exceeded 50 μg/m^3 at least once. These case studies provide insight into the different mechanisms by which Asian aerosols are transported to the surface.

5.2.2 Case studies at LAVO

Both the ambient aerosol and that measured in the snow samples exhibited distinct signatures in elemental composition during three different periods at LAVO. The first, on March 5th, was characterized by an initial peak in the PM10 Fe/Ca ratio greater than 2, while the PM2.5 and PM1.0 Fe to Ca ratio was generally below 1. Fe/Ca was also less than one in the snow water samples collected on this day. The fractional composition of the different size modes is important for determining if aerosols are generated nearby or transported from further away to the observation location. This results from the preferential transport of smaller aerosols, as larger particles are more quickly removed due to gravitational settling [*Mori, et al.*, 2003] and more efficient scavenging by precipitation [*Henzing, et al.*, 2006]. Therefore for coarse mode aerosols, likely source regions are located closer to the observation site, while for smaller particles the source regions may be great distances from where observations are made. The ambient Fe to Ca ratio during the second time of interest, March 14^{th} - 15^{th}, peaked at a value greater than two and maintained a nearly uniform value at all size modes. Measurements of the Fe and Ca in the snow water collected on

this day compared well with the ambient measurement. The last day, March 23rd, was marked by a low (<1) Fe to Ca ratio in the ambient PM10, whereas the Fe was significantly enriched in the fine size mode (PM1.0), peaking at two times the amount of Ca. The Fe mass exceeded the Ca by over a factor of 4 in the snow water on this day. All of these events included a snow event that was collected and analyzed. The differences in the chemical signature of the aerosols, prior to and following each snow event, rule out elemental selectivity during wet removal as an explanation for the observed changes.

5.2.2.1 Case 1: March 5th, 2006

On March 4th and 5th, 2006, the relative fractional contribution of Fe and Ca to the total mass concentrations of the PM1.0 and PM10 aerosol observed at LAVO were different (Figure 5.9). On March 4th, the PM10 Fe to Ca ratio rose from just below 1 to nearly 2.5, while the PM1.0 Fe/Ca ratio went only from 0.5 to 1. When snow began falling on March 5th, both the Fe and Ca returned to the original concentrations observed early on March 4th. As previously stated, the elemental composition of dust is generally not size segregated, which therefore suggests that most of the fine mode (PM1.0) aerosol was composed of a different aerosol than in the coarse mode. The Fe to Ca ratio measured in the snow water collected on March 5th was 0.71, closely matching the ratio observed in the PM1.0 ambient aerosol before and during the snow event. This was evidence that most of the aerosol removed by the snow was from the same source as, or at least similar to, the Ca rich fine mode aerosol observed at the

ground. The total magnitude of the PM10 mass was much greater than the PM1.0, so in order for the fine mode aerosol to dominate in the wash out, there must have been significantly more of the PM1.0 aerosol at higher altitudes than the Fe rich PM10. Thus the Ca rich PM1.0 represented a large scale back ground aerosol that extended to high elevations, while the Fe rich coarse dust was confined to only the lowest layers of the atmosphere.

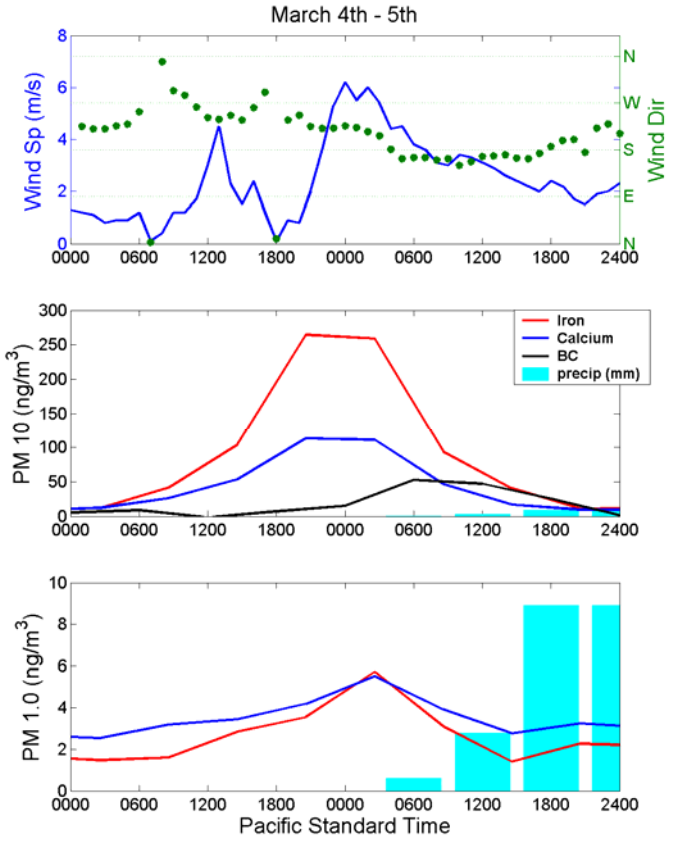

Figure 5.9 Top panel: wind speed (green) and wind direction (blue) Center and bottom panels: Mass concentrations of Fe, Ca, and BC measured at LAVO on March 4th and 5th in the coarse (PM10) and fine (PM1.0) mode respectively.

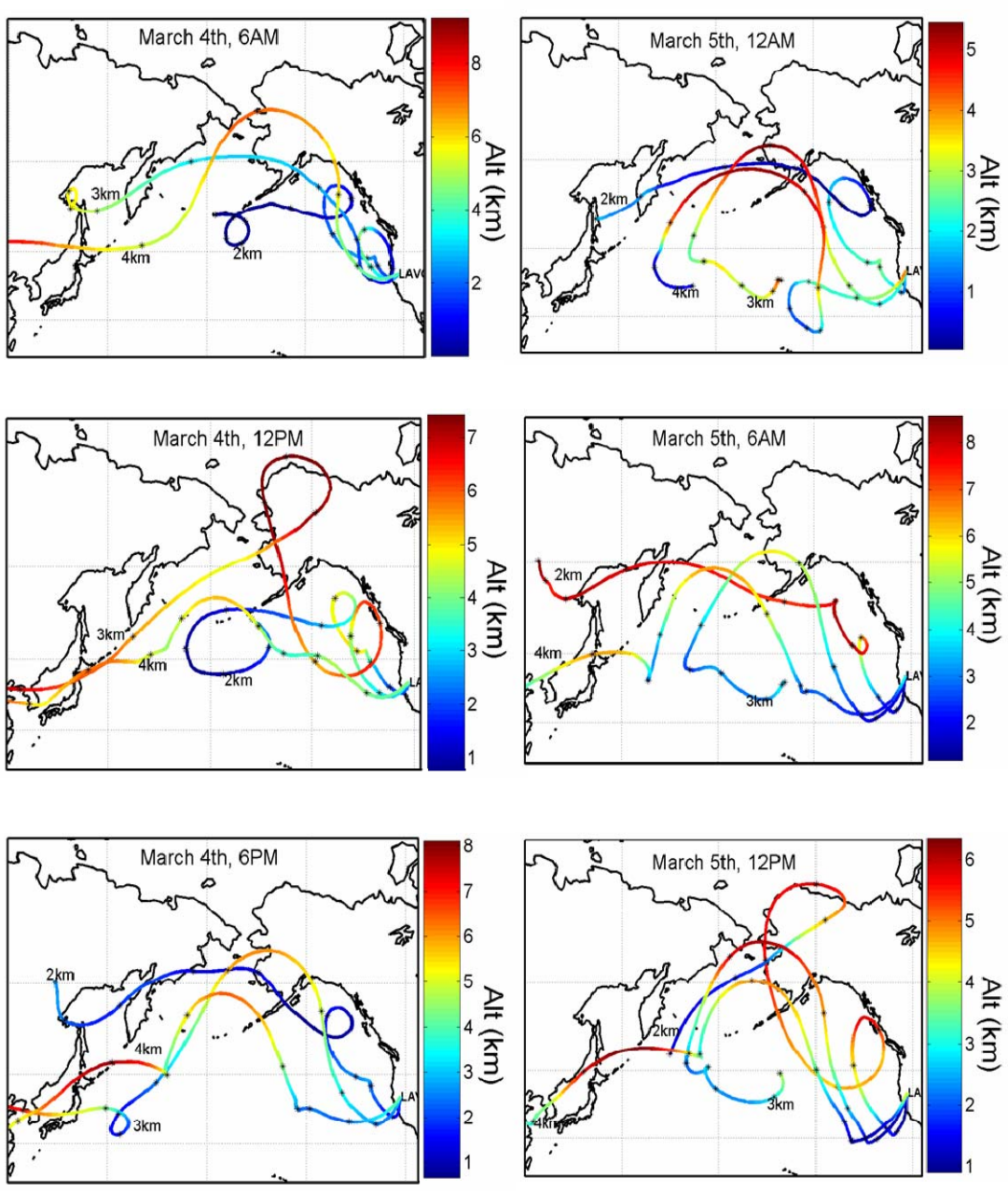

Figure 5.10 NOAA HYSPLIT 10-day air mass back trajectories for March 4th and 5th. Trajectories are shown for air masses arriving at altitudes of 2 km, 3 km, and 4 km amsl over LAVO.

An analysis of the HYSPLIT 10-day air mass back trajectories and the local wind speed and direction provided evidence that both locally (or regionally) generated

dust and a background of transported East Asian fine dust were observed at LAVO during these two days. Initial PM10 aerosol concentrations were low and the Fe/Ca was below 1. As the surface wind direction changed from southwesterly to southerly and wind speed increased to over 6 m/s, the PM10 Fe mass concentration increased by over a factor of 20, while the PM10 Ca mass concentration rose by less than half that amount (Figure 5.9). PM1.0 Fe and Ca increased only by a factor of 4 and 2, a very slight change compared to the PM10. Figure 5.10 shows the 10-day back trajectories for air masses arriving at 2, 3, and 4 km over LAVO at 6AM, 12PM, 6PM, on March 4th and 12AM, 6AM and 12PM on March 5th. The back trajectories indicated that the source regions for these air masses were highly variable, both vertically and temporally, and revealed both East Asian transport pathways, as well as purely marine trajectories originating in the Pacific Ocean. These trajectories clearly showed the potential for long range transport from East Asia in one or more of the layers for each hour shown. The conclusion was therefore drawn that transported fine mode dust from East Asia represented a continuous background aerosol throughout this time period, and that the spike in PM10 dust was a localized event. Average wind speeds over 6m/s, coinciding with the large spike in PM10 Fe, are consistent with the generation of local wind blown dust.

The HYSPLIT 10 day, air mass back trajectories, meteorological data, and the elemental composition of the ambient aerosol and the aerosol removed in the snow provided evidence that, while locally generated dust was observed in the lower atmosphere, transported East Asian fine mode dust was also present, both at the

ground and at higher altitudes. Furthermore, the total aerosol removed by the snow was best represented chemically, by the fine mode, transported aerosol, which means that at higher altitudes the concentration of this fine mode aerosol had to be large enough to completely overwhelm the scavenged contribution of the ground aerosol in the sample. This finding is significant, as it showed that although transported aerosols may be obscured by regional and local pollutants in ground based observations; they can still have more influence on snow falling in the California mountain ranges, than the aerosol observed near the ground. The BC mass concentration showed no correlation to either the Fe or Ca in the fine or coarse mode, and was therefore likely from a source unrelated to either the locally generated dust or the transported dust.

5.2.2.2 Case 2: March 14th - 15th, 2006

The second period of interest was on March 14th and 15th. These two days were marked by light snow flurries, which occurred intermittently throughout the two days, but did not appear to affect the aerosol mass concentration in either the coarse or fine size mode (Figure 5.11). On March 14th, the concentration of PM10 and PM1.0 Fe increased by factors of 4 and 10 respectively. Relative to the Fe, the Ca mass went up only slightly. Unlike in the previous analysis, the large spike in Fe, peaking at roughly 9PM on March 14th, was more drastic in the fine mode than in the coarse mode. Both PM1.0 and PM10 Fe/Ca ratios were greater than 2, indicating a local or regional dust source, based on previously described criteria. Other than the enhanced Fe concentration in the PM1.0 at 9 PM, the Fe/Ca ratio remained consistent between both

size modes for the rest of the period at 1.2 to 1.5, indicative of a well mixed Asian/marine/regional background aerosol.

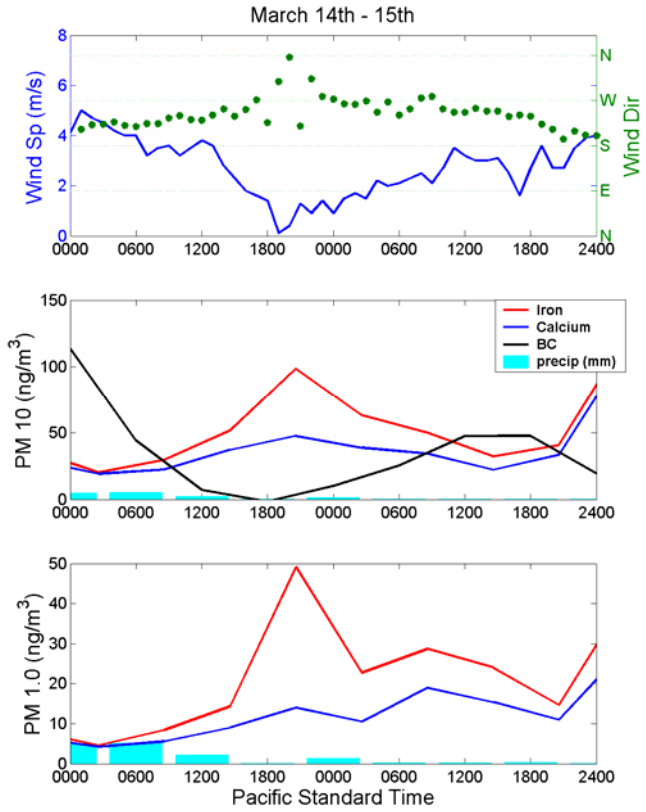

Figure 5.11. Top panel: wind speed (green) and wind direction (blue) Center and bottom panels: Mass concentrations of Fe, Ca, and BC measured at LAVO on March 14th and 15th in the coarse (PM10) and fine (PM1.0) mode respectively.

In contrast to the first case study, the spike in coarse and fine mode aerosol mass was not associated with an increase in surface wind speed, but rather a decrease to almost no wind speeds (Figure 5.11, top panel). Steady southwesterly surface wind direction switched to westerly and northwesterly as wind speed dropped and aerosol

concentration rose. The HYSPLIT 10-day back trajectories for March 14th, 12PM to March 15th 12AM (Figure 5.12) showed uniform trajectories from the west with respect to the three altitudes. The air masses at 2km, 3km, and 4km arriving over

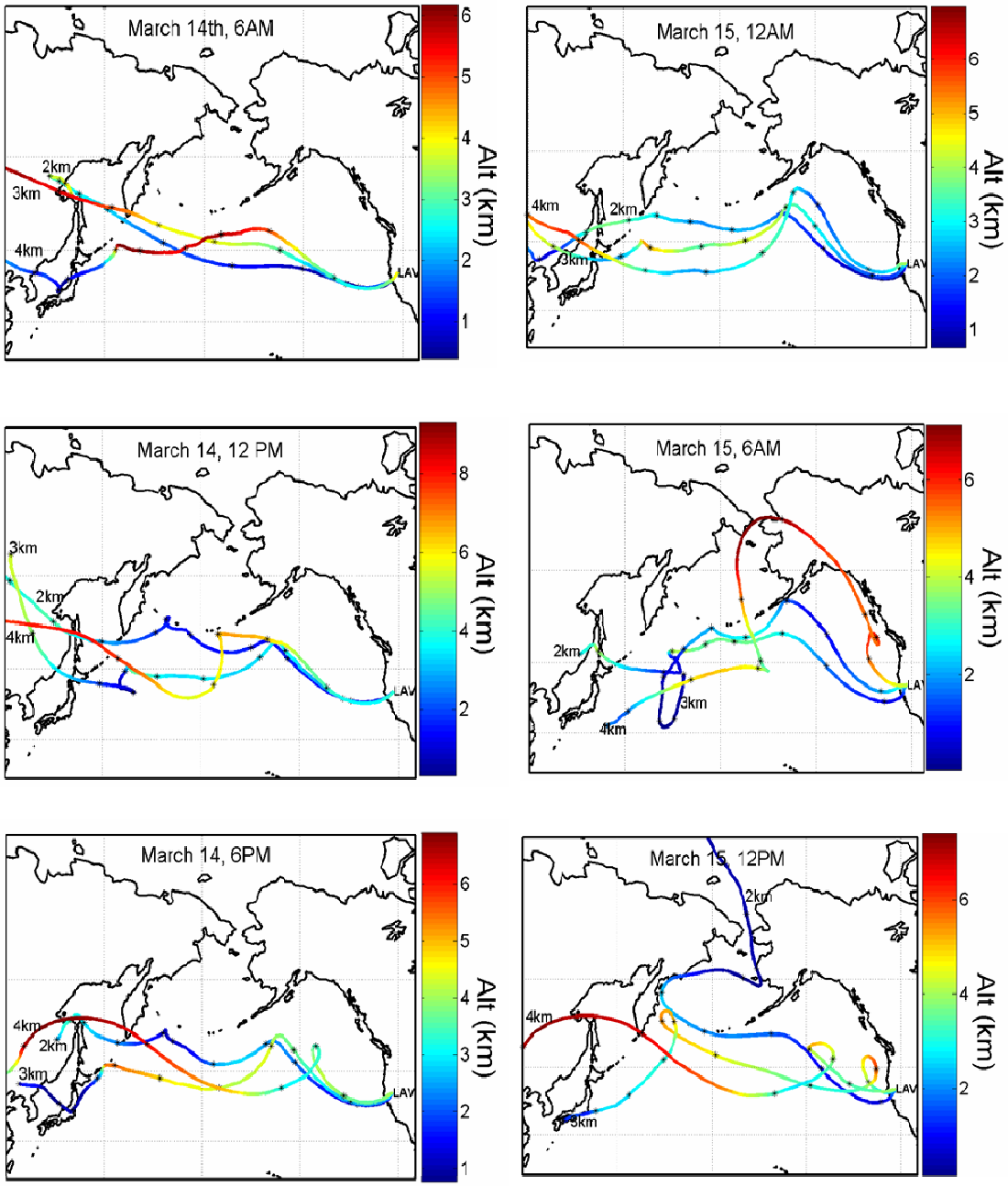

Figure 5.12. NOAA HYSPLIT 10-day air mass back trajectories for March 14th and 15th. Trajectories are shown for air masses arriving at altitudes of 2 km, 3 km, and 4 km amsl over LAVO.

LAVO exhibited almost no vertical variability in the day and a half prior to arrival over LAVO. Almost right above LAVO, a slight upward vertical motion of 2 or 3 hundred meters was observed in the lower 2 and 3 km trajectories. This was most likely from orographic effects of the mountains, accounting for the light snow events observed throughout both days. For orographically induced precipitation, the aerosols measured in the surface air would have had the same source as those in the clouds, as well as the aerosols scavenged by the snow. The XRF analysis of the snow water yielded a Fe/Ca ratio of 2.6, comparable with the ambient aerosol Fe/Ca ratio at the peak concentration. Although back trajectory calculations indicate a strong possibility of trans-Pacific transport; atmospheric stability, characterized by low wind speeds, would have limited the transport of these aerosols to the lower altitudes. Elemental composition of the aerosols pointed to a predominantly North American source mixed with a low concentration of background dust transported from East Asia. Again there appeared to be no connection between the dust and the BC concentration.

5.2.2.3 Case 3: March 23rd - 24th, 2006

The final case study was for March 23rd through March 24th. This period began with enhanced aerosol concentration followed by precipitation and a decrease in measured ambient aerosol mass. As with the first case, the relative concentration of Fe and Ca in the fine and coarse mode were quite different. Unlike the first case study however; this time the PM10 aerosol was enriched in Ca relative to Fe, typically an indication of Asian dust (Figure 5.13). The PM1.0 aerosol, however, was enriched in

Fe relative to Ca, which would not be expected in fine mode dust aerosol from transported from East Asia.

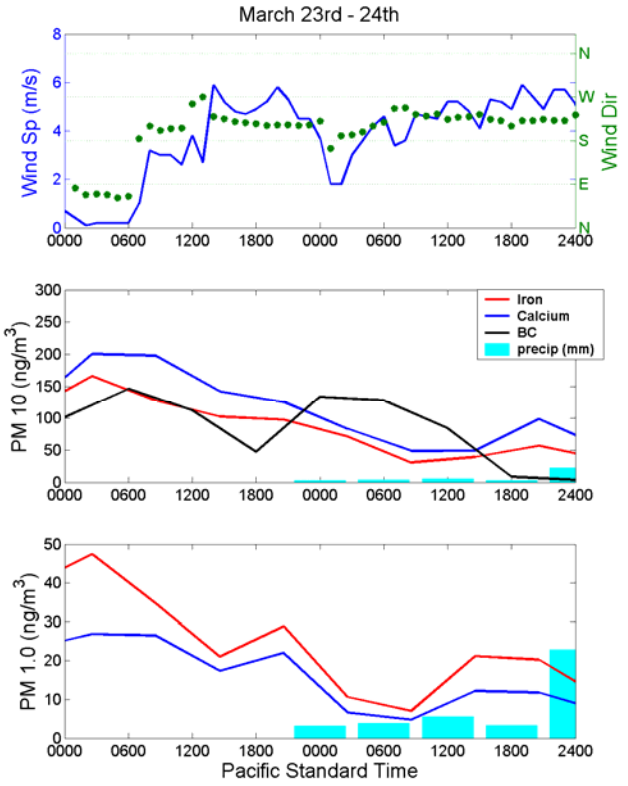

Figure 5.13 Top panel: wind speed (green) and wind direction (blue) Center and bottom panels: Mass concentrations of Fe, Ca, and Cl measured at LAVO on March 23rd and 24th in the coarse (PM10) and fine (PM1.0) mode respectively.

The highest aerosol concentrations occurred early on March 23rd. This maximum coincided with light winds blowing from the east (Figure 5.13, top panel). Low wind speed and easterly flow at this time of day at LAVO most likely represented nocturnal, cold air drainage down the mountain slope. This low-level boundary layer

process would not have been resolved by the HYSPLIT model and there was no evidence of easterly surface flow in the calculated 10-day air mass back trajectories (Figure 5.14). As previously mentioned, dry deserts to the east of LAVO are significantly enriched in Ca relative to Fe, and it's plausible that the observed dust was

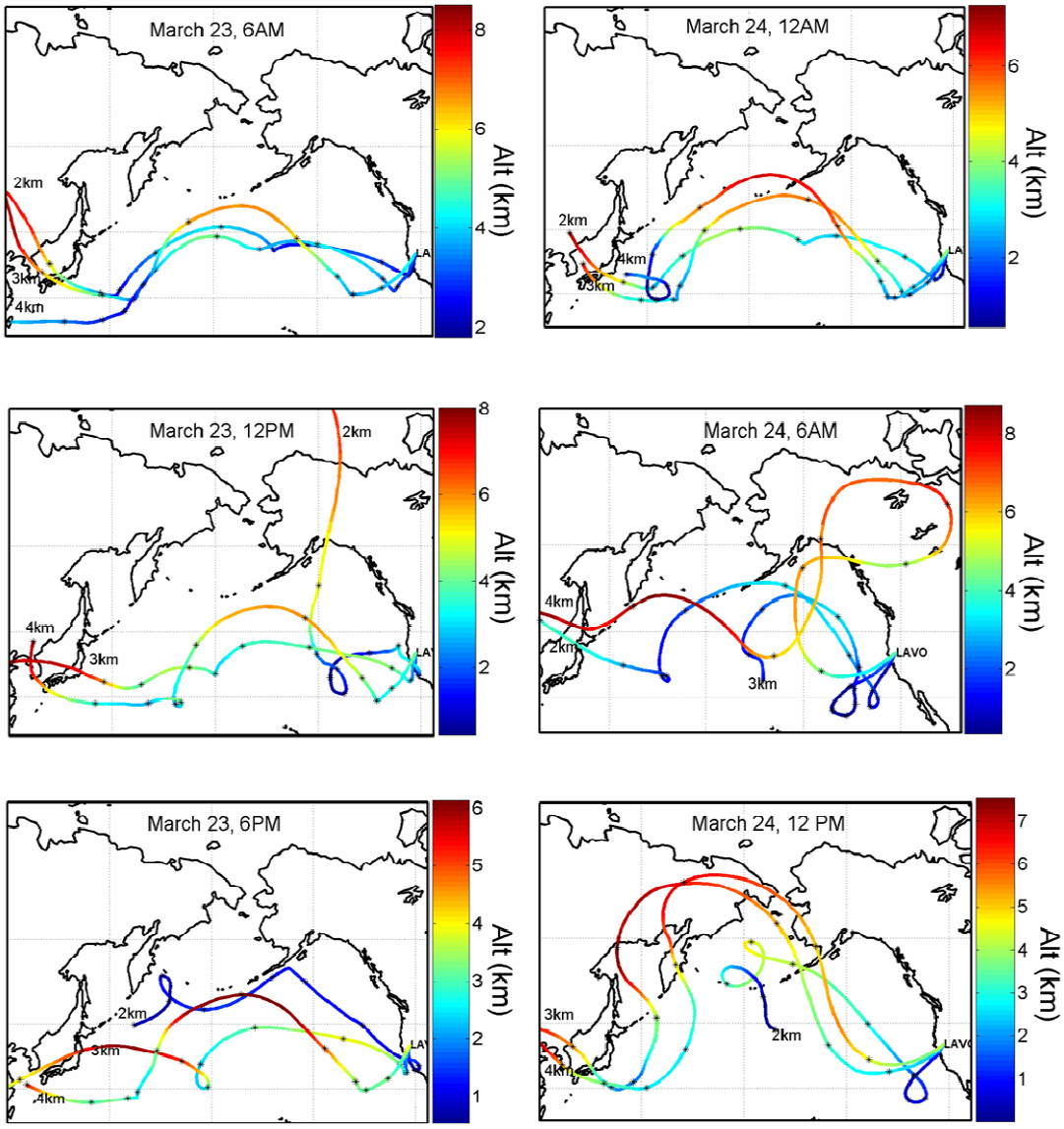

Figure 5.14. NOAA HYSPLIT 10-day air mass back trajectories for March 23rd and 24th. Trajectories are shown for air masses arriving at altitudes of 2 km, 3 km, and 4 km amsl over LAVO.

generated there. This would explain the high Ca concentration in coarse mode dust that was not evident in the fine mode aerosol, as these deserts located directly on the eastern side of the mountain range within a few 100 km of LAVO. The PM10 concentration began to drop shortly after 6AM, when wind speed increased and wind direction returned to a southwesterly flow, in agreement with the HYSPLIT calculations.

During this same time however, the fine mode (PM1.0) aerosol was enriched in Fe compared to the Ca, indicating that, as on March 4th and 5th, the fine mode aerosol was not from the same source as the dust observed in the coarse mode. The XRF analysis of the snow water collected later in the day on the 23rd and on the 24th of March showed that the Fe in the aerosol removed by the snow was greater than the Ca by a factor of 4. Thus it is possible that the enrichment of Fe in the fine mode aerosols observed at LAVO was due to mixing with a fine background aerosol that contained large amounts of Fe relative to Ca and extended to higher altitudes. The BC concentration during this period followed the same trend as the dust, with a high concentration early on the 23rd, followed by a gradual decline. The back trajectories for the 2km layer on March 23rd at 12PM and 6PM indicated that the air mass spent almost 2 days over southern California and was influenced by emissions as far south as Los Angeles, another potential source for high levels of fine mode Fe from industrial processes. As previously stated, PM2.5 and PM1.0 are generally transported greater distances, making Los Angeles a plausible source for fine particles observed at higher altitudes above LAVO.

5.3 Conclusions

Identification of aerosols which have been transported across the Pacific Ocean and mixed with regional pollutants and dust relies on a reconstruction of the history of the observed aerosol, which is based on chemical composition, meteorology and air mass back trajectories. During transport, dust and pollution aerosols react with each other and naturally occurring aerosol, such as sea salt and sulfate. These reactions can cause initially hydrophobic particles like dust and BC to acquire hydrophilic coatings and make them more susceptible to wet removal. Gravitational settling causes the transported aerosol mass distribution to shift to ever smaller sizes the longer they remain in the atmosphere. Thus both the size and chemical composition may be drastically altered by the time these aerosols reach North America [*Mori, et al.*, 2003; *Sullivan, et al.*, 2007].

The largest regional dust source during the wet spring in Northern and Central California was most likely from active plowing of agricultural fields, which typically contain twice as much Fe by mass compared to Ca. Although dry lake beds and deserts to the east and southeast of the Cascades and Sierra Nevadas contain higher concentrations of Ca than Fe, the dominance of westerly winds prevents this dust from having a significant impact on the west facing slopes of the Sierra Nevada and Southern Cascades during March and April. Numerous studies of dust from several regions in China and Mongolia have shown that the Fe/Ca ratios for Asian dust range from 0.5 to just above 1, compared with the North American Fe/Ca ratio for agricultural dust, which is 2. The ratios of Fe/Ca at LAVO indicated that Asian dust

accounted for 87 +/- 18% of the total observed dust in March and early April. An easterly shift in wind direction after April 15th (Chapter 4) likely brought Ca rich desert dust to the site, thus invalidating the use of Fe and Ca as tracers for Asian dust. Using literature values of EC mass relative to PM2.5 dust mass in measured in Beijing and Shanghai [*Yang, et al.*, 2005] of 0.08 to 0.1, and holding the proportions constant during transport, a rough estimate for the fractional contribution of Asian BC to high elevations in California was determined for March and April 2006. In contrast to the large contribution of Asian dust to observed dust in California, Asian BC was only approximately 33 - 40% of the observed BC. This was most likely because local and regional dust emissions in California would have been very low at this time of year due to elevated rainfall in the northern half of the state at this time of year. BC emissions on the other hand are not affected by rain and would not have changed.

The three case studies provided insight into mixing of local, regional, and transported aerosol. The first case presented evidence that although locally wind generated aerosol was dominant in the lower atmosphere, a back ground aerosol containing the fingerprint of East Asian dust constituted the greater part of the fine aerosol mass, both at the surface and aloft. This transported aerosol also represented the bulk of the aerosol removed by the snow, thus it was the transported pollutants at higher elevations, and not the surface aerosol, which made the greatest contribution to impurities in the snow. In the second case, the air mass back trajectories indicated a generally stable atmosphere, and orographic induced precipitation in the lower trajectories. The background Fe/Ca ratio of 1.2 to 1.5 in both the coarse and fine size

mode marked the dust aerosol as mixed North American and Asian. A peak in Fe rich dust during this study was likely local, as was the aerosol measured in the snow water, as both had a Fe/Ca ratio around 2.5. The final case presented more of a mystery, as the Ca mass was greater than the Fe in the coarse mode, but not in the fine. Surface easterlies during the early morning high aerosol concentration indicated that dry deserts to the east and southeast may have been the source of the observed PM10 aerosol observed at the surface. The 2km HYSPLIT back trajectories indicated that pollutants maybe have been transported from Los Angeles and other regions of southern California, another source region for Ca rich dust.

References

Andreae, M. O. (1983), Soot Carbon and Excess Fine Potassium - Long-Range Transport of Combustion-Derived Aerosols, *Science*, *220*, 1148-1151.

Bertschi, I. T., and D. A. Jaffe (2005), Long-range transport of ozone, carbon monoxide, and aerosols to the NE Pacific troposphere during the summer of 2003: Observations of smoke plumes from Asian boreal fires, *J Geophys Res-Atmos*, *110*, doi:10.1029/2004JD005135.

Bey, I., D. J. Jacob, J. A. Logan, and R. M. Yantosca (2001), Asian chemical outflow to the Pacific in spring: Origins, pathways, and budgets, *J Geophys Res-Atmos*, *106*, 23097-23113.

Chow, J., J. Watson, L. Ashbaugh, and K. Magliano (2003), Similarities and differences in PM10 chemical source profiles for geological dust from the San Joaquin Valley, California, *Atmos Environ a-Gen*, *37*, 1317-1340.

de Gouw, J. A., et al. (2004), Chemical composition of air masses transported from Asia to the U. S. West Coast during ITCT 2K2: Fossil fuel combustion versus biomass-burning signatures, *J Geophys Res*, *109*, D23S20, doi:10.1029/2003JD004202.

Draxler, R. R., and G. D. Hess (1998), An overview of the HYSPLIT_4 modeling system for trajectories, dispersion, and deposition, *Australian Meteorological Magazine*, *47*, 295-308.

Eldred, R. A., T. A. Cahill, and R. G. Flocchini (1997), Composition of PM(2.5) and PM(10) aerosols in the IMPROVE network, *J Air Waste Manage*, *47*, 194-203.

Goldstein, A. H., et al. (2004), Impact of Asian emissions on observations at Trinidad Head, California, during ITCT 2K2, *J Geophys Res*, *109*, D23S17, doi:10.1029/2003JD004406.

Hadley, O. L., V. Ramanathan, G. R. Carmichael, Y. Tang, C. E. Corrigan, G. C. Roberts, and G. S. Mauger (2007), Trans-Pacific transport of black carbon and fine aerosols (D < 2.5 mu m) into North America, *J Geophys Res-Atmos*, *112*, D05309, doi:05310.01029/02006JD007632.

Heald, C. L., D. J. Jacob, R. J. Park, B. Alexander, T. D. Fairlie, R. M. Yantosca, and D. A. Chu (2006), Transpacific transport of Asian anthropogenic aerosols and its impact on surface air quality in the United States, *J Geophys Res-Atmos*, *111*, D14310, doi:14310.11029/12005JD006847.

Henzing, J. S., D. J. L. Olivie, and P. F. J. van Velthoven (2006), A parameterization of size resolved below cloud scavenging of aerosols by rain, *Atmos Chem Phys*, *6*, 3363-3375.

Holmes, J., and W. Zoller (1996), The elemental signature of transported Asian dust at Mauna Loa observatory, *Tellus B*, *48*, 83-92.

Jaffe, D., S. Tamura, and J. Harris (2005), Seasonal cycle and composition of background fine particles along the west coast of the US, *Atmos Environ*, *39*, 297-306.

Krueger, B. J., V. H. Grassian, J. P. Cowin, and A. Laskin (2004), Heterogeneous chemistry of individual mineral dust particles from different dust source regions: the importance of particle mineralogy, *Atmos Environ*, *38*, 6253-6261.

Labban, R., J. M. Veranth, J. C. Chow, J. L. P. Engelbrecht, and J. G. Watson (2004), Size and geographical variation in PM1, PM2.5 and PM10: Source profiles from soils in the western United States, *Water Air and Soil Pollution*, *157*, 13-31.

Liang, Q., L. Jaegle, D. A. Jaffe, P. Weiss-Penzias, A. Heckman, and J. A. Snow (2004), Long-range transport of Asian pollution to the northeast Pacific: Seasonal variations and transport pathways of carbon monoxide, *J Geophys Res-Atmos*, *109*, D23S07, doi:10.1029/2003JD004402.

Liu, H. Y., D. J. Jacob, I. Bey, R. M. Yantosca, B. N. Duncan, and G. W. Sachse (2003), Transport pathways for Asian pollution outflow over the Pacific: Interannual

and seasonal variations, *J Geophys Res-Atmos*, *108*, (D20), 8786, doi:8710.1029/2002JD003102.

Luo, C., N. Mahowald, T. Bond, P. Y. Chuang, P. Artaxo, R. Siefert, Y. Chen, and J. Schauer (2008), Combustion iron distribution and deposition, *Global Biogeochemical Cycles*, *22*, -.

Mori, I., M. Nishikawa, T. Tanimura, and H. Quan (2003), Change in size distribution and chemical composition of kosa (Asian dust) aerosol during long-range transport, *Atmos Environ*, *37*, 4253-4263.

Park, S. S., Y. J. Kim, S. Y. Cho, and S. J. Kim (2007), Characterization of PM2.5 aerosols dominated by local pollution and Asian dust observed at an urban site in Korea during Aerosol Characterization Experiments (ACE)-Asia Project, *J Air Waste Manage*, *57*, 434-443.

Shen, Z. X., J. J. Cao, R. Arimoto, R. J. Zhang, D. M. Jie, S. X. Liu, and C. S. Zhu (2007), Chemical composition and source characterization of spring aerosol over Horqin sand land in northeastern China, *J Geophys Res-Atmos*, *112*, doi:10.1029/2006JD007991.

Sullivan, R. C., S. A. Guazzotti, D. A. Sodeman, and K. A. Prather (2007), Direct observations of the atmospheric processing of Asian mineral dust, *Atmos Chem Phys*, *7*, 1213-1236.

Sun, J. M., M. Y. Zhang, and T. S. Liu (2001), Spatial and temporal characteristics of dust storms in China and its surrounding regions, 1960-1999: Relations to source area and climate, *J Geophys Res-Atmos*, *106*, 10325-10333.

Sun, Y. L., G. S. Zhuang, Y. Wang, X. J. Zhao, J. Li, Z. F. Wang, and Z. S. An (2005), Chemical composition of dust storms in Beijing and implications for the mixing of mineral aerosol with pollution aerosol on the pathway, *J Geophys Res-Atmos*, *110*, -.

VanCuren, R. A., and T. A. Cahill (2002), Asian aerosols in North America: Frequency and concentration of fine dust, *J Geophys Res-Atmos*, *107(D24)*, 4804, doi:4810.1029/2002JD002204.

VanCuren, R. A., S. S. Cliff, K. D. Perry, and M. Jimenez-Cruz (2005), Asian continental aerosol persistence above the marine boundary layer over the eastern North Pacific: Continuous aerosol measurements from Intercontinental Transport and Chemical Transformation 2002 (ITCT 2K2), *J Geophys Res*, *110*, D09S90, doi:10.1029/2004JD004973.

White, W. H. (2008), Chemical markers for sea salt in IMPROVE aerosol data, *Atmos Environ*, *42*, 261-274.

Yang, F., K. He, B. Ye, X. Chen, L. Cha, S. H. Cadle, T. Chan, and P. A. Mulawa (2005), One-year record of organic and elemental carbon in fine particles in downtown Beijing and Shanghai, *Atmos Chem Phys*, *5*, 1449-1457.

Chapter 6

Conclusions

6.1 Summary

The research presented in this dissertation has shown how spring time transport of BC from East Asia not only affects the radiation budget over the Pacific Ocean and thus global climate, but also has the potential to impact mountain snow albedo in Northern California. Changes in snow surface albedo influence the rate and timing of snow pack melt rates [*Painter, et al.*, 2007]. Spring transport of Asian pollutants is enhanced due to the position of the jet stream at this time of year, the winter dry season in East Asia, and frequency of cold fronts moving across the dry East Asian deserts, lofting particles to altitudes where they are carried great distances by fast, high level winds [*Liu, et al.*, 2003]. The timing of this enhanced transport is especially relevant to high elevation sites in western North America, where the transported pollutants are often detected at the ground level and constitute a significant fraction of the observed aerosol. Spring marks the onset of snow melt as ambient temperatures approach 0°C, the temperature at which snow melt is the most sensitive to BC induced albedo reduction at visible wavelengths. When the surface air temperature is significantly below freezing, BC in snow absorbs energy at the surface, but cannot overcome the thermal inertia needed to initiate melt. If the ambient temperature is more than a few degrees above freezing, the efficiency of water, in any form, at absorbing infra-red radiation completely overwhelms the added contribution of melt due to BC absorption.

Chapter 2 presented a model calculation, using the CFORS (Chemical weather FORecast System), of the total amount of transported BC and fine aerosol mass in to North America between 30°N and 60°N between March 26th and April 25th, 2004. The total BC and aerosol mass transported across 130°W during the aforementioned period amounted to 28.5 +/- 3.25 Gg and 1000 +/- 100 Gg respectively. The model output was validated using aerosol and BC data collected onboard an the Wyoming King Air aircraft during the CIFEX (Cloud Indirect Effects Experiment) field study, as well as at over 30 ground stations operated by the IMPROVE (Interagency Monitoring of Protected Visual Environments) network. These aerosol observation sites were located in Alaska, Hawaii, Washington, Oregon and California. The monthly averaged BC and aerosol concentration from the IMPROVE stations compared well to the average concentrations predicted by CFORS above 1 km altitude; however the model over-predicted dust and BC concentration at lower elevations. Both the average, vertical distribution, as well as a time series of aerosol mass concentration, collected on board the aircraft agreed with the CFORS model above 2 km. Again the model output was much higher than observations in the lowest atmospheric layers. At an elevation of 2 km, CFORS predicted that approximately 40 to 50% of the BC was from East Asian emissions. Based on these results, the remainder of this dissertation focused on determining the amount of BC removed via wet deposition to the California mountain snow pack and estimating the contribution from trans-Pacific transport.

Chapter 3 provided a detailed description as to how the snow and rain samples were prepared and analyzed for BC mass concentration. Results from the field study were given in Chapters 4 and 5. Chapter 4 presented the measurements of BC, Fe, Ca, K, and Al mass concentration in rain and snow. The average BC concentration found in the snow at Lassen Volcano National Park and Central Sierra Snow Laboratory was roughly 6 ng/g and 7 ng/g respectively. Based on previous modeling studies of radiation interactions with "dirty" snow [*Clarke and Noone*, 1985; *Flanner, et al.*, 2007; *Grenfell, et al.*, 2002; *Hansen and Nazarenko*, 2004; *Jacobson*, 2004], the range of BC concentrations found in the California snow was enough to lower the albedo by 0.3% to 1.2%. A comparison between the ambient BC concentration prior to a precipitation event at LAVO and the total amount removed during the event showed that the two values were highly correlated, strong evidence that below cloud scavenging was the primary source of BC in the snow. This conclusion was further supported by the corresponding decrease in ambient BC during heavy precipitation events. A comparison between the mass concentration of excess fine potassium (K_{exc}), an indicator for biomass burning, and the ambient BC, indicated that during March, when snow samples were collected, approximately 76% of the observed atmospheric BC was from fossil fuel burning. This suggested urban and industrial processes as the primary source of BC for this period. During the latter half of April and early May, BC concentration increased by a factor of three, as did the relative concentration of K_{exc}, indicating that biomass burning contributed nearly 50% to the total BC observed at LAVO and that the source region was therefore likely to be more

rural. These conclusions were supported by NOAA HYSPLIT [*Draxler and Hess*, 1998] back trajectory calculations, as well as surface wind direction, which indicated areas to the east and northeast of LAVO as likely source regions for the regional aerosol. There are no cities located within a 1000 km of LAVO in that direction.

A similar analysis for the Ca, Fe, and K at both LAVO and CSSL resulted in weaker, but still significant, correlations between the total mass removed in a precipitation event and the ambient concentration prior to the event. The weaker correlation suggested that the dust aerosol observed at the ground was not as representative of what was measured in the precipitation as for the BC aerosol. This was probably because local and regional dust emissions would have been largely suppressed during the extremely wet spring in 2006; however BC emissions would have been unaffected. Therefore, long range transport likely contributed more to the observed dust aerosol in the snow samples and the ambient air compared to the BC mass. This conclusion was validated in Chapter 5.

Chapter 5 focused on the elemental XRF (X-ray fluorescence spectroscopy) measurements of both atmospheric aerosols and snow water contaminants to identify episodes of trans-Pacific transport of dust from Asia. The data indicated that approximately 87% the background aerosol was primarily fine mode East Asian dust, mixed with variable contributions from local and regional dust. This agrees with conclusions reached during similar analysis for the ITCT 2K2 field experiment in 2004 [*VanCuren, et al.*, 2005]. Fe enhancement in the fine (PM1.0 and PM0.75) mode relative to Ca was observed at both LAVO and CSSL, in short duration, episodic

bursts, which indicated local or near regional sources, most likely biomass burning and metal based industrial processes [*Luo, et al.*, 2008]. A strong correlation between K_{exc} and the excess fine Fe further supports this conclusion. An estimate of potential BC contribution from Asian aerosol transport was based on previous measurements of the relative BC mass to PM2.5 soil mass measured on the Asian coast, which was on average about 0.08 to 0.1 [*Shen, et al.*, 2007; *Yang, et al.*, 2005]. Assuming that this proportion remained constant during transport, the Asian contribution to BC observed at LAVO was 33 to 40 %, slightly lower, but still in agreement with the range of estimates predicted by the CFORS (Chemical weather FORecast System) model presented in Chapter 2.

An examination of three unique aerosol events at LAVO showed that depending on meteorology, aerosols observed near the ground are not always the primary factor determining the magnitude of impurities found in the snow Both boundary layer and synoptic scale meteorology influence how transported and regionally produced aerosols are mixed and incorporated into falling snow or rain. Size resolved mass concentrations of Fe and Ca were consistent with both local meteorological data and the air mass back trajectories, where nearby sources could adequately explain the elemental composition of the coarse mode aerosol and fine mode aerosols were transported from regions further away. The elemental analysis of the snow and rainwater aerosol mass concentrations were generally better correlated with the PM2.5 and PM1.0 ambient aerosol concentration, indicating that the fine mode aerosols extended to higher altitudes and were efficiently scavenged by falling

snow and rain. This was consistent with the conclusion that a large fraction of the fine aerosols were from far away sources, as transport typically occurs between 2 and 8 km [*de Gouw, et al.*, 2004; *Roberts, et al.*, 2006; *Stith and Ramanathan*, 2007].

6.2 Historical Context

The two studies, for which analysis was completed in this dissertation, corresponded to aerosol transport and concentration in March and April in 2004 and 2006. The following section provides a historical and spatial context for the results presented in Chapters 2 through 5 using aerosol data collected at three sites in the Southern Cascade and Sierra Nevada Mountain ranges and extending from January 2001 through December 2006. These data were taken from the IMPROVE (Interagency Monitoring of Protected Visual Environments) network [*Chow, et al.*, 2001] and include ambient EC (elemental carbon), PM2.5 soil dust, PM2.5 aerosol, and Fe (iron) and Ca (calcium) mass concentrations. The three sites comprise Kaiser (KAIS, 37.2°N, 119.15°W, 2597 amsl), Hoover (HOOV, 38.1°N, 119.2°W, 2560 amsl), and Lassen Volcano National Park (LAVO, 40.54°N, 121.6°W, 1730 amsl). The last of these, LAVO, was where the most intensive observational efforts took place for the data and results presented in Chapters 4 and 5. Thus the comparison between LAVO and the other two sites illustrated whether the results from LAVO were anomalous or generally representative of high altitude mountain locations in Northern California.

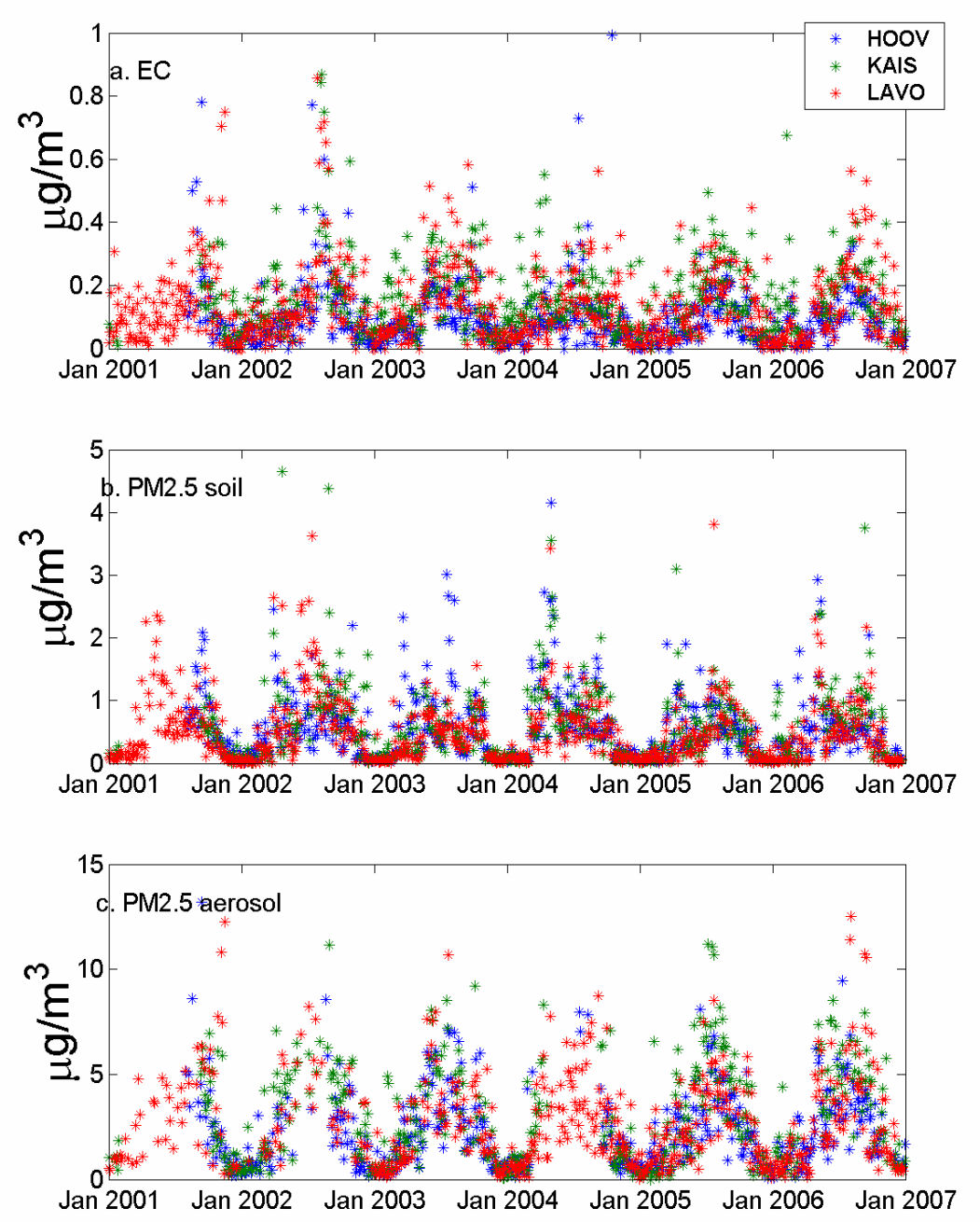

Figure 6.1. Six years of ambient EC, fine soil dust, and PM2.5 aerosol mass concentration at Hoover, Kaiser, and Lassen Volcano National Park.

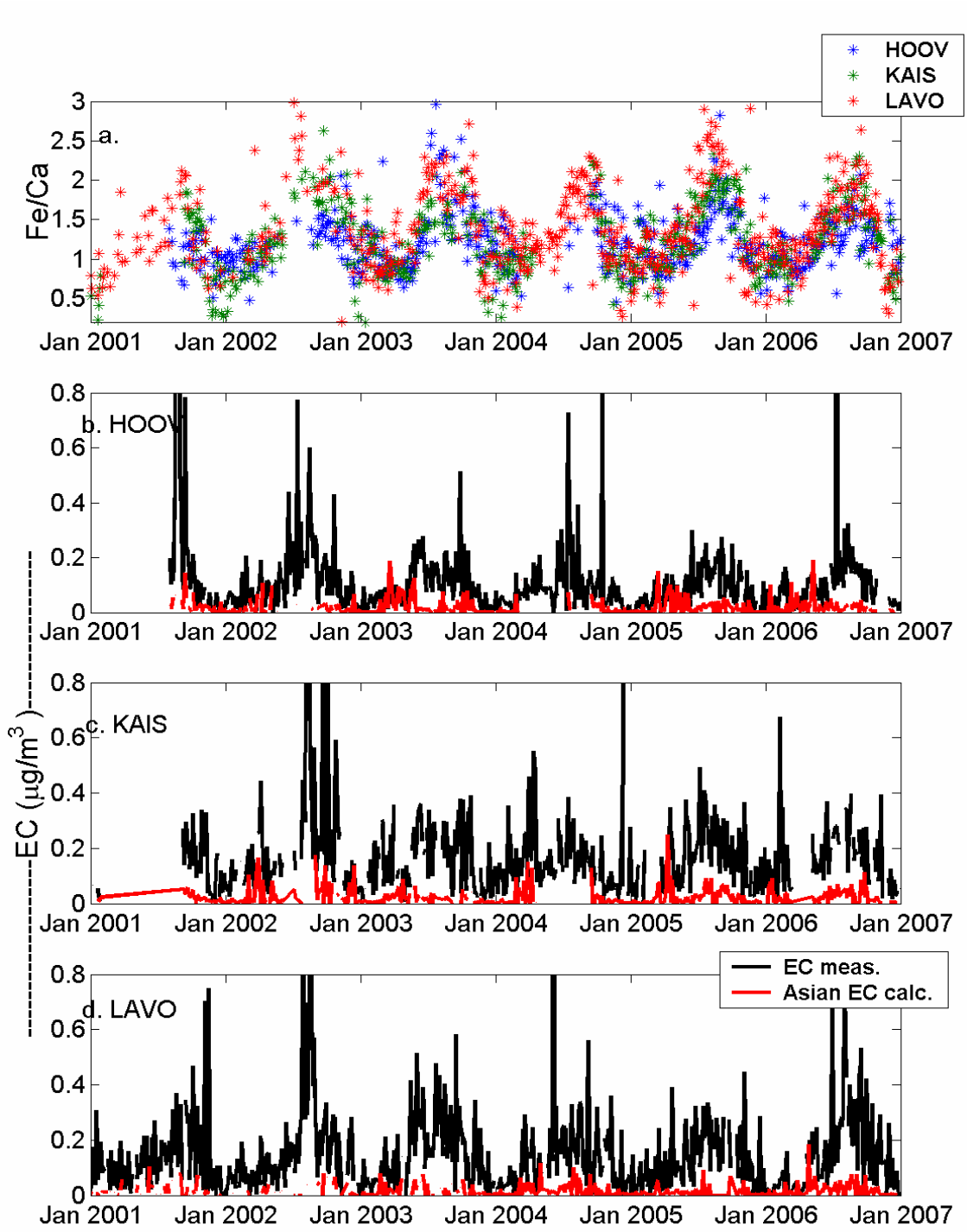

Figure 6.2 Six years of (a) Fe/Ca ratio in soil dust, and observed EC compared with calculated Asian contribution of EC at (b) Hoover, (c) Kaiser, and (d) Lassen Volcano National Park.

Similar to the four year time series of the Pb (lead) mass concentration shown in Chapter 2, the six year time series of: EC, the fine soil (PM2.5), and the PM2.5 aerosol, exhibit a clear and consistent annual variation in the magnitude of their mass concentrations (Figure 6.1). All three variables peak in July and August, which is the dry season in Northern and Central California. In the winter and early spring months, the mass concentrations are very low due to enhanced wet removal of atmospheric aerosols, as well as a suppression of dust emissions by comparatively wet conditions. Relative to the EC and total PM2.5, the fine soil mass concentration reduction during the winter and spring is more pronounced (Figure 6.1b), which is most likely due to the suppression of dust emissions, rather than just wet removal as with EC and PM2.5. The amplitude of the annual signal has remained consistent over the past 6 years at all three locations. Variables at all three sites are also well correlated and the relative magnitudes generally well matched.

In Chapter 5, the ratio of Fe to Ca was used to identify Asian and North American dust measured at LAVO. Asian dust corresponded to a ratio equal to or below 1, while North American dust was distinguished by Fe/Ca ratio greater than 2 [*VanCuren, et al.*, 2005]. A six year time series of the Fe/Ca ratios measured at the three previously mentioned IMPROVE observations sites (Figure 6.2a) provides support for this source apportionment technique. A clear annual signal in the Fe/Ca ratio that corresponds to the PM2.5 and fine soil concentrations (Figure 6.1) shows that in the winter and spring the ratio fluctuates around 1, indicating predominantly Asian dust. In the late summer and early fall, the peak of California dry dust emission

season, the Fe/Ca ratios are clustered around 2, typical of North American dust. As in Chapter 5, the Asian dust contribution was separated from the total PM2.5 soil mass concentration and used to make a rough estimate of the expected Asian BC associated with the Asian dust outflow (Figure 6.2 b, c, & d). Again the Asian BC mass concentration was estimated at roughly 8% to 10% of the Asian dust mass [*Shen, et al.*, 2007; *Yang, et al.*, 2005].

During March and April from 2001 to 2006, the average estimated Asian BC contribution to the observed BC varied between 25 and 45%. There was no systematic difference between the 3 sites and the estimated Asian contribution to BC is within reasonable agreement with the CFORS model result for Asian BC vs. total BC over North America (Chapter 2, Figure 2.10). BC and dust do not generally share the same source and, therefore, their relative magnitudes are not consistent in the day to day exported aerosol. For example, during a severe dust storm, the ratio of BC mass to dust would be greatly reduced. Therefore the calculation for the Asian BC fraction relies on seasonal averages of the exported BC mass concentration vs. the exported dust mass concentration from East Asia. Furthermore, calcium rich dust generated in North America may occasionally cause false Asian dust readings. The estimates of the Asian BC fraction of observed BC presented in this section represent general seasonal averages.

The six year time series of BC, fine dust, and PM2.5 elemental composition from the IMPROVE data network indicate that the results presented in this dissertation, although limited to data collected in two different years during spring, are

spatially and temporally representative of conditions in the Southern Cascades and Sierra Nevada Mountains in Central and Northern California. The annual variability in the Fe/Ca ratio, low in the winter and spring and high during the late summer and fall, validate its usefulness as a tracer for Asian dust. Lastly the average contribution of Asian BC accounts for roughly 25 to 45% and therefore likely contributes one quarter to a half of the BC observed in the snow pack at high elevation sites in Northern and Central California.

References

Chow, J. C., J. G. Watson, D. Crow, D. H. Lowenthal, and T. Merrifield (2001), Comparison of IMPROVE and NIOSH carbon measurements, *Aerosol Sci Tech*, *34*, 23-34.

Clarke, A. D., and K. J. Noone (1985), Soot in the Arctic Snowpack - a Cause for Perturbations in Radiative-Transfer, *Atmos Environ*, *19*, 2045-2053.

de Gouw, J. A., et al. (2004), Chemical composition of air masses transported from Asia to the U. S. West Coast during ITCT 2K2: Fossil fuel combustion versus biomass-burning signatures, *J Geophys Res*, *109*, D23S20, doi:10.1029/2003JD004202.

Draxler, R. R., and G. D. Hess (1998), An overview of the HYSPLIT_4 modeling system for trajectories, dispersion, and deposition, *Australian Meteorological Magazine*, *47*, 295-308.

Flanner, M. G., C. S. Zender, J. T. Randerson, and P. J. Rasch (2007), Present-day climate forcing and response from black carbon in snow, *J Geophys Res-Atmos*, *112*, -.

Grenfell, T. C., B. Light, and M. Sturm (2002), Spatial distribution and radiative effects of soot in the snow and sea ice during the SHEBA experiment, *J Geophys Res-Oceans*, *107*, 8031, doi:8010.1029/2000JC000414.

Hansen, J., and L. Nazarenko (2004), Soot climate forcing via snow and ice albedos, *P Natl Acad Sci USA*, *101*, 423-428.

Jacobson, M. Z. (2004), Climate response of fossil fuel and biofuel soot, accounting for soot's feedback to snow and sea ice albedo and emissivity, *J Geophys Res-Atmos*, *109*, D21201, doi:21210.21029/22004JD004945.

Liu, H. Y., D. J. Jacob, I. Bey, R. M. Yantosca, B. N. Duncan, and G. W. Sachse (2003), Transport pathways for Asian pollution outflow over the Pacific: Interannual and seasonal variations, *J Geophys Res-Atmos*, *108*, (D20), 8786, doi:8710.1029/2002JD003102.

Luo, C., N. Mahowald, T. Bond, P. Y. Chuang, P. Artaxo, R. Siefert, Y. Chen, and J. Schauer (2008), Combustion iron distribution and deposition, *Global Biogeochemical Cycles*, *22*, -.

Painter, T. H., A. P. Barrett, C. C. Landry, J. C. Neff, M. Cassidy, C. R. Lawrence, K. E. McBride, and G. L. Farmer (2007), Impact of disturbed desert soils on duration of mountain snow cover, *Geophys Res Lett*, *34*, L12502, doi:12510.11029/12007GL030284.

Roberts, G., G. Mauger, O. Hadley, and V. Ramanathan (2006), North American and Asian aerosols over the eastern Pacific Ocean and their role in regulating cloud condensation nuclei, *J Geophys Res-Atmos*, *111*, D13205, doi:13210.11029/12005JD006661.

Shen, Z. X., J. J. Cao, R. Arimoto, R. J. Zhang, D. M. Jie, S. X. Liu, and C. S. Zhu (2007), Chemical composition and source characterization of spring aerosol over Horqin sand land in northeastern China, *J Geophys Res-Atmos*, *112*, doi:10.1029/2006JD007991.

Stith, J., and V. Ramanathan (2007), The Pacific Dust Experiment (PaCDEX) Field Campaign: A summary of accomplishments during the field campaign and examples of early results, paper presented at American Geophysics Union Fall Meeting, San Francisco.

VanCuren, R. A., S. S. Cliff, K. D. Perry, and M. Jimenez-Cruz (2005), Asian continental aerosol persistence above the marine boundary layer over the eastern North Pacific: Continuous aerosol measurements from Intercontinental Transport and Chemical Transformation 2002 (ITCT 2K2), *J Geophys Res*, *110*, D09S90, doi:10.1029/2004JD004973.

Yang, F., K. He, B. Ye, X. Chen, L. Cha, S. H. Cadle, T. Chan, and P. A. Mulawa (2005), One-year record of organic and elemental carbon in fine particles in downtown Beijing and Shanghai, *Atmos Chem Phys*, *5*, 1449-1457.